SOLID STATE NMR INVESTIGATIONS OF CRYSTALLINE ORGANIC INCLUSION COMPOUNDS

BY

ALI MAHDYARFAR

A THESIS PRESENTED TO THE UNIVERSITY OF ST. ANDREWS

FOR THE DEGREE OF DOCTOR OF PHILOSOPHY

MARCH 1994

DECLARATIONS

I, Ali Mahdyarfar, hereby certify that this thesis, which is approximately 30000 words in length, has been written by me, that it is a record of my work carried out by me and that it has not been submitted in any previous application for a higher degree.

Date. 24/3/94

Signature of Candidate. .

I was admitted as a research student under Ordinance No. 12 in January 1991 and as a candidate for the degree of Ph.D. in January 1992; the higher study for which this is a record was carried out in the University of St. Andrews between 1991 and 1994.

Date. 24/3/94

Signature of Candidate. .

I hereby certify that the candidate has fulfilled the conditions of the Resolution and Regulations appropriate to the degree of Ph.D. in the University of St. Andrews and that the candidate is qualified to submit this thesis in application for that degree.

Date 24.3.94

Signature of Supervisor. . . .

©COPYRIGHT

ACKNOWLEDGEMENTS

I would like to express my appreciation to my previous supervisor Dr Kenneth Harris for his guidance within the period of his supervision; I have learned enormously from many instructive and informative discussions on scientific matters with him. Also, I would like to acknowledge the help and guidance that I received from my current supervisor Professor Colin Vincent in the period of his supervision.

I am grateful to all members of our research group for their help and assistance throughout this period. My special thanks to Dr Sharon Smart for introducing me to the computer simulation program for ^{2}H NMR and Dr Abil Aliev for his assistance with NMR spectrometer.

I would like to thank Dr Peter Jupp (from the Department of Mathematics, the University of St. Andrews) who has developed the essential mathematical framework related to the Markov chain model for inclusion compounds; the results and conclusions presented in chapter 4 could not have been obtained without his effort.

I wish to thank many members of the technical staff in the School of Chemistry, specially Mr Jim Bews for his help with computer, Mrs Melanja Smith for her assistance with MSL spectrometer, Mr Colin Smith (glass-blowing), Mr James Rennie (workshop) and Mr Jim Allen from photographic department.

Finally, I am greatly indebted to the CVCP and the School of Chemistry for their financial support that allowed me to study for a Ph.D. degree at the University of St. Andrews.

ABSTRACT

The work presented here is concerned with structural and dynamic investigations of crystalline organic inclusion compounds primarily using high-resolution solid state NMR spectroscopy. The focus has been on two types of host systems; urea and tri-ortho-thymotide (TOT).

High-resolution solid state ^{13}C NMR spectra of 1-haloalkane/urea inclusion compounds indicate the existence of two different interactions between end-groups of these guest molecules. This conclusion is derived from the presence of the two signals due to the related end-groups. The chemical shift variation of these signals as a function of the chain length of haloalkanes is reported. A noticeable trend is observed for some of these guest molecules.

The areas under these signals are related to the relative numbers of these two interactions. However mathematical analysis shows that it is not possible to derive intrinsic interactions between the end-groups from measurements on these inclusion compounds. It is shown that such information can be obtained *via* measurement on inclusion compounds containing two types of guest molecules, and then applying the standard results of a Markov chain on these measurements.

The migration of the potential guest molecules from the external liquid phase into the tunnel structure of urea inclusion compounds is reported by solid state ^{13}C NMR spectroscopy. Several evidence is presented to support the exchange mechanism for this observation.

The dynamics of deuterated benzene and pyridine in their TOT inclusion compounds is investigated by variable temperature ^{2}H NMR. These guest molecules are undergoing well defined motion in the solid cage structure. The detailed mechanism of their motions is investigated using computer simulation of the spectra.

CONTENTS

CHAPTER III

SOLID STATE ^{13}C NMR STUDIES OF ORIENTATIONAL DISORDER OF UNSYMMETRIC GUEST MOLECULES IN THEIR UREA INCLUSION COMPOUNDS

CHAPTER IV

INVESTIGATION OF WEAK INTERMOLECULAR INTERACTIONS BETWEEN FUNCTIONAL GROUPS IN UREA INCLUSION COMPOUNDS; SOLID STATE NMR AND A STATISTICAL ANALYSIS STUDIES

CHAPTER V

STUDY OF DIFFUSION OF GUEST MOLECULES INTO THE TUNNEL STRUCTURE OF UREA INCLUSION COMPOUNDS

CHAPTER VI

^{2}H NMR INVESTIGATION OF GUEST DYNAMICS IN TRI-ORTHO-THMOTIDE INCLUSION COMPOUNDS

CHAPTER I

BASIC PRINCIPLES OF SOLID STATE NMR SPECTROSCOPY

Introduction

Solution NMR spectroscopy has been used widely for the investigation of unknown molecular structures. The primary information which is provided by high-resolution NMR spectroscopy is:

1. The chemical shifts; using this parameter different chemical environments present within the sample can be determined.
2. The relative intensities; which provide the relative proportions of these environments.
3. Coupling constants; which provide information on connectivites, geometry, etc.

If solution NMR techniques are applied directly to solid samples, the spectra will be characteristically broad and featureless. This is due to the existence of several spin interactions which are anisotropic in nature . These interactions are largely eliminated in solution by rapid isotropic molecular motion.

The application of a variety of solid materials such as glasses, ceramics, catalysts, polymers, coals, woods in industry demands detailed structural information for these materials [1]. However most of these solids are amorphous in nature and therefore utilisation of X-ray diffraction techniques is uninformative.

In this chapter we describe briefly the phenomenon of nuclear magnetic resonance and some basic experimental considerations of recording the spectra; then we illustrate different approaches that can be

invoked in order to record high-resolution NMR spectra of solids. Finally some recent applications of this technique in different areas of solid state chemistry are presented.

1.1. Basic NMR Interactions

The nuclei which contain an odd number of either protons or neutrons or both, possess spin angular momentum (**P**) and therefore a magnetic moment μ:

$$\mu = \gamma \mathbf{P} \qquad (1)$$

where $\mathbf{P} = h\,(I(I+1))^{1/2}$ and I is the spin quantum number. The constant γ in this equation is called the "gyromagnetic ratio" and is a nuclear constant of the order of $10^7\ T^{-1}\ s^{-1}$. The quantization law predicts the presence of 2I + 1 states for the angular momentum (I is the nuclear spin quantum number) [2].

The interaction (Zeeman interaction) between an external static magnetic field (B_0) and the nuclear spin system removes the degeneracy of these states;

$$H_Z = \mu.\mathbf{B}_0 \qquad (2)$$

The result of this interaction is the generation of discrete energy levels;

$$E_m = -\frac{1}{2\pi} m\,\gamma\,h\,B_{loc.} \qquad (3)$$

where m = (I+1, I-1). In this equation $B_{loc.}$ is the combination of the external field B_0 and the internal component B_{int} which is arised from the interaction of the nuclei with their surrounding environments;

$$B_{loc} = B_0 + B_{int} \qquad (4)$$

Determination of these internal fields is of central interest in NMR spectroscopy, since they convey structural information. The complete Hamiltonian which describes different interactions between spins can be written as:

$$\begin{aligned} H_{NMR} &= H_{ext} + H_{int} \\ &= (H_Z + H_{RF}) + (H_S + H_D + H_Q) \end{aligned} \qquad (5)$$

The first two terms are not related to the molecular or structural characteristics of the system and are imposed externally. These include the Zeeman interaction (H_Z) and the radio frequency interaction H_{RF}, which describes the interaction of the spins with the periodically fluctuating magnetic component of the radiofrequency field used in the NMR experiment. This term (H_{RF}) does not have any effect on the line shapes of NMR spectra, but it is of pivotal importance in understanding pulsed NMR experiments. Other terms in this equation which are internal with respect to the spin systems are; chemical shielding interaction (H_S), dipolar interaction (H_D), and quadrupolar interaction (H_Q).

1.2. Nuclear Spin Tensor Interactions

All the internal Hamiltonian contributions involve tensor quantities. A tensor is a property which links two vectors. For example shielding tensor, σ, links the magnetic field which arises from the shielding, B_S, to the applied magnetic field, B_0, by the equation:

$$B_S = - \sigma B_0 \qquad (6)$$

In general the linked vectors are not parallel, though for shielding we are only interested in the component of B_S that is along B_0. Since vectors have three components, any tensor R (in its cartesian form) can be represented by a matrix of 9 components:

$$R = \begin{vmatrix} R_{11} & R_{12} & R_{13} \\ R_{21} & R_{22} & R_{23} \\ R_{31} & R_{32} & R_{33} \end{vmatrix}$$

If the tensor is symmetric i.e. Rji = Rij it is possible to transform R to the diagonal form by choosing an appropriate axis system (Principal Axis System, "PAS"):

$$\begin{vmatrix} R_{xx} & 0 & 0 \\ 0 & R_{yy} & 0 \\ 0 & 0 & R_{zz} \end{vmatrix}$$

R_{xx}, R_{yy}, R_{zz} are principal components of the tensor and the required information is within them. Euler angles required to transform from a general frame to the PAS .

Instead of using R_{xx}, R_{yy}, R_{zz} to describe the system, it is very common to define alternative parameters;

(A) the isotropic average $R_{iso} = 1/3\ (R_{xx}+R_{yy}+R_{zz})$

(B) the asymmetry η, this is a dimensionless quantity which is between 0 and 1;

$$\eta = \frac{|Rxx-Ryy|}{|Rzz|}$$

where $|R_{zz}| \geq |R_{yy}| \geq |R_{xx}|$.

1.3. Magnetic Dipole-Dipole Interaction

The magnetic dipole-dipole interaction describes the effect of the local magnetic fields associated with the magnetic moments of surrounding nuclei. There are two different mechanisms for this interaction: through-space coupling (direct coupling) and the indirect spin-spin coupling which occurs *via* polarisation of bonding electrons. In NMR spectra of solids, the first term is usually dominant. The corresponding Hamiltonian describing the interaction between two spins with gyromagnetic ratios γ_1 and γ_2 and internuclear distance r is;

$$H_D = \frac{\gamma_1\gamma_2 h^2}{4\pi^2 r^3} \text{ I. D. S.} \qquad (7)$$

The second rank tensor "D" characterising the spatial part of the dipolar two spin Hamiltonian is always axially symmetric and traceless (i.e. R_{iso} = 0). This simplifies the mathematical description of the interaction.

For a single crystal, the interaction between two isolated spins can be evaluated. The spectrum will contain two lines with the peak separation $\Delta\upsilon$ given by:

$$\Delta\upsilon = \frac{\gamma_1\gamma_2 h^2}{4\pi^2 r^3}(1 - 3\cos^2\theta) \qquad (8)$$

where the θ is the angle between the internuclear vector and the applied magnetic field. For a particular nucleus, pairwise interactions between a nucleus and all its neighbours exist, although because of the $1/r^3$ factor the near neighbour interactions are dominant. In a polycrystalline material the above equation must be averaged over all possible angles of θ corresponding to the random orientational distribution of polycrystallites and therefore of internuclear vector orientations.

The net result of these two factors is to generate a severe broadening of the spectrum, which is field independent. For most systems of spin 1/2 nuclei this is the main line broadening interaction and is the largest for ^1H containing systems as ^1H has the largest γ value of any nucleus and its small size allows for small internuclear distances (r). For proton-proton interactions dipolar line broadening can range up to about 80 kHz, and ^{13}C-^1H interactions can give a line broadening of up to 40 kHz in the ^{13}C NMR spectrum.

1.4. Chemical Shift Interaction

The chemical shift describes the effect of magnetic electron-nucleus interactions which affect the local field experienced by the nucleus and therefore influence its resonance frequency. Such influences comprise, (a) diamagnetic shielding by closed electronic shells, (b) paramagnetic deshielding by the angular momenta of admixed excited electronic states, (c) shielding or deshielding by rapidly fluctuating paramagnetic electron spins, and (d) shielding or deshielding effects due to conduction electrons at the Fermi edge (Knight shift). Although these contributions are physically distinct, they are inseparable in the experiment. The chemical shift Hamiltonian, describing the composite effect of these interactions is:

$$H_S = \mathbf{I}\,(1-\sigma)\,\mathbf{B}_0 \qquad (9)$$

Here σ is a second rank tensor and, as described before, it can be rotated into a coordinate system, the principal axis system, in which it has diagonal form, with σ_{xx}, σ_{yy}, σ_{zz} as the only non zero components. A complete description of the chemical shift tensor includes six parameters, the three diagonal components and the three Euler angles that relate the orientation of the principal axis system to the crystal or molecular axis of

the solid considered. In general such detailed knowledge necessitates orientation-dependent measurements of the resonance frequencies of single crystals. The situation is comparatively simple, if a molecular axis of higher symmetry is present. In this case, the symmetry axis fixes the PAS and only two chemical shift components parallel and perpendicular to this axis need to be specified.

The chemical shift tensor components can provide valuable quantitative information about local symmetry [4]. For example, if we observe a lineshape such as in Fig 1.1(b) we can conclude that a higher local symmetry axis (C_3, C_4, C_6) is present. In amorphous solids, a

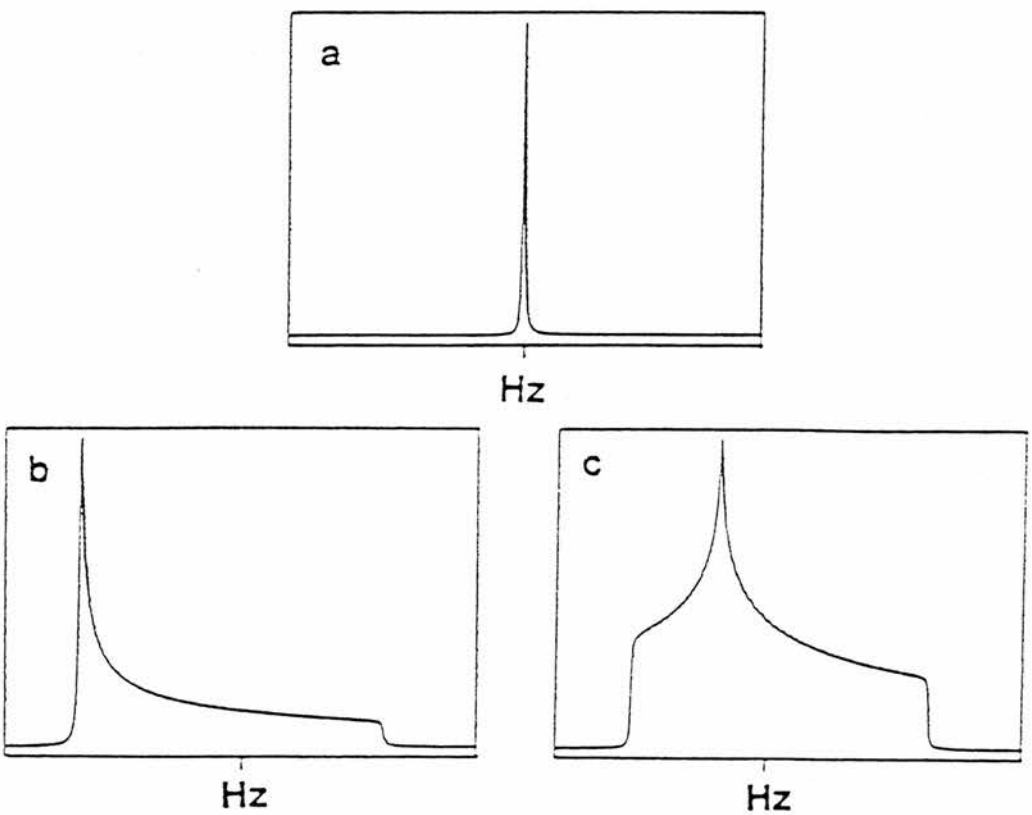

Fig. 1.1 Typical chemical shift-dominated NMR powder patterns: (a) spherically symmetric chemical shift tensor, (b) axially symmetric chemical shift tensor, and (c) asymmetric chemical shift tensor.

distribution of chemical shift parameters usually exists. In cases in which chemical shift anisotropy is small, this distribution may obscure structured lineshapes. The isotropic chemical shift;

$$\delta_{iso} = 1/3\,(\delta_{xx} + \delta_{yy} + \delta_{zz}) \qquad (10)$$

is the main observable in the line-narrowing experiments such as magic angle spinning (MAS) NMR. δ_{iso} depends sensitively on the chemical and electronic environment of the nucleus under study.

1.5. Nuclear Electric Quadrupole Interaction

Another perturbation on the nuclear magnetic energy levels arises from the interaction of non-spherically symmetric nuclear charge distributions (quadrupole moment) with electric field gradients (EFG) generated by asymmetric electron distributions in molecules or lattice sites. Quadrupolar interaction only affects nuclei with $I > 1/2$, and only if these nuclei are in non-cubic environments. The Hamiltonian describing this interaction is:

$$H_Q = \frac{e^2qQ}{4I(2I-1)}\{3I_z^2 - I^2 + \eta(I_x - I_y)\} \qquad (11)$$

Fig 1.2 shows the resulting energy level diagram and the resulting powder lineshape for a nucleus with I=1. By convention, the quadrupolar interaction is then characterised by two parameters, e^2qQ/h (the quadrupole coupling constant) and η (the asymmetry parameter) which are unique for each nucleus within a specific environment. In principle, e^2qQ/h and η can be evaluated from the line shape of powder patterns of the type shown in Fig 1.2.

In many cases, however, these transitions extend over such a wide spectral region that they often escape experimental detection. The quadrupolar nucleus which is most widely used by chemists in studies of condensed phases is deuterium, with I = 1. ^{2}H NMR lineshapes are very sensitive to the exact details of motions occurring in molecular solids. By analysis of the lineshapes it is possible to deduce detailed mechanistic information about the relevant motion. The motions appropriate for investigation by this technique are those with frequency in the range 10^3 to 10^8 s^{-1}.

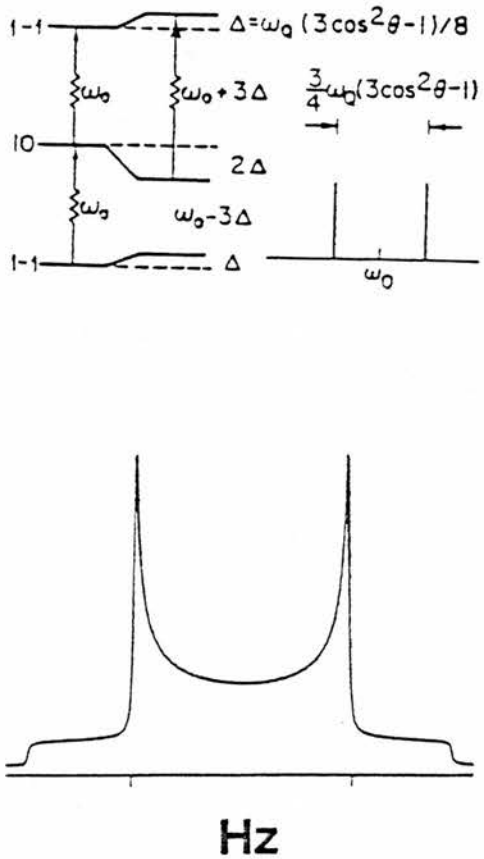

Fig. 1.2 Energy level diagram and the lineshape for I=1 in single crystals (upper right) and powders (lower part).

1.6. Experimental Pulsed NMR

In NMR spectroscopy the magnetic component of an applied radiofrequency field generates transitions between various nuclear energy levels. There are two common approaches used to bring about these transitions: (1) variation of the external magnetic field under continuous irradiation of a monochromatic frequency υ_0 (continuous wave NMR), and (2) polychromatic excitation of the entire spectrum by short pulses at a carrier frequency υ_0 and a fixed magnetic field strength. Due to the widespread use of pulsed NMR, here we only discuss the second method in detail [5].

In order to explain pulsed NMR experiments, we consider that the interaction of the nuclear magnetic moments with the magnetic field forces the nuclei to precess around the field direction at the Larmor frequency:

$$\upsilon_p = (2\pi)^{-1} \gamma B_{loc} \qquad (12)$$

The macroscopic magnetisation, which forms at spin-lattice equilibrium as a result of the Boltzmann distribution, is the target of the pulsed NMR experiment. To measure the NMR spectrum of the sample, this magnetisation is converted to a nuclear induction signal. The principle is illustrated with vector diagrams depicted in the "rotating frame", i.e. a coordinate system that rotates with the carrier frequency υ_0 about the magnetic field axis (see Fig. 1.3).

A short (1-10 μs), intense (100-1000 Watt) radiofrequency pulse (90° pulse) is applied that tips the magnetisation into the plane perpendicular to the magnetic field direction . The pulse must be applied at the carrier frequency υ_0 in the vicinity of υ_p. Precise resonance is, however, not required, since pulsed excitation is itself polychromatic.

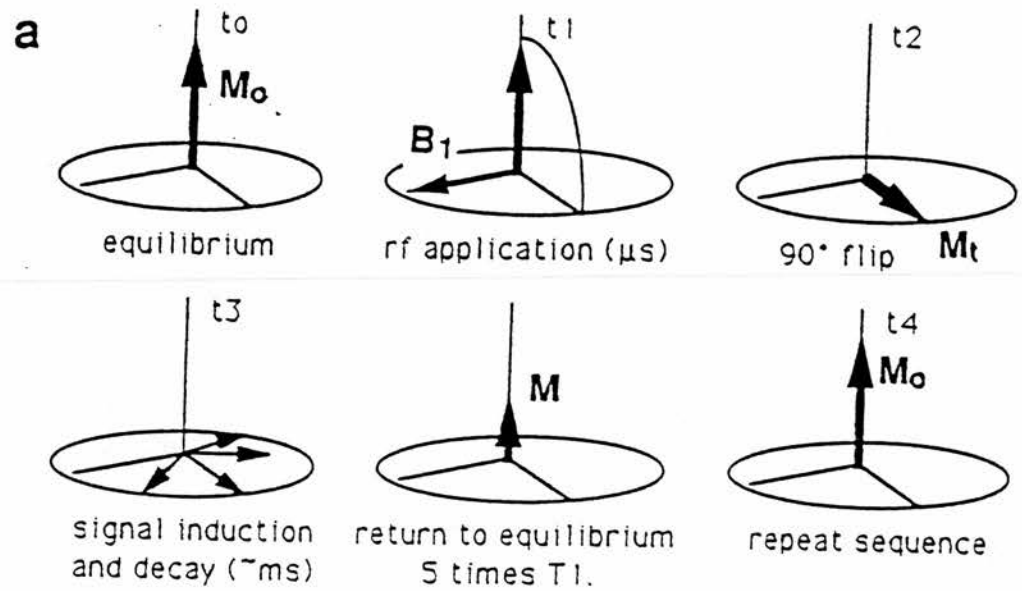

Fig. 1.3 Detection of NMR signal by pulsed spectroscopy, shown in the rotating coordinatine system associated with the oscillating magnetic field component at the applied radio frequency ω_0 at various stages (t_0-t_4) of the experiment.

Since samples with multiple sites have a range of values of υ_p, it is important, however, that the Fourier spectrum of the pulse includes the entire range of such precession frequencies. In polycrystalline solids the required range is typically 100-200 kHz, which is easily covered by short pulses (ca. 5 μs or less). In certain cases, site distribution effects or strong quadrupolar interactions generate much wider ranges of resonance frequencies.

Following the 90° flip by the RF excitation pulse, the magnetisation precesses with the υ_p components of the nuclei present and induces an a.c. voltage in the detector coil of the NMR probe. This voltage signal decays in time because the magnetisation vectors lose their phase-coherence due to their differences in υ_p as well as due to spin-spin interactions. The free-

induction decay signal is amplified, and is mixed in the receiver section of the spectrometer with the carrier frequency υ_0. The resulting signal then oscillates at the difference frequency $\upsilon_{offset} = |\upsilon_p - \upsilon_0|$ and is typically in the audio frequency range (0-200 kHz). If more than one chemically distinct site is present in the sample, this signal is a decaying interferogram (beating pattern) of several different frequency components. Fourier transformation of this digitised interferogram then provides the various components of υ_{offset} (and hence the υ_p) . Chemical shifts are determined by comparison of υ_{offset} for the sample of interest with that of a chosen standard.

Since the acquired signals are generally weak, signal averaging by repetitive pulsing is usually necessary. A 90° pulse creates a set of equally populated nuclear spin levels, hence no z-magnetisation is present immediately after the pulse, and one must allow for sufficient time for the spin system to relax to its equilibrium state. For quantitative applications, the repetition time must exceed 5 times the longest spin-lattice relaxation time for any nuclear environment in the sample.

1.7. Techniques for Line Narrowing in Solids

1.7.1. Introduction

The presence of the interactions described in section 1.1 the solid state and their anisotropic nature leads to severe line broadening in the spectra of solid materials. One main challenge in the field of solid state NMR has been the invention of appropriate techniques to eliminate this line broadening and to acquire spectra with resolution comparable to solution state NMR spectra [5]. Here we present some of the important line narrowing techniques which are now routinely used in recording the spectra of solids.

1.7.2. Magic Angle Spinning

The anisotropic nature of dipolar interactions and chemical shielding is the major source of line broadening for spin 1/2 nuclei in solids. In solution, rapid isotropic motion averages these interactions to zero and consequently we observe sharp signals at the isotropic values. Both dipolar coupling and chemical shift anisotropy in the solid state possess an angular dependence of:

$$3\cos^2\theta - 1 \qquad (13)$$

where θ is the angle between a specific direction that depends on the orientation of the molecule and the static magnetic field B_0.

Fig. 1.4 shows a schematic diagram for the MAS experiment. A given internuclear vector forms an angle χ with respect to the axis of the cylindrical sample (S).

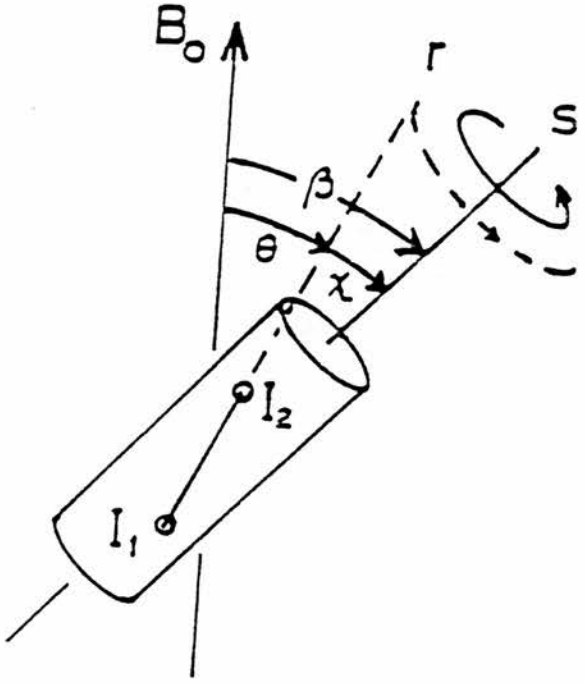

Fig. 1.4 Definition of the angles for the MAS experiment.

If spinning about axis S occurs, for the indicated nuclear pair, θ will vary between $\beta-\chi$ and $\beta+\chi$, where β is the angle between the axis of spinning and B_0. Clearly the average NMR interaction depends on $<3\cos^2\theta - 1>$. Simple geometric arguments show that this dependence is given by following equation;

$$<3\cos^2\theta - 1> = 1/2\,(3\cos^2\beta - 1)\,(3\cos^2\chi - 1) \qquad (14)$$

In this equation χ can take all possible values between π and $-\pi$. The value β is at the choice of the experimentalist. In the special case when $\theta = 54^\circ 44'$ then;

$$3\cos^2\theta - 1 = 0$$

Consequently if the sample holder containing polycrystalline material oriented at this specific angle (magic angle) with respect to B_0 is spun fast enough, broadening due to these interactions is essentially eliminated. In practice, it is generally not possible to achieve such spinning rates, therefore for many systems it is impossible to eliminate the effect of these two contributions by means of magic angle spinning (MAS) alone.

Nevertheless in some types of compound, MAS alone is sufficient to generate reasonably sharp signals to allow the determination of isotropic chemical shifts for different sites in the sample. In most inorganic compounds there are relatively few or no protons, to produce broadening due to heteronuclear dipolar coupling between protons and the nucleus of interest. Although other nuclei might exist within these systems, the proton is usually the main source of heteronuclear dipolar broadening. If the CSA is small, magic angle spinning will generate relatively sharp signals. In order to succeed using MAS experiment in line narrowing, the

rotation frequency must be at least of the order of the CSA linewidth which is often a few kilohertz; many MAS experiments can be conducted at the rate of about 3 kHz. When the CSA linewidth is larger than the spinning frequency, a set of sharp lines (isotropic peak + spinning sidebands) spaced at the rotation frequency are generated.

Fig. 1.5.a. shows the ^{207}Pb NMR spectrum of a static sample of lead (II) nitrate [6]. Since this is a dilute spin case and there are no protons in the sample, there will be no contribution from dipolar broadening and the line broadening is determined by CSA. Fig 1.5.b. shows the ^{207}Pb NMR spectrum of lead (II) nitrate with magic angle spinning (MAS) at 3.2 kHz. In effect, the intensity of the sideband manifold maps the amplitude of the CSA pattern. For example, in lead nitrate the line is 2.5 kHz wide for a static sample. In a spectrum acquired with 500 Hz MAS (Fig. 1.5.c.) the most intense component is not at the isotropic chemical shift but rather at the maximum of the CSA powder pattern.

Another system for which MAS alone will produce narrow lines is the case of plastic crystals. In such crystals there is long range order, in that individual molecules occupy well defined lattice positions, but the molecules are free to rotate in the crystal. This motion may be fast enough to average substantially the dipole-dipole interactions, which sharpens the signals to a point where the magic angle can further reduce the linewidth to less than the chemical shift differences. Adamantane is a classical example of such a material.

We should also mention that, in some cases, it is not possible to spin the sample fast enough to remove all of the effects of the CSA. The resulting spectra will therefore contain spinning side bands and are consequently difficult to analyse. However, when there is a small number of spinning sidebands (as is usually the case for ^{13}C nucleus), it is possible to eliminate the sidebands from the spectrum by a technique first

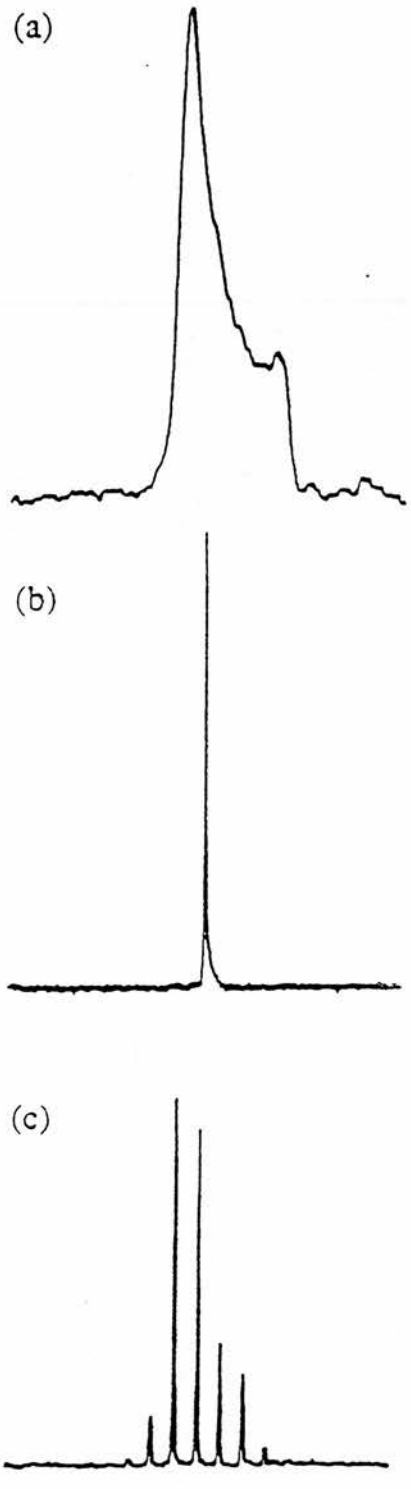

Fig. 1.5 41.7 MHz ^{207}Pb spectra of polycrystalline $Pb(NO_3)_2$ with a spectral width of 200 ppm. In (a) the sample is static, in (b) the sample is spinning at the magic angle at 3.2 KHz and in (c) the sample is spinning at 500 Hz.

introduced by Dixon [7]. In this method (so called "TOSS"; total suppression of spinning sidebands) sidebands are inverted by the pulse sequence but the isotropic peak is unaffected. The addition of spectra with normal and inverted sideband intensities gives a spectrum with only the isotropic peaks.

1.7.3. Dipolar Decoupling

The major source of line broadening in the ^{13}C NMR spectra of organic solids is dipolar coupling to protons. Consequently a heteronuclear decoupling experiment similar to solution NMR can be used to remove the coupling between ^{13}C and ^{1}H. The only difference concerns the magnitude of coupling in solids which is much higher than in solution; therefore the decoupling power required for solid materials is substantially bigger. In solution NMR spectroscopy, the decoupler power is typically five watts or less, whereas for solid materials the dipolar decoupling power is of the order several hundred watts. The combination of MAS and dipolar decoupling will remove both CSA and heteronuclear dipolar broadening and will result in a spectrum very similar to solution state NMR.

1.7.4. Multiple Pulse Line Narrowing

Application of the dipolar decoupling experiment for removing homonuclear dipolar interaction simply removes the whole of the spectrum. For example in ^{1}H NMR spectroscopy the line broadening is primarily due to homonuclear ^{1}H-^{1}H dipolar interaction. However there are several pulse sequences which remove the homonuclear dipole-dipole interaction. These multiple pulse line narrowing pulse sequences utilise the fact that, when applied with suitable widths and delays, a series of pulses can average the dipolar interaction by reorienting the spins. To a

simple approximation, the sequences produce an averaging of the spin vectors in the rotating frame to the magic angle with respect to the applied magnetic field. Two famous pulse sequences of this type are WAHUHA (after Waugh, Huber, and Haeberlen) [8]. and MREV-8 (after Mansfield, Rhim, Elleman, and Vaughan) [9]. These line narrowing sequences can also be combined with magic angle spinning to remove CSA and further sharpen the signals. The ^1H NMR signals obtained using this method are considerably narrower than ordinary ^1H NMR spectrum of solids. The usual linewidth obtained using this technique is about 1 ppm. Considering that the total range of isotropic chemical shifts for ^1H is ca. 10 ppm, this linewidth still can not provide very good resolution.

1.8. Intensity Enhancement via Cross Polarisation (CP)

Spin-lattice relaxation times for dilute nuclei such as ^{13}C in solids are often considerably longer than for ^1H. These can sometimes be of the order of an hour. In fact it is possible to transfer magnetisation from nuclei with high-γ to nuclei with low-γ by exploiting the dipolar coupling between them. The technique "cross polarisation" (CP) based on this idea (first introduced by Pines, Gibby, and Waugh) [10], can be used to increase the signal-to-noise ratio (S/N) of the spectrum of the dilute nucleus X; however, the resolution of the spectrum will not be affected. The basic idea of the pulse sequence (illustrated in Fig. 1.6) is to enhance the magnetisation of the dilute nucleus X from the magnetisation reservoir of the abundant proton spin system. The sequence starts by the rotation of the proton spin magnetisation by 90° to align it with the Y axis in the rotating frame. The phase of this on resonance pulse is now shifted by 90° so that it ($\mathbf{B}_H$) and the proton magnetisation are both aligned along the Y axis. The proton spins will now precess around $\mathbf{B}_H$, and are said to be spin-locked, the fast decay due to T_2 processes which would normally

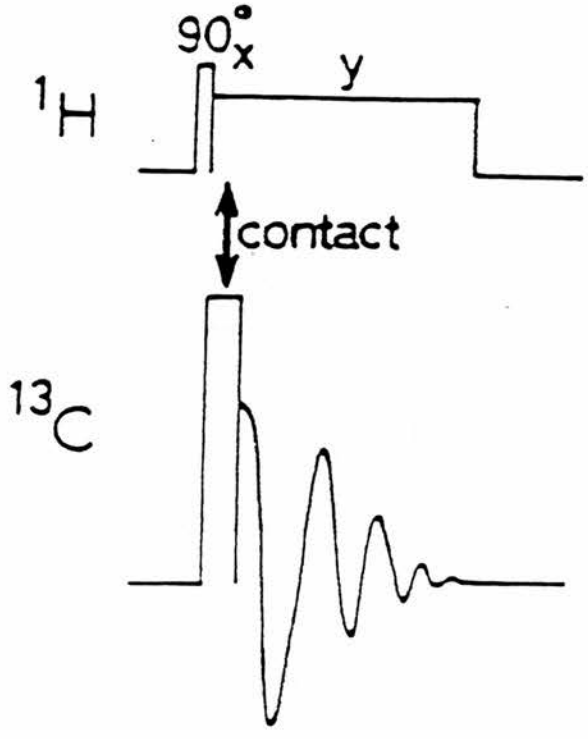

Fig. 1.6 The cross-polarization pulse sequence, using the case ^{1}H-^{13}Cas an example.

occur is prevented by the spin-locking field $\mathbf{B}_H$. Simultaneous with the phase-shift of the proton pulse, an on-resonance RF pulse $\mathbf{B}_X$ is applied to the dilute nucleus X, with the magnitudes of $\mathbf{B}_H$ and $\mathbf{B}_X$ chosen so that they satisfy the 'Hartman-Hahn' condition:

$$\gamma_H \mathbf{B}_H = \gamma_X \mathbf{B}_X \qquad (15)$$

The X-nucleus magnetisation now grows by transfer of magnetisation from the proton reservoir during the 'contact time' τ_1 in which the Hartman-Hahn condition is satisfied. At the end of this time, the X-pulse is turned off, and the X-nucleus free induction decay is recorded in the time period τ_2, during which the proton field $\mathbf{B}_H$ acts as a

decoupling field. After the recycle delay τ_3, the sequence is repeated. In principle, several 'contacts' of the X-spins could be performed within a single proton spin-locking pulse, but in practice, single contacts are usually used.

The enhancement of signal-to-noise of the X-nucleus by cross polarisation experiment is accomplished *via* two mechanisms:

1. The magnetisation of the X-nucleus is increased by polarisation transfer from the proton reservoir (maximum increase by the factor γ_H/γ_X).
2. The relaxation time T_1 for the proton magnetisation is generally shorter than that for the X-nuclei. In the CP experiment, the X-nucleus magnetisation depends only on growth from the proton magnetisation during the 'contact time'. Since the recycle delay depends on T_1 for ^1H, the experiment can therefore be repeated after much shorter recycle delay which enables substantial recovery of the proton magnetisation. This mechanism provides an indirect enhancement of the S/N of the X-nucleus spectrum in a given period of time. However it should be stressed that the CP experiment does not in any way affect the resolution of the spectrum.

The combination of cross polarisation and magic angle spinning (CP-MAS), together with high power ^1H decoupling therefore provides spectra with reasonable resolution and S/N ratios for a variety of dilute nuclei in solid samples.

1.9. General Applications of High-Resolution Solid State NMR

1.9.1. Amorphous Materials

Many materials (e.g. glass, ceramics, polymers and composites) are amorphous. Structural information about these materials is essential in order to understand their properties and also to design new kinds of material with novel properties. The lack of long range ordering in

amorphous materials precludes the application of conventional diffraction techniques for structural characterisation.

Typical structural information that can be obtained from NMR spectra is from the chemical shifts of the resonances and their relative intensities (also from relaxation times). Chemical shifts depend on the local ordering, since disorder will create a range of local environments and therefore a range of chemical shifts. The result of this phenomenon will be line broadening. Due to this effect the signals for amorphous materials are usually broader than the signals for crystalline materials. In spite of relatively broad NMR signals for these materials, NMR spectroscopy provides considerable structural information which can not be obtained from other characterisation techniques. Examples of these materials are glasses, surfaces and surface-immobilised species, and polymer resins [1].

1. Inorganic glasses; these are typically composed of Al, B, Na, O, and Si. In these glasses there is no hydrogen present and therefore a MAS experiment is generally sufficient to obtain adequate NMR spectrum of the system. In these systems solid state NMR spectra can be obtained for ^{11}B, ^{27}Al, ^{29}Si and possibly ^{23}Na. A detailed description of these systems can be obtained when measurements on several of these nuclei are combined [11].

2. Surfaces and surface-immobilised species; high-resolution solid state ^{29}Si NMR investigations have provided considerable information about the surface of silica gel, silica attached species, and aluminosilicates [12]. For example only silicon atoms near the surface of silca gel are cross polarised effectively from the proton nuclei (water molecules attached on the surface) and therefore observable in reasonable experimental time. All the ^{29}Si nuclei inside the structure possess exceedingly long relaxation times and hence it is difficult to observe their signals.

3. Polymer resins; solid state NMR provides complementary structural information to solution NMR experiments about polymers [13]. This information is needed since many properties of polymers are related to the actual structures in the solid state.

There are other cases in which the polymers are amorphous and entirely insoluble, and therefore no solution state NMR or diffraction studies are available. Therefore solid state NMR is the major source of information about these materials.

1.9.2. Incomplete Diffraction Data

A major application of solid state NMR is to provide complementary information to X-ray diffraction data [1]. For example the diffraction data from crystalline polymers are limited by the incomplete three dimensional order in these systems, and solid state NMR provides complementary information for complete structural elucidation.

Zeolites are also materials for which X-ray diffraction data is often incomplete. These are basically open framework structures containing tunnels and cavities and are made of AlO_4 and SiO_4 tetrahedra. It is generally not possible to prepare large single crystals of these materials, therefore only powder X-ray diffraction can be used for structural elucidation. In addition Si and Al have nearly identical scattering factors. Hence even if it is possible to deduce the crystal structure it is not possible to locate the Si and Al atoms within the structure. Since the NMR resonance of both ^{29}Si and ^{27}Al nuclei are detectable and they present information regarding local structure, solid state NMR provides considerable information about these structures [14].

1.9.3. Molecular Motion and Chemical Exchange

Many molecules in the solid state undergo large amplitude motions [5]. In principle, if molecular motion is not symmetric (i.e. the orientation of the molecule in each of the positions occupied during the motion is not identical in space) it is possible to detect the motion using diffraction measurements, but even in this case diffraction data do not provide any quantitative insight into the dynamics of the solid phase. A variety of solid state NMR techniques can be used to derive such information.

Such molecular motions can be detected by wide line proton NMR spectroscopy and quantified by relaxation time measurements which provide information such as the activation energy for the specific dynamic process.

In some cases, the molecular reorientation is combined with a chemical exchange process, for example in the case of many fluxional organometallic molecules. In these cases variable temperature NMR can provide direct information of the mechanism of the exchange process itself. Fig. 1.7 shows the ^{13}C CP-MAS NMR spectrum of the fluxional organometallic cyclooctatetraene-diiron pentacarbonyl [15]. All eight carbons of the cyclooctatetraene ring show a single sharp absorption due to the exchange between these carbons which occurs even down to 77 K.

Also, detailed mechanistic and kinetic information about molecular motion can be obtained from solid state ^{2}H NMR lineshape analysis (see chapters II and VI). Broad patterns of solid-state ^{2}H NMR spectra are affected drastically by appropriate motion (i.e. motion faster than 10^3 Hz) within the sample. The mobility of many solid materials including polymers [16], membranes [17], guest molecules in inclusion compounds and also surface absorbed species [18] have been studied (for some examples related to these topics, see chapters II and VI).

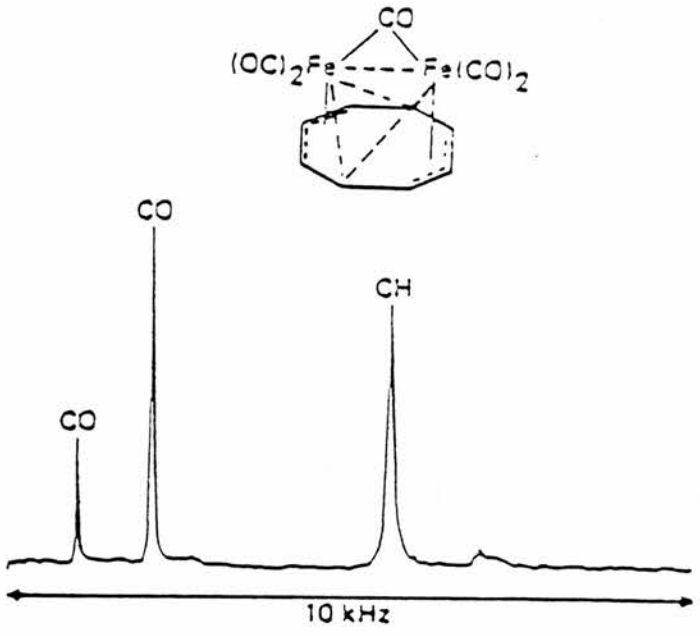

Fig. 1.7 Solid state ^{13}C CP/MAS NMR spectrum of the fluxional organometallic cyclooctatetraene-diiron pentacarbonyl at 113 K.

References:

[1] Fyfe, C. A. in "Multinuclear Magnetic Resonance in Liquids and Solids". Ed. by Granger, P. and Harris R. K., Kluwer Academic Publishers, 1990, Dordecht, Boston, London.

[2] Abragam, A., "The Principles of Nuclear Magnetism" Clarendon Press, Oxford, 1961.

[3] Eckert, H. "Progress in Nuclear Magnetic Resonance" Vol. 24, Part 3.Pergamon Press, 1992.

[4] Fukushima, E. and Roeder, S. B. W., "Experimental pulse NMR. A Nuts and Bolts Approach", Addison-Wesely, Reading, MA. 1981.

[5] Fyfe, C. A., "Solid State NMR for Chemists", CRC Press, Guleph, Ontario, 1984.

[6] Sanders, J. K. M., Hunter, B. K. "Modern NMR Spectroscopy" Chapter 9, Oxford University Press, 1993.

[7] Dixon, W. T. *J. Mag. Res.* 1981, **44**, 220.

[8] Waugh, J. S., Huber, L. M., Haeberlen, V. *Phy. Rev. Phys. Lett.* 1968, **20**, 180.

[9] Rhim, W. K., Elleman, D. E., Vaughan, R. W. *J. Chem. Phys.* 1973, **59**, 3740.

[10] Pines, A., Gibby, M. G., Waugh, J. S. *J. Chem. Phys.* 1973, **59**, 569.

[11] Fyfe, C. A., Gobbi, G. C., Hartman, J. S., Lenkinski, R. E., O'Brien, J. H., Beange, E. R., Smith, M. A. R. *J. Mag. Res.* 1982, **47**, 168.

[12] Maciel, G. E., Sindorf, D. W., *J. Am. Chem. Soc.* 1980, **102**, 7606.

[13] Fyfe, C. A., Rudin, A., Tchir, W. *Macromolecules*, 1980, **13**, 1320.

[14] Lippma, E., Magi, M., Samoson, A., Grimmer, A. R., Engelhardt, G. *J. Am. Chem. Soc.* 1980, **102**, 4889.

[15] Fyfe, C. A., Lyerla, J. R., Yannoni, C. S. *Acc. Chem. Res.* 1982, **15**, 208.

[16] Davis, j. H., Jeffrey, K. P., Bloom, M., Valic, M. E., Higgis, T. P. *Chem. Phys. Lett.* 1976, **42**, 390.

[17] Scheler, G., Haubenreisser, U., Rosenberger, H. *J. Mag. Res.*. 1981, **44**, 134.

[18] Maciel, G. E., Sindorf, D. W., Bartuska, V. J. *J. Choromatography,* 1981, **205**, 438.

CHAPTER II

REVIEW OF SOLID STATE NMR INVESTIGATIONS OF CRYSTALLINE ORGANIC INCLUSION COMPOUNDS

Introduction

Inclusion compounds are defined as systems in which one species (the guest) is spatially confined within another species (the host).

Generally inclusion compounds can be divided into two subgroups. In one type of inclusion compound, the host is a molecular species, and this host molecule itself has the ability to accommodate another species (either ionic or molecular). In general this type of inclusion compound can exist both in solution and in the solid state.

In the second type of inclusion compound the host is a crystalline solid, and within this solid structure there is some type of cavity, within which guest molecules can be located. These inclusion cavities have various different topologies; for example linear non intersecting tunnels, intersecting tunnels, isolated cages and systems of interconnected cages (Fig. 2.1). It is this second type of inclusion compound that is the focus of the discussion in this chapter.

There are examples of both inorganic host systems (including zeolites, clays, graphite), and also organic host materials (for example urea, thiourea, tri-ortho-thymotide and perhydrotriphenylene). Here we do not provide an extensive review of all classes of inclusion compound. The discussion in this review chapter is therefore entirely devoted to crystalline inclusion compounds with organic host materials.

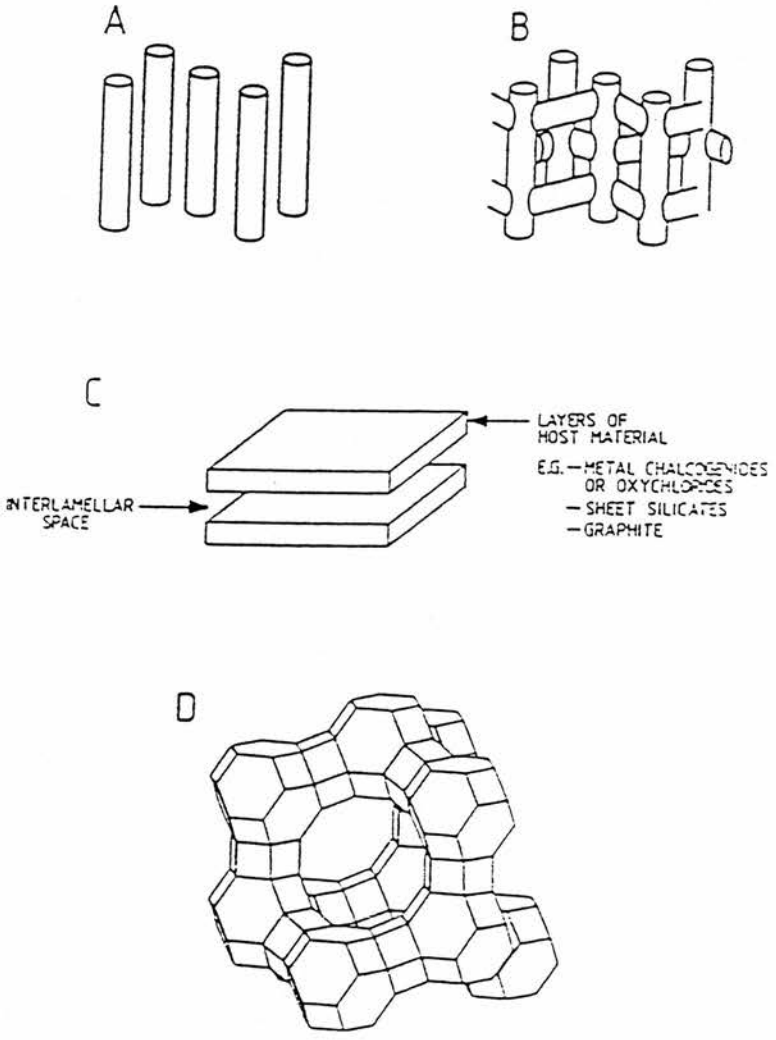

Fig. 2.1 Schematic illustrations of different types of host solid structures; (a) one-dimensional tunnel structure; (b) intersecting tunnels; (c) sheet structure; (d) three dimensionally linked cavities.

In general it is possible to obtain reasonably good quality single crystals from organic crystalline inclusion compounds, therefore a substantial contribution has been made by X-ray crystallography in structural elucidation of the host components [1-3]. However guest species within these inclusion compounds have a tendency to adopt a disorder state (both static and dynamic) and are often incommensurate with respect to the host structure. In either situation structure determination is not straightforward, and other experimental techniques should be invoked in order to obtain such information.

Here we illustrate (using several examples of inclusion systems) the capability of solid state NMR spectroscopy to provide structural and dynamic information relating to organic crystalline inclusion compounds. Three classes of organic crystalline inclusion compounds (urea, thiourea and tri-ortho-thymotide) have been chosen to demonstrate the power and versatility of the technique in providing such information.

2.1 Structural Characteristics of Urea Inclusion Compounds

Urea can form crystalline inclusion compounds with a wide variety of organic molecules, provided these molecules are based on a sufficiently long n-alkane chain and provided they have a sufficiently low degree of substitution [4]. Structurally, the urea molecules in these inclusion compounds form an extensively hydrogen bonded array (Fig. 2.2), containing linear, parallel, non-intersecting tunnels within which the guest molecules are located (Fig. 2.3).

The effective diameter of these tunnels ranges between *ca.* 5.1 Å and 5.9 Å. The guest molecules are densely packed along these tunnels. The host framework is unstable if the guest molecules are subsequently removed from the inclusion compound; the urea then recrystallises in its pure crystalline phase, which does not contain any empty tunnels [5-7].

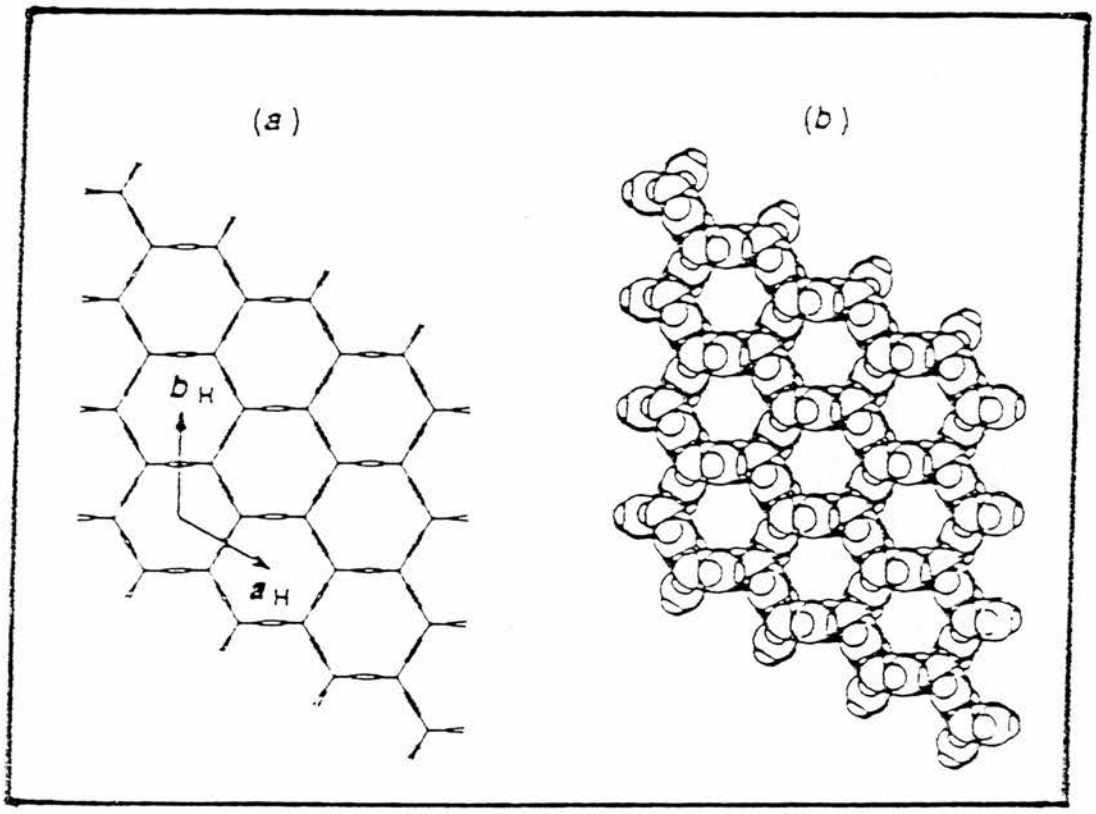

Fig. 2.2 (a) Two reprensations of the urea host structure (a) with atomic radii equal to zero (b) with considering van der Waals radii.

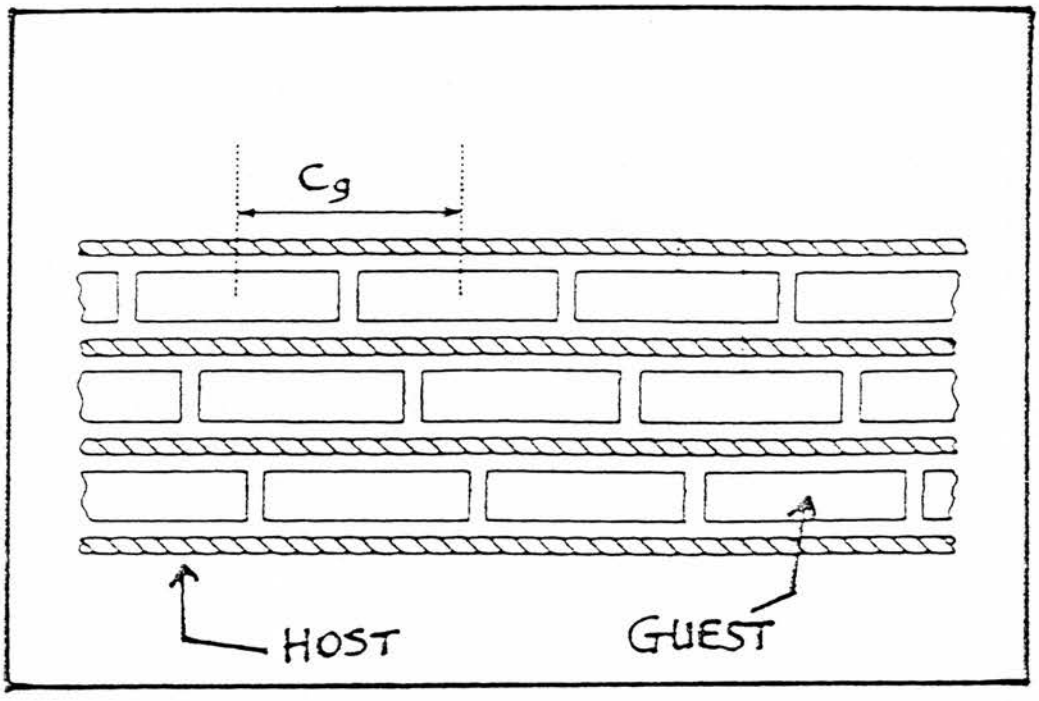

Fig. 2.3 Schematic representation of the arrangement of the guest molecules in the urea tunnel structure (viewed along the crystallographic c axis).

This represents an important difference between urea inclusion compounds on the one hand and their topologically-similar zeolitic analogues on the other. In zeolitic systems the host framework generally remains as a stable structure if the guest molecules are subsequently removed.

The chirality of the urea host structure is also noteworthy. While each urea molecule is achiral, these molecules adopt a spiral arrangement in forming the walls of the tunnel, and a homochiral collection of spirals is present within any particular single crystal.

2.2 Solid State NMR Studies of Urea Inclusion Compounds

Solid state NMR has been used widely to investigate different structural and dynamic aspects of the guest molecules (as well as NMR properties like chemical shifts) in the tunnel structure of urea inclusion compounds. These types of information can not generally be obtained *via* diffraction-based techniques.

The influence that the constrained environment of the urea tunnel has on the ^{13}C chemical shift values of the guest species is an interesting issue. Imashiro et al. [8] analysed the ^{13}C chemical shifts of a number of n-alkanes (C_7-C_{20}) trapped in urea inclusion compounds based on the simple additivity rules which hold for n-alkanes in solution. The additivity constant for solids, solution and liquid phases, and for the n-alkane molecules within the urea host structure are different, as a consequence of the presence of conformational isomers which occur in different amounts within the different phases. In the solid phase and in the urea inclusion compounds, the extended all-trans conformation is expected as the predominant conformation. Okazaki and McDowell [9] have also discussed chemical shifts of the guest molecules in terms of

changes in substituent effects which occur when tridecane, myristyl alcohol, dioctylamine, myristic acid, and stearonitrile are included in urea.

The guest molecules in urea inclusion compounds usually experience a high degree of mobility. Numerous NMR techniques have therefore been used to investigate dynamic properties of different guest molecules in these inclusion compounds.

Early ^{1}H second moment NMR measurements on fatty acid inclusion compounds of urea [**10**] showed that at room temperature there is extensive motional averaging for these guests.

Meirovitch et al. [11] examined the stearic acid/urea system in detail by following the evolution of ^{2}H lineshapes in the slow motional region for selectively deuterated samples of stearic acid in the urea tunnel structure (Fig. 2.4). Results are consistent with the steric acid dimmers reorienting about the tunnel axis between three equivalent sites. Motion of the methyl group is more complicated, and the lineshapes appear to fit a diffusive model rather than a model with distinct jump sites. A diffusive model was also proposed for 1-bromooctane/urea, however the three fold jumps model with a broad distribution in correlation times would appear to fit these results as well.

Okazaki et al. [12] have studied the ^{13}C NMR lineshape of the cyano group in stearonitrile, obtained under magic angle spinning conditions, and split by residual dipolar interaction with ^{14}N. The analysis of the lineshape leads to the conclusion that the molecule rotates about its long axis when trapped in the urea tunnel.

Harris et al. have investigated the mobility of n-d_{34}-hexadecane in its urea inclusion compound using ^{2}H NMR [13]. The result of this investigation shows that at room temperature the guest molecules undergo 60° jumps about their long axis, torsional libration about the penultimate C– C bond and rapid rotation of the CD_3 group about its 3-

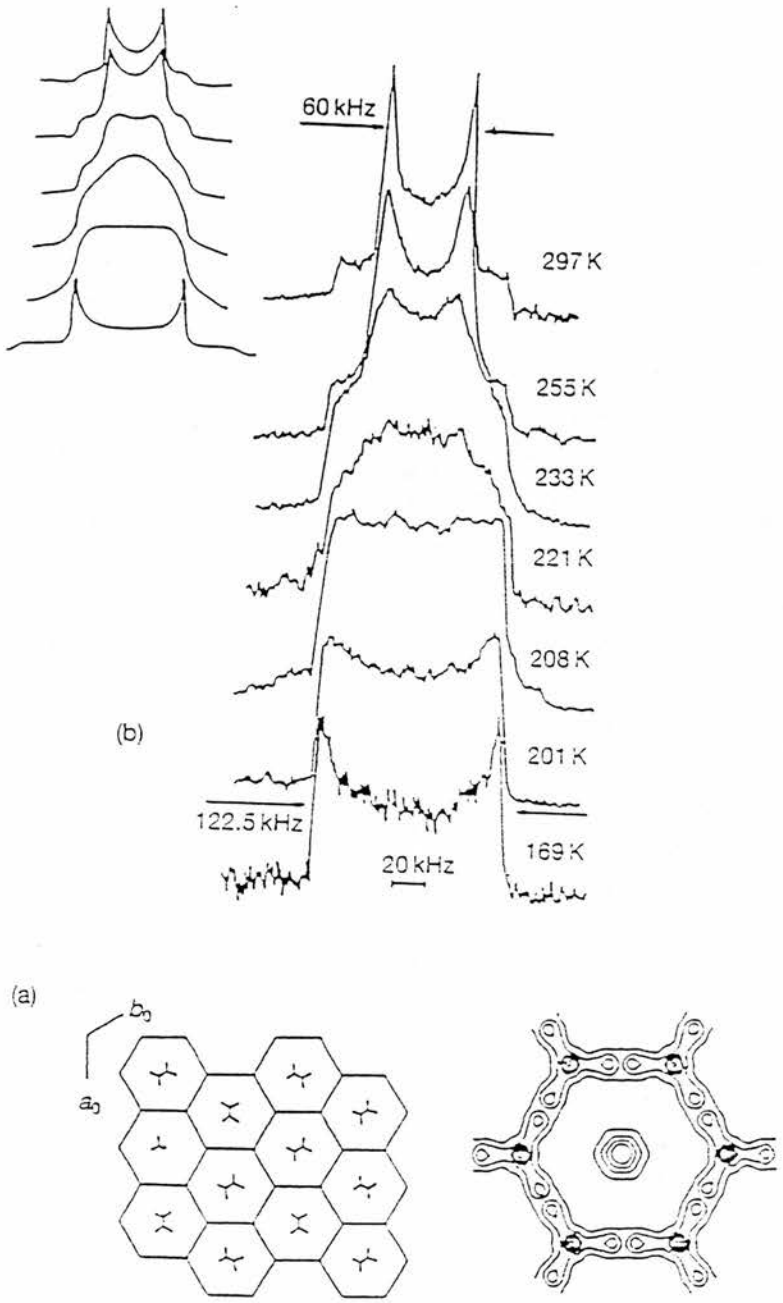

Fig. 2.4 (a) Schematic tunnel structure and electron density projections along the tunnel axis for the n- $C_{16}H_{34}$/urea inclusion compound; (b) ^2H NMR spectra as a function of temperature for the polycrystalline 2,2-d_2-stearic acid/urea inclusion compound. Inset: calculated lineshapes for a three equivalent site model.

fold symmetry axis. The phase transition which occurs at ~ 147 K for this compound is associated with an abrupt discontinuity in the motional freedom of the guest molecules.

A ^{2}H NMR study [14] of the trioxane /urea inclusion compound with either the host or the guest sub-structure deuterated is an excellent example of the detailed dynamic information which can be obtained, adding considerably to less definite information derived from previous ^{1}H [15] and ^{14}N [16] NMR studies. In the lowest temperature phase IV, three fold rotation of all trioxane molecules was deduced from slow motional lineshapes with an activation energy of 20.1 kJ mol^{-1}. In phases III and II, stable between -33 and -84° C, two populations of trioxane guests with distinct mobilities were observed. In the highest temperature phase I, again a single mobile population of trioxane molecules is observed which shows the onset of ring inversion with an activation energy of 48.9 kJ mol^{-1}, very similar to the value for the same molecule in solution. As for other urea inclusion compounds [17], evidence for two fold flips of the urea host molecules about the C=O bond was also observed.

2.3 Structural Characteristics of Thiourea Inclusion Compounds

In the presence of appropriate guest molecules, thiourea also forms a crystalline inclusion compound with a uni-dimensional, infinite, linear tunnel structure. The thiourea host structure however possesses a tunnel diameter of approximately 6.1 Å which is larger than the corresponding value for the urea host structure (about 5.3 Å) [4].

Thiourea inclusion compounds are generally rhombohedral crystals. The arrangement of thiourea molecules in the crystal is similar to that of urea molecules in the urea inclusion compounds.

Due to the larger diameter of the tunnels, thiourea is capable of forming inclusion compounds with bulky and also branched guest molecules. The thiourea tunnel for example, can include cyclohexane and some of its derivatives as well as certain compounds containing a benzene ring. Even molecules as large as ferrocene can form an inclusion compound with thiourea; such guest molecules do not form inclusion compounds with urea. On the other hand, linear n-alkanes cannot form inclusion compounds with thiourea. This is due to the lack of mutual compatibility between the host tunnel and the guest molecules, which prohibits the formation of such inclusion compounds (i.e. the guest is not bulky enough).

The stability of thiourea inclusion compounds generally increases as the length of the guest molecule increases; this behaviour is similar to the situation with urea inclusion compounds[4].

2.4 Solid State NMR Studies of Thiourea Inclusion Compounds

Dynamic investigation and also conformational analysis of the guest molecules in thiourea inclusion compounds have been the subject of numerous studies.

The cyclohexane/thiourea inclusion compound has been studied by several techniques. The results of these studies indicate the existence of three distinct phases for this compound [**18**]. The ^{14}N NQR line multiplicities have been used to identify the number of thiourea molecules within the unit cell [**19**]. Also it has been shown that motional narrowing in the ^{1}H NMR spectrum of cyclohexane/thiourea-d_4 occurs between 120 K and 150 K in two distinguishable steps [**20**]. The rhombohedral unit cell parameters change continuously between 123 K and 150 K, and at 153 K the rhombohedral phase changes to a monoclinic structure [**20**]. ^{2}H NMR provides details of the molecular motion in this system [**21**]. In the low

temperature phase (phase III) at 134 K, the cyclohexane molecule is oriented upright in the tunnel, and rotates rapidly about the molecular threefold axis (Fig. 2.5). In phase II, the cyclohexane rotation axis tips with respect to the tunnel axis. The average tipping angle changes from 36° at 159 K to 42.9° at 240 K in phase I. The tipping angle then continues to evolve through the magic angle and, in addition, the single powder pattern now indicates that there is fast inversion

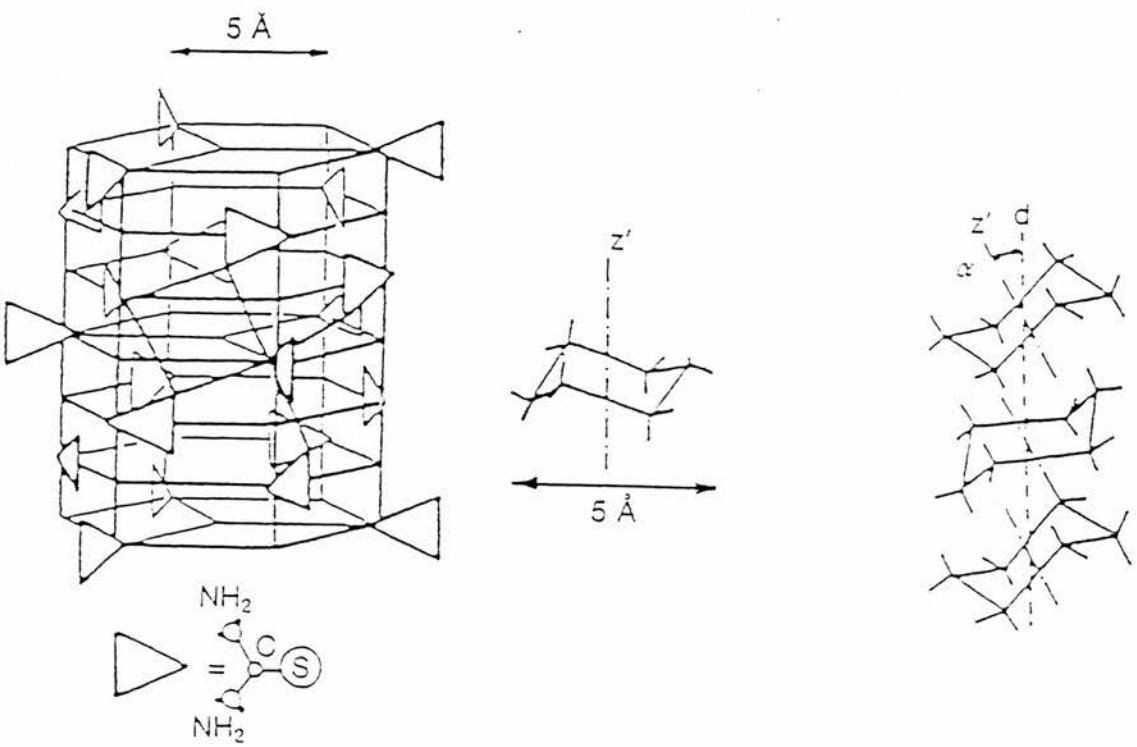

Fig. 2.5 (a) Structure of the cyclohexane/thiourea inclusion compound; (b) the chair conformer of cyclohexane; (c) orientation of cyclohexane molecules in the thiourea tunnels.

of the cyclohexane ring. Cyclopentane-d_{10} trapped in the thiourea tunnel performs rapid reorientation about the tunnel axis at a tilt angle of either 42.5° or 70°, in addition to rapid ring inversion at temperatures over 140 K [22].

Ferrocene trapped in the thiourea tunnels has been studied by ^{13}C [**23**], ^{1}H [**24**] and ^{2}H [**25**] NMR. ^{13}C NMR spectra obtained for an oriented sample (several single crystals aligned with their long axes parallel to each other) [**23**] showed (via the existence of two signals) that two different types of ferrocene molecules exist, one set with molecular symmetry axis along the tunnel axis, the other with the molecular symmetry axis oriented at right angles to the tunnel axis. There are three preferred orientations separated by 120°. Both types of ferrocene molecule perform rapid reorientation about the molecular symmetry axis. Exchange between the two populations gives rise to line broadening, followed by line coalescence, at 222 K. Below the phase transition at 220 K, the activation energy for the exchange process between the two populations is 12.1 kJ mol^{-1}, and the fraction of the ferrocene in the perpendicular orientation is 53 percent. Above the phase transition temperature, these figures are 7.1 kJ mol-1 and 63 percent. No evidence of other motional changes were found at the other observed heat capacity anomalies which occur at 147.2 K, 171.4 K, and 185.5 K [**26**].

Analysis of the ^{2}H NMR lineshapes has allowed delineation of two distinct reorientational processes among the five distinguishable orientations of ferrocene suggested to be populated in this inclusion compound. Kinetic parameters have been estimated as $E_a = 6.4 \pm 0.5$ kJ mol^{-1} with $A = (2.15 \pm 0.5) \times 10^7\ s^{-1}$ for the direct interchange between the three orientations

perpendicular to the host tunnel axis, and $E_a = 10.1 \pm 1.0$ kJ mol^{-1} with $A = (1.5 \pm 0.6) \times 10^8\ s^{-1}$ for parallel-perpendicular orientational interchange [24].

The ability of guest-host and guest-guest interactions to influence guest conformation is well illustrated in studies of substituted cyclohexanes trapped in thiourea [**27, 28**]. In solution, the equatorial and

axial conformers exist in a state of rapid exchange, with the equatorial conformer preferred. ^{13}C CP/MAS NMR spectra have shown that methylcyclohexane, cyclohexanol and cyclohexylamine trapped in the thiourea tunnel structure exists in the equatorial conformation, whereas the trapped chlorocyclohexane, bromocyclohexane and iodocyclohexane prefer the axial conformation. Fluorocyclohexane appears to prefer the equatorial conformation. In all cases there is a rapid exchange between axial and equatorial conformations.

2.5 Structural Characteristics of TOT inclusion Compounds

Although tri-*ortho*-thymotide (TOT) was first prepared in 1865 [**29**] (Fig. 2.6), the TOT inclusion compounds were discovered and first studied in 1952 [**30**].

The existence of two pairs of enantiomeric TOT conformations in solution has been detected by NMR spectroscopy [**31**]. The major form

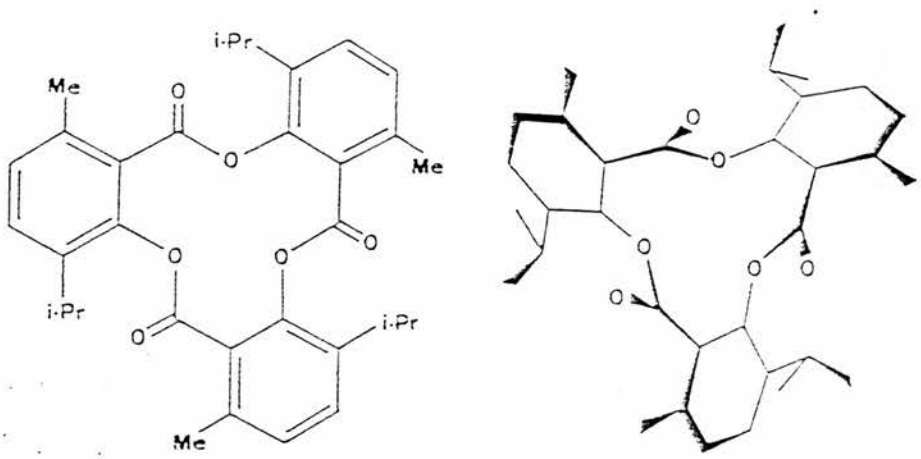

Fig. 2.6 Tri-ortho-thymotide. Constitution and idealised view of the (M)-(−) configuration.

was referred to as the propeller conformation and has all three carbonyl groups pointing to one side of the central twelve-membered ring. The minor form was referred to as the helical conformation and has one carbonyl pointing in a direction opposite to that of the other two. Only the propeller form has been observed in the TOT inclusion compounds studied so far.

TOT is capable of forming two distinct types of inclusion compounds with different guest molecules:

(a) the guest molecules are enclosed in discrete cavities (cages) and are not in mutual contact. This is the most extensively studied type of TOT inclusion compound, and is formed with guests of length not greater than about 9 Å [**32**].

(b) the guest molecules are accommodated in continuous "linear" tunnels running through the crystal along characteristic crystallographic directions. The guest molecules are generally, but not always, in contact with each other in the tunnels. Long chain hydrocarbons are an example of the type of guest molecules which can be accommodate in this type of structure [**33**]. The space group of the host structure in these inclusion compounds is $P6_1$, $P6_2$ and $P3_1$.

The unit cell dimensions of cage type inclusion compounds increase slightly and in a regular manner to accommodate larger included molecules. For the tunnel type inclusion compounds the cell dimensions are more nearly constant but vary in a periodic way as the length of the included guest molecules increases.

2.6 Solid State NMR Studies of TOT Inclusion Compounds

It has been shown that ^{13}C NMR spectra provide a straightforward indication of chiral discrimination for several TOT inclusion compounds of secondary-butyl compounds, and can provide a quantitative

determination of enantiomeric excesses [**34**]. Also, differences between the dynamic states of the enantiomers are revealed by the NMR measurements. Polycrystalline samples of TOT inclusion compounds were prepared with 2-chloro-, 2-bromo-, 2-iodobutane and 2-butanol as guests. In the inclusion compounds, the ^{13}C NMR spectra of the host molecule consist of "triplets" in accordance with the loss of threefold molecular symmetry. The observable guest resonances are as follows: C(2) gives rise to a distinct doublet for all the guests, and C(4) gives rise to a distinct doublet for halo-derivatives; the remaining signals, including the C(3) resonance, are singlets (the C(1) resonance is obscured by the TOT spectrum at low field). For the C(2) and C(4) guest doublets the lines of higher intensity were assigned to the (P)-TOT/(S)-guest and (M)-TOT/(R)-guest combinations. These host-guest preferences have been established from independent studies [**35-36**]. Thus solid state NMR provides a direct method of estimating enantioisomeric excesses in mixed diastereomeric crystalline systems. The NMR results on the enantomeric excesses for these compounds are in agreement with results obtained from other techniques.

The dipolar dephasing technique (a technique used for the detection of mobility or carbons remote from protons in organic compounds) [**37**] was used to obtain further insight into the dynamic properties of sec-butyl compounds in the cage structure of TOT and into their chiral discrimination [**34**]. The ratio I_{DD}/I of ^{13}C signal intensities measured under dipolar diphasing and normal cross-polarisation/magic angle spinning conditions is a semiquantitative measure of the dynamic state of the molecular group. For locked methylene or methine carbon atoms $I_{DD}/I = 0$, whereas enhanced molecular motion increases the I_{DD}/I ratio up to a maximum value of 1. For 2-chloro- and 2-bromobutane, C(2) has $I_{DD}/I = 0$ for the major enantiomers, and a value of *ca.* 0.4 for the

minor enantiomer. Similarly the ratios for the C(4) atom have values of *ca.* 0.6 and *ca.* 0.9 for the major and minor enantiomers, respectively. These results suggest that the preferred enantiomer fits rigidly into the cage, whereas the minor component is subject to a reorientation process analogous to single axis rotation. The C(2) atoms of both enantiomers of 2-butanol have $I_{DD}/I = 0.4$ so that they both display the same degree of motional freedom in the cavity. The conclusion, arrived at on the basis of these solid state NMR observations was, therefore, that enantioselectivivity seems to be reflected more by the dynamic guest properties (static major enantiomers, mobile minor enantiomers) than by the equilibrium guest positions determined by X-ray diffraction. The NMR model is of great interest because it is somewhat at variance with the X-ray structural models for chiral recognition. X-ray diffraction results are consistent with computational results based on this assumption that the least repulsion energy will exist between the preferred guest enantiomer and with the cage. However, this preferred enantiomer is not necessarily the less mobile component (as predicted based on the NMR model).

The results relating to chiral recognition have now been confirmed by examination of the ^2H NMR lineshapes of 2-bromobutane-1,1,1-d_3 (Fig. 2.7) [38]. The quadrupole coupling constant for the favoured P-S and M-R guest-host pair is considerably larger than that for the less favoured P-R and M-S pair, indicating decreased mobility for the former. In a host-guest system without specific binding sites this may be taken as a sign of stronger guest-host binding for the favoured pair.

In the past, the reaction of guest molecules in the TOT host structure with reactive small molecules such as oxygen and HBr to give chiral products with some enantiomeric excess has been followed by wet chemical methods [39]. Questions remain as to whether these reactions

actually occur within the intact lattice, or even whether the reactions may have occured during the subsequent extraction procedure. The reaction between cis-2,3-epoxybutane, trapped in TOT, and HBr was followed

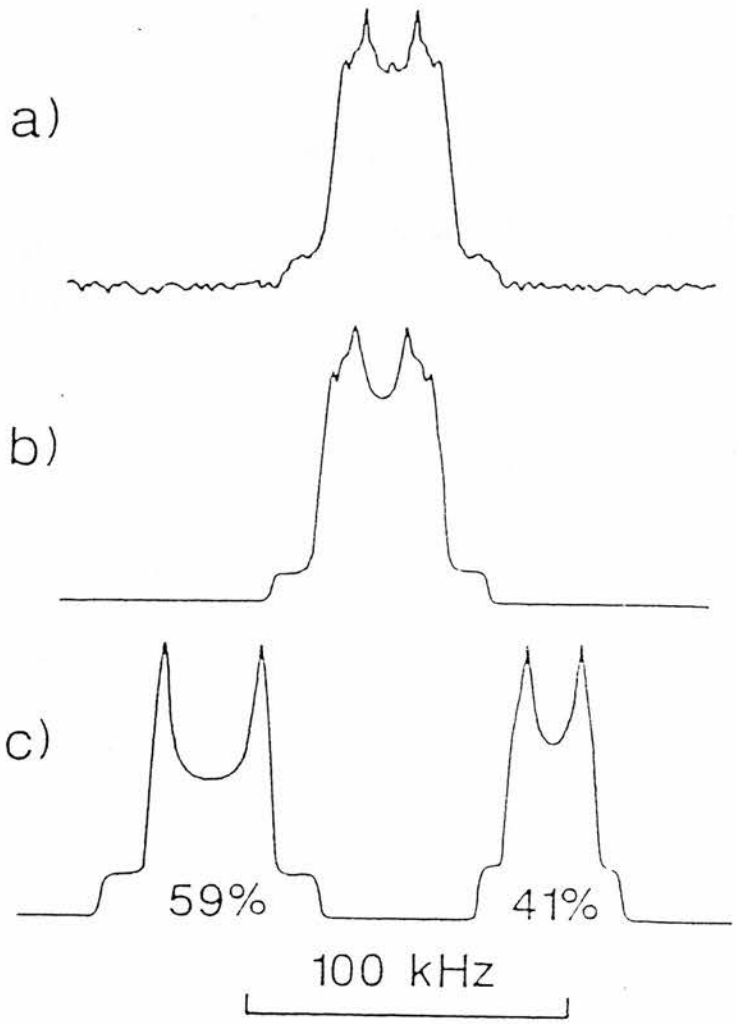

Fig. 2.7 ^{2}H NMR lineshapes of R/S 2-bromobutane-(1,1,1-d_3) trapped in tri-ortho-thymotide at 273 K (a) experimental, (b) simulated, (c) simulated components.

directly by ^{13}C CP/MAS NMR in the solid state (Fig. 2.8) [38], and the results showed that indeed there is a direct conversion from reactant to product in the intact lattice.

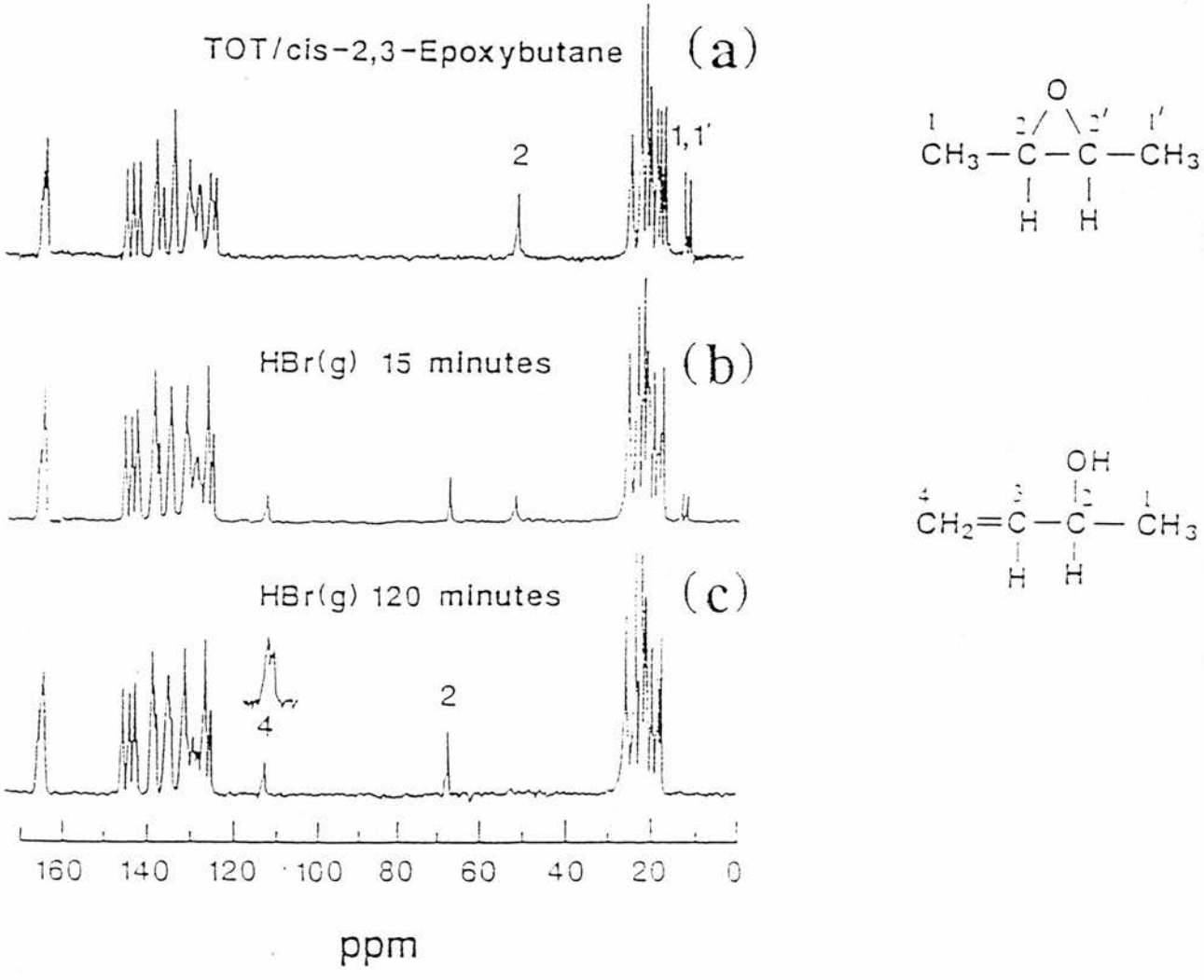

Fig. 2.8 Progress of the reaction of cis-2,3-epoxybutane trapped in tri-ortho-thymotide with HBr gas as revealed by ^{13}C CP/MAS NMR. In the spectrum (b) both reactant and product are present in an intact lattice; also the splitting of the product line (inset), showing doubling due to the presence of both enantiomeric products.

References:

[1] Schlenk, W. *Justus Liebigs Ann. Chem.*. 1949, **565**, 204.

[2] Schlenk, W. *Justus Liebigs Ann. Chem.*. 1951, **573**, 142.

[3] Lawton, D.; Powell, H. M. *J. Chem. Soc.*. 1958, 2339

[4] Takemoto, K.; Soneda, N. in "Inclusion Compounds", (Ed. Atwood, J. L. Davies, J. E. D.; MacNicol, D. D. Vol. 2, Academic Press, 1984, p. 47.

[5] Knight, M. B.; Witnauer, L. P.; Coleman, J. F.; Noble, W. R.; Swern, D. *Anal. Chem.*. 1952, **24**, 1331.

[6] McAdie, H. G. *Can. J. chem.*. 1962, **40**, 2195.

[7] Harris, K. D. M. *J. Phys. Chem. solids*.. 1992, **53**, 529.

[8] Imashiro, F.; Maeda, T.; Nakai, T.; Saika, A.; Terao, T. *J, Phys. Chem.*. 1986, **90**, 5498.

[9] Okazaki, M.; McDowell, C. A.; *J. Mol. Struct*.. 1984, **118**, 149.

[10] Umemoto, K.; Danyluk, S. S. *J. Phys. Chem.*. 1967, **71**, 3757.

[11] Meirovitch, E.; Belsky, I. *J. Phys. Chem.*. 1984, **88**, 6407.

[12] Okazaki, M.; Naito, A.; McDowell, C. A. *Chem. Phys. Lett.* 1983, **100**, 15.

[13] Harris, K. D. M.; Jonsen, P. *Chem. Phys. Lett*.. 1989, **154**, 593.

[14] Gelerinter, E.; Luz, Z.; Poupko, R.; Zimmerman, H. *J. Phys. Chem.* 1990, **94**, 5391.

[15] Clement, R.; Gourdji, M.; Guibe, L. *J. Mag. Reson.* 1975, **20**, 345.

[16] Clement, R.; Gourdji, M.; Guibe, L. *Mol. Phys.* 1975, **30**, 825.

[17] Heaton, N. J.; Vold, R. L.; Vold, R. R. *J. Am. Chem. Soc.* 1989, **111**, 3211.

[18] Cope, A. F. G.; Gannon, D. J.; Parsonage, N. G. *J. Chem. Thermodyn.* 1972, **4**, 829.

[19] Clement. R.; Gourdji, M.; Guibe, L. *Mol. Phys.* 1971, **21**, 247.

[20] Clement, R.; Mazieres, C.; Gourdji, M.; Guibe, L. *J. Chem. Phys.* 1977, **67**, 5381.

[21] Meirovitch, E.; Krant, T.; Vega, S. *J. Phys. Chem.* 1983, **87**, 1390.

[22] Meirovitch, E.; *J. Phys. Chem.* 1984, **88**, 6411.

[23] Nakai, T.; Terao, T.; Imashiro, F.; Saika, A. *Chem. Phys. Lett.* 1986, **132**, 554.

[24] Clement. R.; Gourdji, M.; Guibe, L. *Chem. Phys. Lett.* 1980, **72**, 466.

[25] Heyes, S. J.; Clayden, N. J.; Dobson, C. M. *J. Phys. Chem.* 1991, **95**, 1547.

[26] Sorai, M.; Ogasawara, K.; Suga, H. *Mol. Cryst. Liq. Cryst.* 1981, **73**, 231.

[27] McKinnon, M. S.; Wasylishen, R. E. *Chem. Phys. Lett.*. 1986, **130**, 565.

[28] Harris, K. D. M.; Aliev, A. E. *J. Am. Chem. Soc.* 1993, **115**, 6369.

[29] Naquet, G. *Bull. Soc. Chim. Fr.* 1865, **4**, 93.

[30] Newman, A. C. D.; Powell, H. M. *J. Chem. Soc.* 1952, 3747.

[31] Ollis, W. D.; Sutherland, I. O. *J. Chem. Soc., Chem. Comm.* 1966, 402.

[32] Allemand, J. ; Gerdil, R. *Acta Crystallogr.* 1983, **C39**, 260.

[33] Williams, D. J.; Lawton, D. *Tetrahedron Lett.* 1975, 111.

[34] Ripmeester, J. A.; Burlinson, N. E. *J. Am. Chem. Soc.* 1985, **107**, 3713.

[35] Helmkamp, G. K.; Joel, C. D.; Sharman, H. *J. Org. Chem.* 1956, **21**, 844.

[36] Arad-Yellin, R.; Green, B. S.; Knossow, M.; Tsoucaris, G. *Tetrahedron Lett.* 1980, **21**, 387.

[37] Alemany, L. B.; Grant, D. M.; Alger, T. D.; Pugmire, R. J. *J. Am. Chem. Soc.* 1979, **101**, 5854.

[38] Facey, G. A.; Ripmeester, J. A. *J. Chem. Soc., Chem. Commun.* 1990, 1585.

[39] Gerdil, R.; Barchietto, G. *Tetrahedron Lett.* 1987, **28**, 4685.

CHAPTER III

SOLID STATE ^{13}C NMR STUDIES OF ORIENTATIONAL DISORDER OF UNSYMMETRIC GUEST MOLECULES IN THEIR UREA INCLUSION COMPOUNDS

Introduction

Guest molecules embedded within urea inclusion compounds experience a high degree of mobilty. This includes rotation of the guests about the tunnel axis and also translation along this axis. Several experimental techniques including solid state NMR [1-3] and neutron scattering [4] have clearly revealed the existence of dynamic disorder within the guest substructure in these compounds. In view of the motion of the guest molecules, substantial difficulties arise in attempting to deduce structural information about the guest substructure (e.g. to determine the guest substructure) via X-ray diffraction techniques. Nevertheless, there is sufficient ordering within the guest to determine an average periodicity [5,6].

Several aspects of the guest substructure have been controversial for a long time. One aspect concerns the orientation of unsymmetric guests within the tunnel structure [7]. The type of unsymmetric molecules which are appropriate to form inclusion compounds with urea are of the types $CH_3(CH_2)_n$-X-$(CH_2)_mCH_3$ ($n \neq m$) or X-$(CH_2)_n$-Y. It is clear that two orientations of such guest molecules in the tunnel can be envisaged, leading to head-head, head-tail and tail-tail end-group interactions(see Fig. 3.1). It is possible that only one specific end-group interaction (for example only head-head and tail-tail or only head-tail)

exists for guest molecules, or alternatively it is possible that all end-group interactions exist in a random fashion, and therefore generating 'local orientational disorder'.

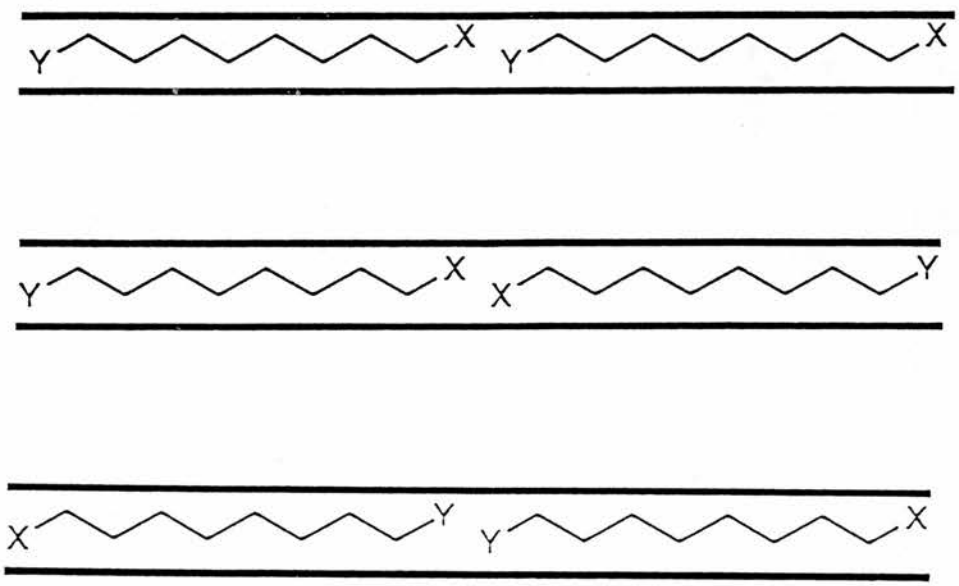

Fig. 3.1 Schematic representation for the different end-group interactions between unsymmetric guest molecules containing X and Y end-groups located in the urea tunnel structure.

In fact, it has been shown that some unsymmetric guest molecules are ordered inside the tunnel. For example in urea inclusion compounds of carboxylic acids, the average periodicity of the guest molecules is twice the length of the molecule [8]. This arises from hydrogen bonding between two molecules (head-head) which leads to the formation of dimers. Hence, in the case of carboxylic acids only

head-head and tail-tail end-group interactions exist. But there is no general way via X-ray diffraction techniques to probe local orientational disorder for unsymmetric guest molecules. X-ray diffraction provides averaged information about the structure, and local structural features (such as the question of head-head versus head-tail end-group interactions) cannot be investigated *via* this technique. We have therefore exploited solid state NMR as an alternative technique to investigate this problem based on the fact that this technique can, in principle, reveal information concerning the local structure in the solid state. The unsymmetric guest molecules that we have chosen for our investigation are 1-haloalkanes $CH_3(CH_2)_nX$ (X = F, Cl, Br, I; n typically 5-11).

In this chapter we discuss how solid state NMR can reveal the existence of this type of disorder in urea inclusion compounds and also discuss how the different halogen end group interactions manifest themselves upon the ^{13}C spectrum for different 1-haloalkanes. Also, we present a specific method for precise characterisation of signals associated with different intermolecular environments, of the guest molecules. Furthermore, we have noticed that the chemical shifts of the signals related to different intermolecular environments vary as a function of chain length of 1-haloalkanes. The variation of chemical shifts as a function of chain length is reported and discussed for the 1-haloalkane guest molecules.

3.1 Synthesis and Characterisation of Urea Inclusion Compounds

3.1.1 General Method of Preparation

Urea and 1-haloalkanes ($X(CH_2)_nCH_3$; X = F, Cl, Br, I n typically 5-11) were obtained commercially and used without further purification. Urea inclusion compounds were prepared *via* the following procedure.

An excess amount of 1-haloalkane (excess with respect to the expected stoichiometry of the inclusion compound) was added to a saturated solution of urea in methanol in a conical flask at 50°C. In the preparation of 1-iodoalkane/urea compounds, the conical flasks were covered in order to eliminate possible photochemical decomposition of 1-iodoalkanes. Further methanol was added to dissolve completely the 1-haloalkane and any crystals of inclusion compound that may have formed at this stage. For longer 1-haloalkanes (typically n=9-11) and for all 1-iodoalkanes, a few drops of t-amyl alcohol were needed to dissolve completely the 1-haloalkane. The conical flask was then stoppered and immersed in a Dewar flask containing water at 50 °C and allowed to cool slowly to room temperature. The crystals that had formed at this stage were collected and washed with cold 2,2,4-trimethylpentane to remove any non-included 1-haloalkane adsorbed on the surface of the collected materials. Urea inclusion compounds containing a mixture of two different types of guest molecule were prepared using a similar procedure. The ratio of the two guests in these urea inclusion compounds (which can be substantially different from the corresponding ratio in solution) was determined by elemental analysis (C, H, N).

3.1.2 Characterisation of Products

The external morphology of the collected crystals was examined under the optical microscope. The observed morphology of the crystals was consistent with the expected morphology of urea inclusion compounds i.e., long hexagonal prisms. In addition, powder X-ray diffraction confirmed that these inclusion compounds have the conventional urea tunnel structure [9].

3.2 Experimental Aspects of Recording NMR Spectra

High-resolution solid state ^{13}C NMR spectra were recorded at 125.7 MHz on a Bruker MSL 500 spectrometer. A cross polarisation pulse sequence was used under the Hartman-Hahn condition using 1 ms contact time with high power ^{1}H decoupling applied during acquisition of the spectrum and with the sample subjected to magic angle spinning (typically ca. 7 kHz). Experiments with different recycle delays (1s, 5s, 10s, 20s) were performed to determine the appropriate recycle delay. A recycle delay of 10s was chosen as a suitable value. The digital resolution for the spectra was 4.695 Hz/pt.

Single pulse ^{13}C experiments can also be performed on these compounds with the same recycle delay used in the CP experiment. The feasibility of the single pulse technique for the urea inclusion compounds is explained on the basis of the high degree of mobility of the guest molecules. The only difference between the results obtained from single pulse experiments and cross polarisation experiments concerns the relative intensities of the signals for the end-group carbons. For instance the relative intensity of the methyl carbon signals compared to other signals in the spectrum obtained by cross polarisation is less than the corresponding relative intensities obtained *via* the single pulse experiment (this is due to the fact that the methyl carbon is comparatively more mobile, and therefore cross polarisation is less efficient than for the other carbons).

The chemical shifts were measured compared to tetrakis(trimethylsilyl)silane (TTMS) as an internal standard where its chemical shift was set at 3.50 ppm. For 1-iodoalkane/urea compounds adamantane was used as the internal standard).

3.3 Solid State ^{13}C NMR Studies of 1-iodoalkane/Urea Inclusion Compounds

3.3.1 General Spectral Features

The solid state ^{13}C NMR spectrum of the 1-iodoheptane/urea inclusion compound is shown in Fig. 3.2 to illustrate the general spectral features of the series of 1-iodoheptane/urea inclusion compounds. In Fig. 3.2.a the entire spectrum (including the urea signal) is shown and in Fig. 3.2.b an expanded region showing only the signals due to 1-iodoheptane is presented. In the spectrum of this compound *two* signals are observed for the CH_3 carbon atom and similarly there are *two* signals for the CH_2I carbon atom. In contrast, only one peak is observed for each of the other carbon environments in the 1-iodoheptane molecule.

The same spectral features are observed for other 1-iodoalkane/urea inclusion compounds. Fig. 3.3 shows the signals for the CH_3 and CH_2I carbons for a series of 1-iodoalkanes ($CH_3(CH_2)_nI$ n=5-11). In the spectra of all these inclusion compounds, two resolved signals are observed for both the CH_3 carbon and the CH_2I carbons. We ascribe the existence of two peaks for CH_3 carbons and CH_2I carbons of 1-iodoalkanes to the two different possible end-group interactions that each of these end-groups can experience within the urea tunnel structure; specifically, CH_3...CH_3 (head-head), CH_3...CH_2I (head-tail) and CH_2I...CH_2I (tail-tail). Therefore CH_3 carbon atoms exist in two different intermolecular environments, also there are two different intermolecular environments for CH_2I carbon atoms. These differences in local intermolecular environments are manifested as individual resolved peaks in the ^{13}C NMR spectrum. Hence solid state NMR results suggest that two different types of orientation of these guest molecules exist within the tunnel structure. We now present

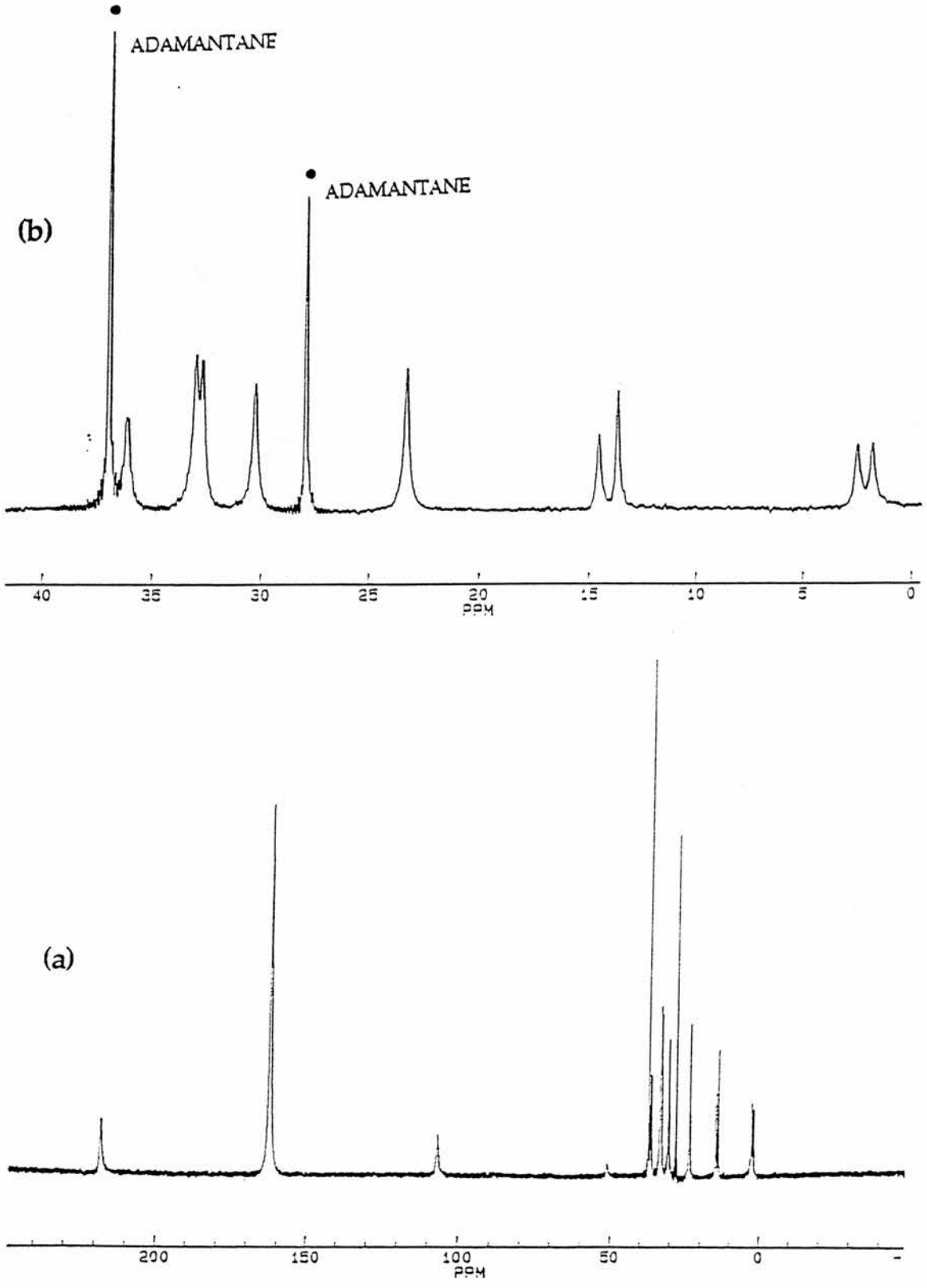

Fig. 3.2 (a) Solid state ^{13}C NMR spectrum of 1-iodoheptane/urea; (b) the expanded region containing only the signals for 1-iodoheptane.

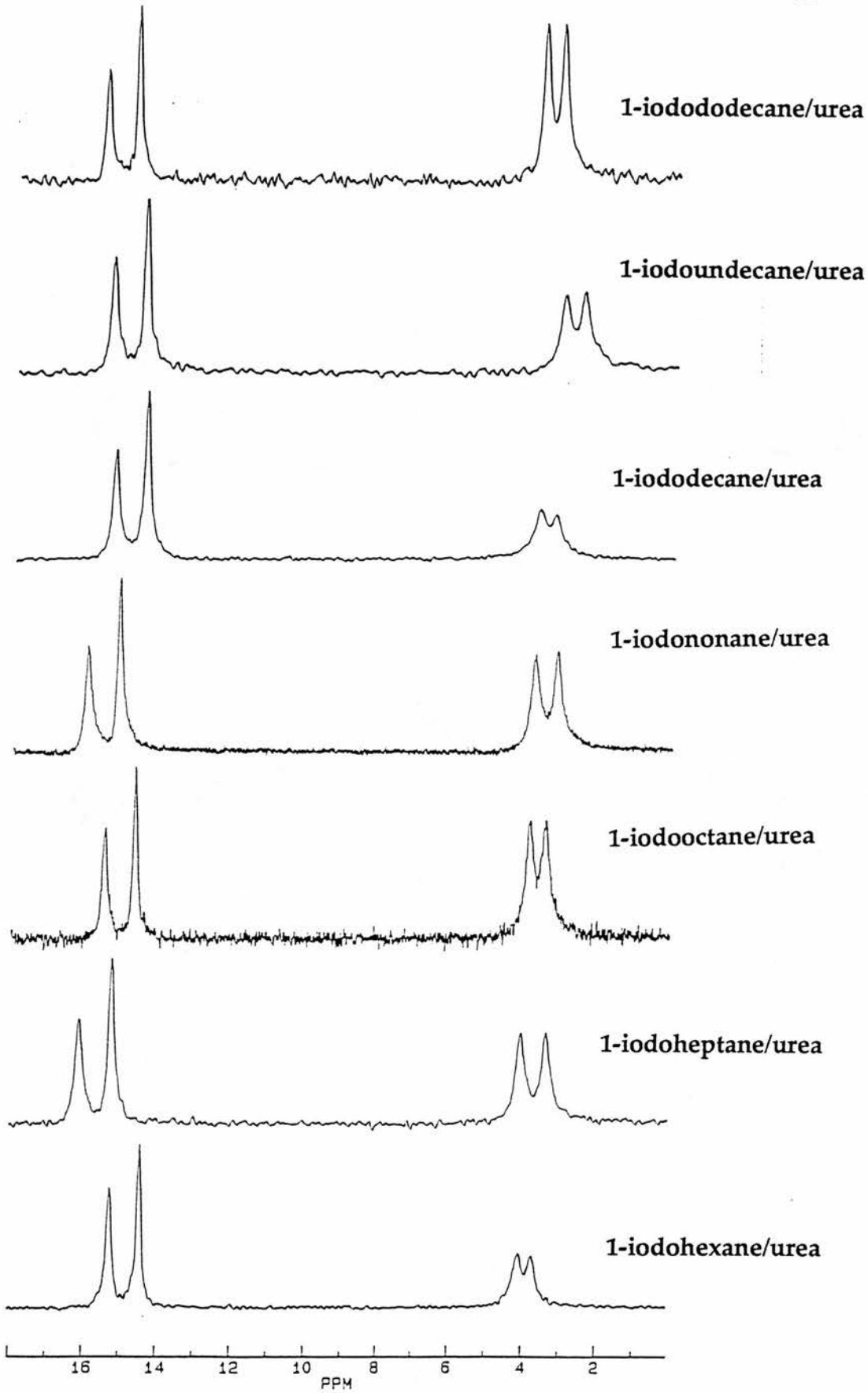

Fig. 3.3 ^{13}C NMR signals for the CH_3 and CH_2I carbons of 1-iodoalkanes ($CH_3(CH_2)_5I$-$CH_3(CH_2)_{12}I$).

evidence to support the proposed orientationally disordered structure for these guest molecules in their urea inclusion compounds, deduced from our ^{13}C NMR results.

Consider urea inclusion compounds containing n-alkanes. In such compounds only one type of intermolecular environment for CH_3 end-groups can be envisaged, i.e. $CH_3...CH_3$. Therefore, based on the previous discussion, we would expect to observe only one signal for this carbon in ^{13}C NMR spectra. The spectrum of the decane/urea inclusion compound (see Fig. 3.4.a) confirms our expectation that only one signal is observed for the CH_3 carbon. Similarly in the ^{13}C NMR spectra of α,ω-diiodoalkane/urea inclusion compounds, one signal is expected for CH_2I carbon atoms since there is only one type of intermolecular environment for CH_2I end-groups (i.e. $CH_2I...CH_2I$). Fig. 3.4.b shows the ^{13}C NMR spectrum of the 1,8 diiodooctane/urea inclusion compound. Only one signal is observed for CH_2I carbons in this spectrum. These results confirm that two types of end-group interaction exist for the 1-iodoalkanes in their urea inclusion compounds.

It might also be argued that the existence of two signals for CH_2I and CH_3 carbon atoms is related to two distinguishable domains of the guest substructure within the urea host. If this assumption is correct, we would expect to observe two distinguishable signals for all the carbon atoms in 1-iodoalkanes. However in the NMR spectra of these compounds, only one signal is observed for each of the other carbon atoms of 1-iodoalkanes, which suggests that there is only one distinguishable domain of guest substructure within the host structure. This evidence (in conjunction with X-ray diffraction results which do not show evidence for the existence of two different domains) strongly suggests the presence of two different types of end-group interaction. In

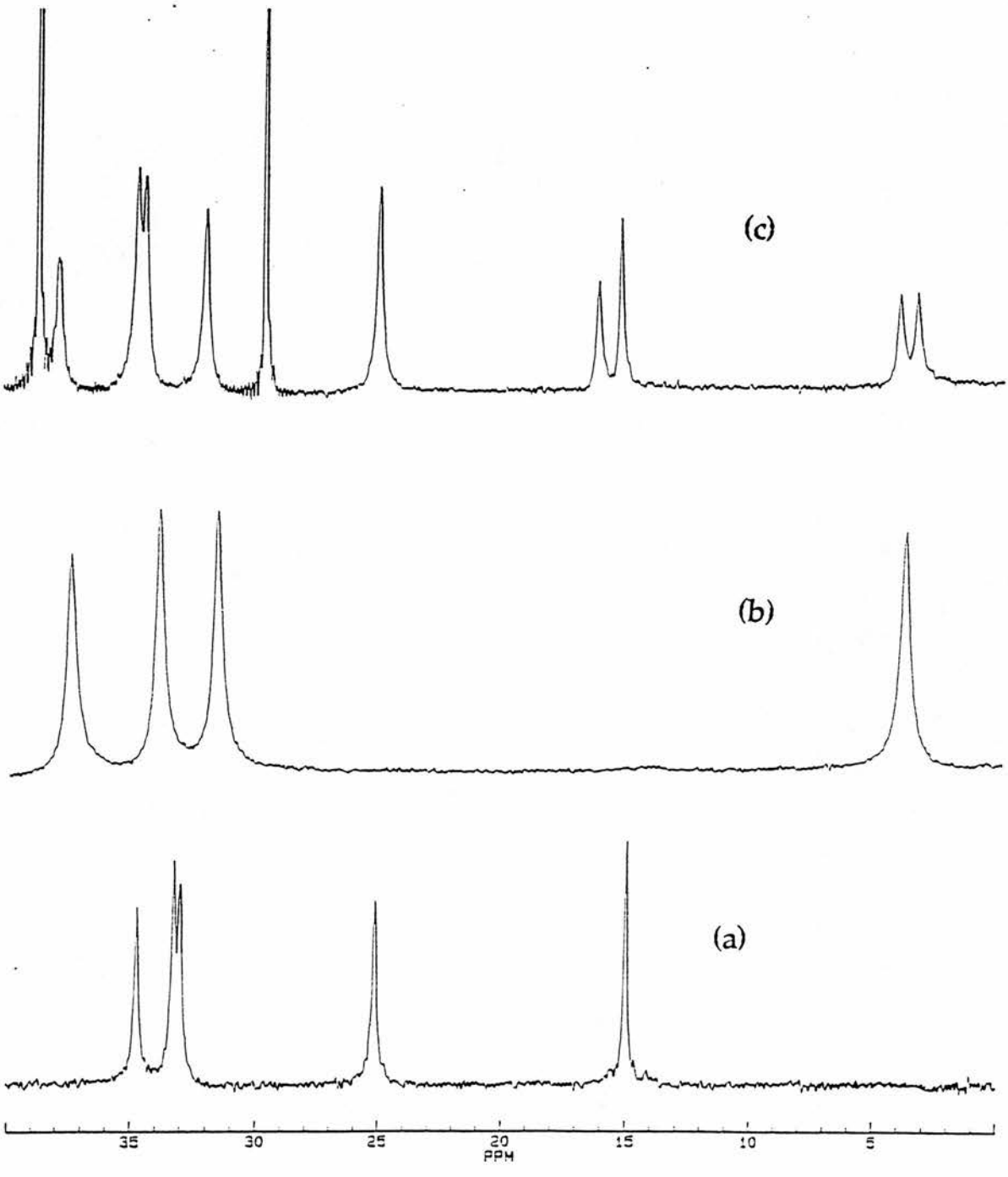

Fig. 3.4 Solid state ^{13}C NMR spectra of (a) decane/urea; (b) 1,8-diiodooctane/urea; (c) 1-iodoheptane/urea.

the following section, we provide further evidence to support this model by employing inclusion compounds containing two different types of guest molecule. It is obvious that quantitative measurement of the relative areas under these signals can reveal information about the relative populations of the different end-group interactions. We elaborate upon this issue in chapter IV.

3.3.2 Characterisation of Signals Associated With Different Intermolecular Environments

3.3.2.a Introduction

The important question which arises from regarding the observation discussed above is whether we can assign the intermolecular environment corresponding to each individual signal. We now present a method for unambiguous assignment of the signals associated with different intermolecular environments. In this method, the relative numbers of end-group interactions can be varied *via* including a symmetric guest species (containing only one type of end-group) in addition to the unsymmetric guest molecule. This method will be described in detail in the next section.

3.3.2.b Alteration of the Relative Populations of Different End-Group Interactions *via* Preparation of Inclusion Compounds Containing Two Different Guests

In the synthetic procedure for preparation of urea inclusion compounds if crystallisation occurs from a solution containing two (or more) potential guest species, both guests will be accommodated within the tunnel structure. We can increase or decrease the relative amount of a particular end-group interaction by preparing inclusion compounds containing different ratios of appropriate guests and

therefore the relative intensities of the corresponding peaks in the NMR spectrum will change. This is the basis for the characterisation of signals which arise due to different intermolecular environments. Consider the guest molecule $X(CH_2)_nY$ containing two types of end-group X and Y. As discussed above, there are three types of interaction for these end-groups X...X , Y...Y and X...Y. Now if we prepare an inclusion compound containing two types of guests $X(CH_2)_nX$ and $X(CH_2)_nY$, we will increase the relative number of X...Y interactions versus Y...Y interactions (this fact is substantiated later).

Consequently, if different NMR signals are observed for the end-group interactions involving group X, we expect an increase in the intensity of the peak which corresponds to the X...X interaction. On this basis, we can characterise the end-group interaction corresponding to each individual signal by observing the change in signal intensities. We demonstrate the applicability of this method to assign signals in the ^{13}C NMR spectra of 1-iodoalkane/urea inclusion compounds.

3.3.2.c Characterization of CH_3 Carbon Signals

We now employ the method described in the previous section to assign the end-group interaction corresponding the CH_3 carbon signals in the ^{13}C NMR spectra of 1-iodoalkane/urea inclusion compounds. In urea inclusion compounds containing 1-iodoalkane and α,ω-diiodoalkane guest molecules, the number of CH_3...CH_2I interactions is increased relative to the number of CH_3...CH_3 interactions on increasing the relative amount of α,ω-diiodoalkane guest molecules, and therefore we expect a change in the relative intensity of the signal for the CH_3...CH_2I interaction. Fig. 3.5.b shows CH_3 carbon signals for an inclusion compound containing 65.4% 1-iodooctane and 34.6% 1,8-diiodooctane. Comparison of these signals with the CH_3 carbon signals

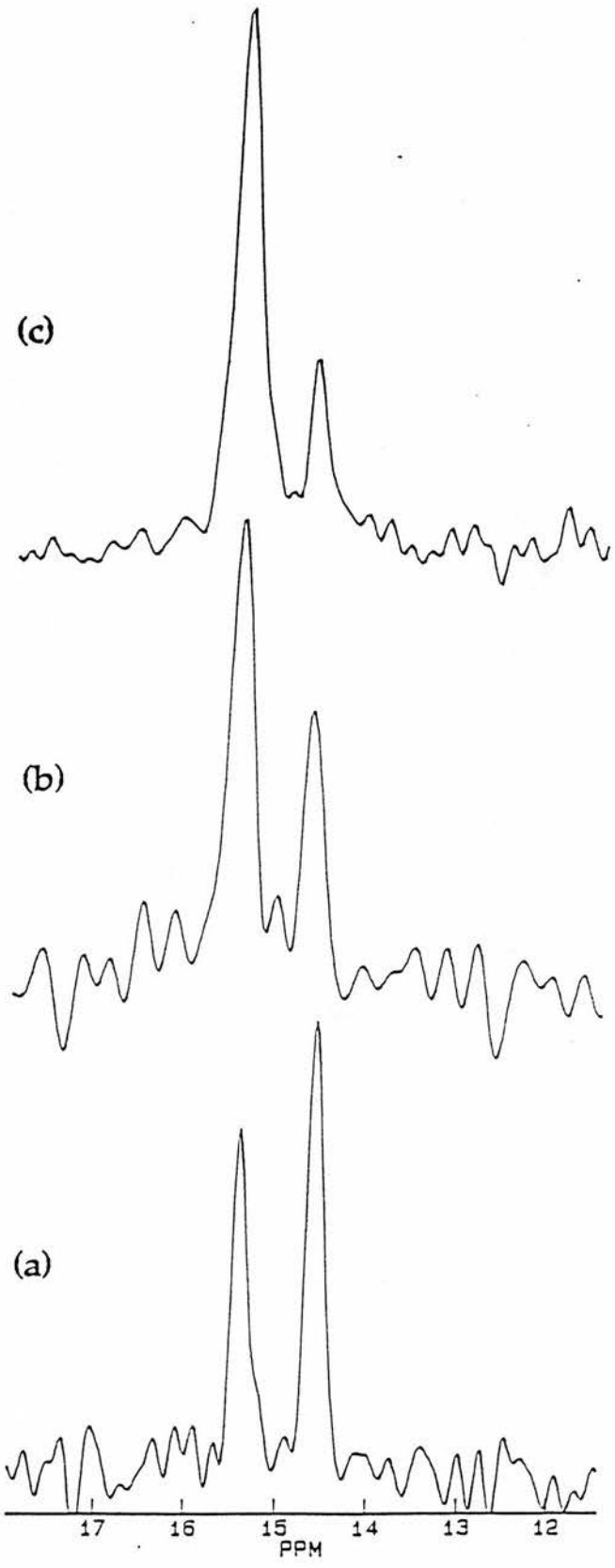

Fig. 3.5 ^{13}C NMR signal of the CH_3 carbon of (a) 1-iodooctane/urea; (b) urea inclusion compound containing 65.4% 1-iodooctane/urea, 34.6% 1,8- diiodooctane (c) urea inclusion compound containing 47.8% 1-iodooctane/urea 52.2% 1,8diiodooctane.

of 1-iodooctane/urea (Fig. 3.5.a) shows a decrease in intensity of the signal at 14.58 ppm. Fig. 3.5.c shows the CH_3 carbon signals for another inclusion compound containing 47.8% 1-iodooctane and 52.2% 1,8 diiodooctane. In this inclusion compound, the relative number of CH_3...CH_3 interactions has been further reduced and there is therefore a further decrease in the intensity of the signal at 14.58 ppm. Consequently the signal at 14.58 ppm is assigned to represent CH_3...CH_3 interaction and the signal at 15.41 ppm is assigned to represent CH_3...CH_2I interaction. While chemical shifts of these two signals are slightly different for different 1-iodoalkanes (see section 3.3.3) this difference is small compared to the separation between the two peaks, and it is reasonable to assume that in all the 1-iodoalkanes the CH_3 carbon signal at higher chemical shift represents CH_3...CH_2I interaction and the signal at lower chemical shift represents CH_3...CH_3 interaction.

3.3.2.d Characterization of CH_2I Carbon Signals

For characterisation of CH_2I carbon atom signals, the inclusion compounds containing 1-iodoalkanes and α,ω-diiodoalkanes are not appropriate compounds, since CH_2I carbon signals originate from both guest molecules and therefore cannot provide unambiguous information about the intermolecular environment associated with each individual signal. However, a combination of 1-iodoalkanes and n-alkanes can provide the required information. In inclusion compounds containing 1-iodoalkane and n-alkane guest molecules, the relative number of CH_2I...CH_2I contacts is decreased (compared with the number of CH_2I...CH_3 contacts) as the proportion of n-alkane guest molecules is increased. Therefore a corresponding decrease in the signal intensities of related peak due to the CH_2I...CH_2I contacts is

expected. Fig. 3.6.b shows the spectrum of an inclusion compound containing 67.4% 1-iodoundecane and 32.6% undecane. In this compound the relative number of $CH_2I...CH_2I$ contact have been decreased. Therefore the corresponding peak should exhibit a decrease in intensity. The relative intensity of the peak at 3.58 ppm is decreased in comparison with to the spectrum of the compound containing only 1-iodooctane. Fig 3.6.c shows the spectrum of a compound containing 25.1% 1-iodoundecane and 74.9% n-undecane. In this inclusion compound, the relative number of $CH_2I...CH_2I$ contacts has been further reduced and as a consequence the relative intensity of the peak at 3.58 ppm is also further decreased. In view of the results obtained from these experiments, the signal at 3.58 ppm is assigned to represent $CH_2I...CH_2I$ interaction and the signal at 3.08 ppm is assigned to represent to $CH_2I...CH_3$ interaction. In conclusion, in the spectra of 1-iodoalkane/urea compounds, the CH_2I carbon signal at higher chemical shift represents $CH_2I...CH_2I$ interaction and the peak at lower chemical shift represents $CH_2I...CH_3$ interaction.

3.3.3 Chain Length Dependence of Chemical Shifts

Chemical shifts of CH_3 and CH_2I carbon signals vary as a function of chain length of 1-iodoalkanes. Table 3.1 illustrates chemical shift values for these carbon atoms in 1-iodoalkanes ($CH_3(CH_2)_nI$; n=5-11) in their urea inclusion compounds. Also Δ_1 and Δ_2 are the chemical shift differences between the two signals for CH_3 and the two signals for CH_2I, respectively.

The variation of chemical shifts in 1-iodoalkanes containing an odd number carbon atoms shows a pattern which is different from 1-iodoalkanes containing an even number of carbon atoms. The CH_3 carbon chemical shift of even numbers (6, 8, 10, 12) gradually increases

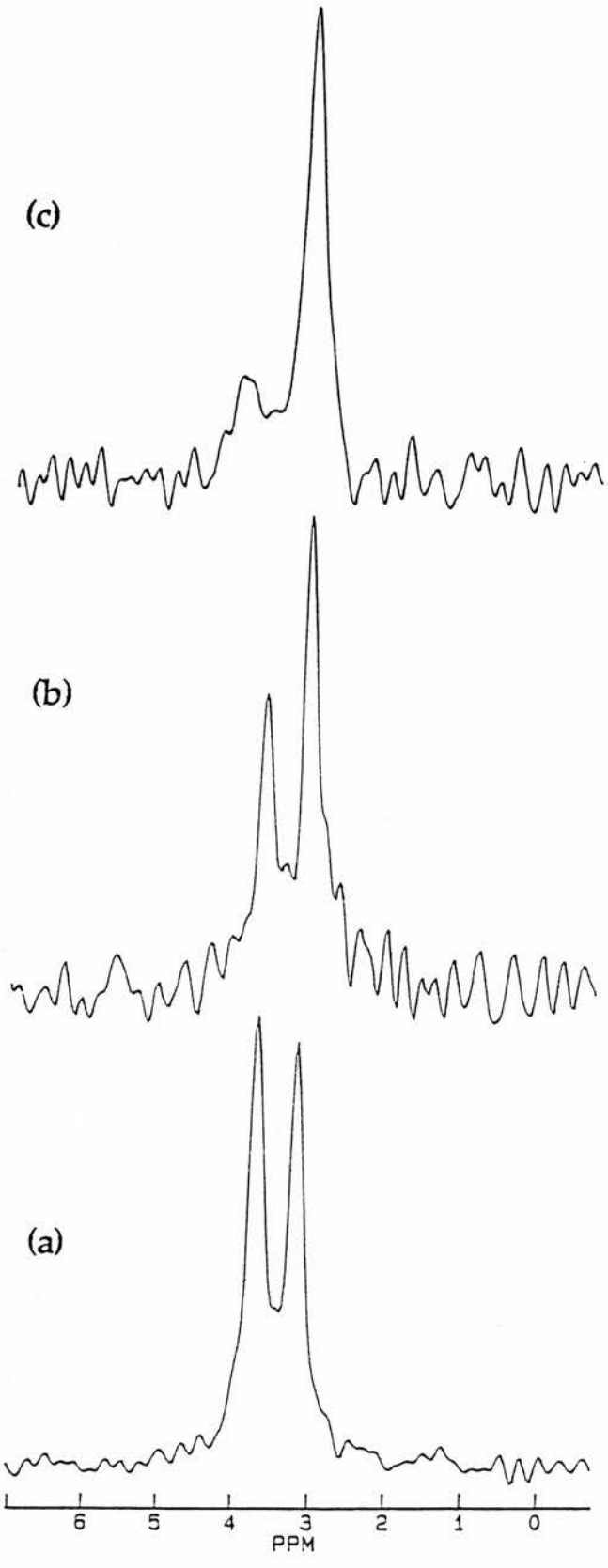

Fig. 3.6 ^{13}C NMR signal of the CH_2I carbon of (a) 1-iodoundecane/urea; (b) urea inclusion compound containing 67.4% 1-iodoundecane, 32.6% decane (c) urea inclusion compound containing 25.1% 1-iodoundecane 74.9% undecane.

TABLE 3.1: ^{13}C NMR chemical shifts for CH_3 carbons and CH_2I carbons of 1-iodoalkanes ($CH_3(CH_2)_{n-1}I$) in their urea inclusion compounds.[a]

	CH_3 Carbon Signals			CH_2I Carbon Signals		
n	$CH_3...CH_3$	$CH_3...CH_2I$	Δ_1[b]	$CH_2I...CH_3$	$CH_2I...CH_2I$	Δ_2[c]
6	14.35	15.17	0.82	3.67	4.01	0.34
8	14.58	15.41	0.83	3.41	3.81	0.40
10	14.80	15.62	0.82	3.21	3.71	0.50
12	14.91	15.81	0.90	3.06	3.64	0.58
7	15.17	16.05	0.88	3.34	4.01	0.67
9	15.08	15.94	0.86	3.13	3.73	0.60
11	14.97	15.85	0.88	3.08	3.58	0.50

[a]Values are given in units of ppm. [b]Δ_1 represents the chemical shift difference between the two signals associated with CH_3 carbons. [c]Δ_2 represent the chemical shift difference between the two signals associated with CH_2I carbons.

whereas for odd numbers (7, 9, 11) it decreases on increasing the chain length. The CH_2I carbon chemical shift for odd and even carbon numbers gradually decreases by increasing the chain length. It is interesting to note how the separation between signals varies with chain length. In the series of 1-iodoalkanes, the separation between the two signals for CH_3 carbons is constant (0.85 ± 0.03 ppm; compared to the digital resolution of the recorded spectra which is 0.04 ppm/pt), whereas the separation between signals related to CH_2I carbons fluctuates as chain length is varied (see table 3.1).

3.4 Solid State ^{13}C NMR Studies of 1-bromoalkane/Urea Inclusion Compounds

3.4.1 General Spectral Features

The solid state ^{13}C NMR spectrum of the 1-bromodecane/urea inclusion compound is shown in Fig. 3.7 to illustrate the general spectral features of 1-bromoalkane/urea inclusion compounds. In this spectrum two individual signals are observed for the CH_3 carbon atom. The signal due to the CH_2Br carbon is resolved from the other CH_2 carbons, and therefore it is not possible to investigate intermolecular effects on the chemical shift of the CH_2Br carbon. Similar features are observed in the spectra of all the 1-bromoalkane/urea compounds studied ($CH_3(CH_2)_5Br$ - $CH_3(CH_2)_{12}Br$; see Fig. 3.8). The only compound for which the signals for all CH_2 carbons are individually resolved is 1-bromohexane/urea. In the spectrum of this compound there are *two* signals due to the CH_3 carbon, but only *one* signal is observed for each of the other carbon environments (including the CH_2Br carbon). Thus, while an intermolecular chemical shift effect is observed for the CH_3 carbon in 1-bromohexane, this effect is not resolved for the CH_2Br carbon. In the following section we present evidence which suggests that this behaviour is general for the 1-bromoalkane/urea inclusion compounds.

3.4.2 Identification of the CH_2Br Carbon Signal Using ^{13}C Labelled 1-bromodecane

The ^{13}C NMR resonance for the CH_2Br carbon can be detected readily if we prepare the urea inclusion compound with a 1-bromoalkane which is specifically labelled with ^{13}C isotope at the CH_2Br position. The intensity of this signal will be much stronger than the signals of the other carbons. Fig. 3.9 shows the spectrum of the urea inclusion

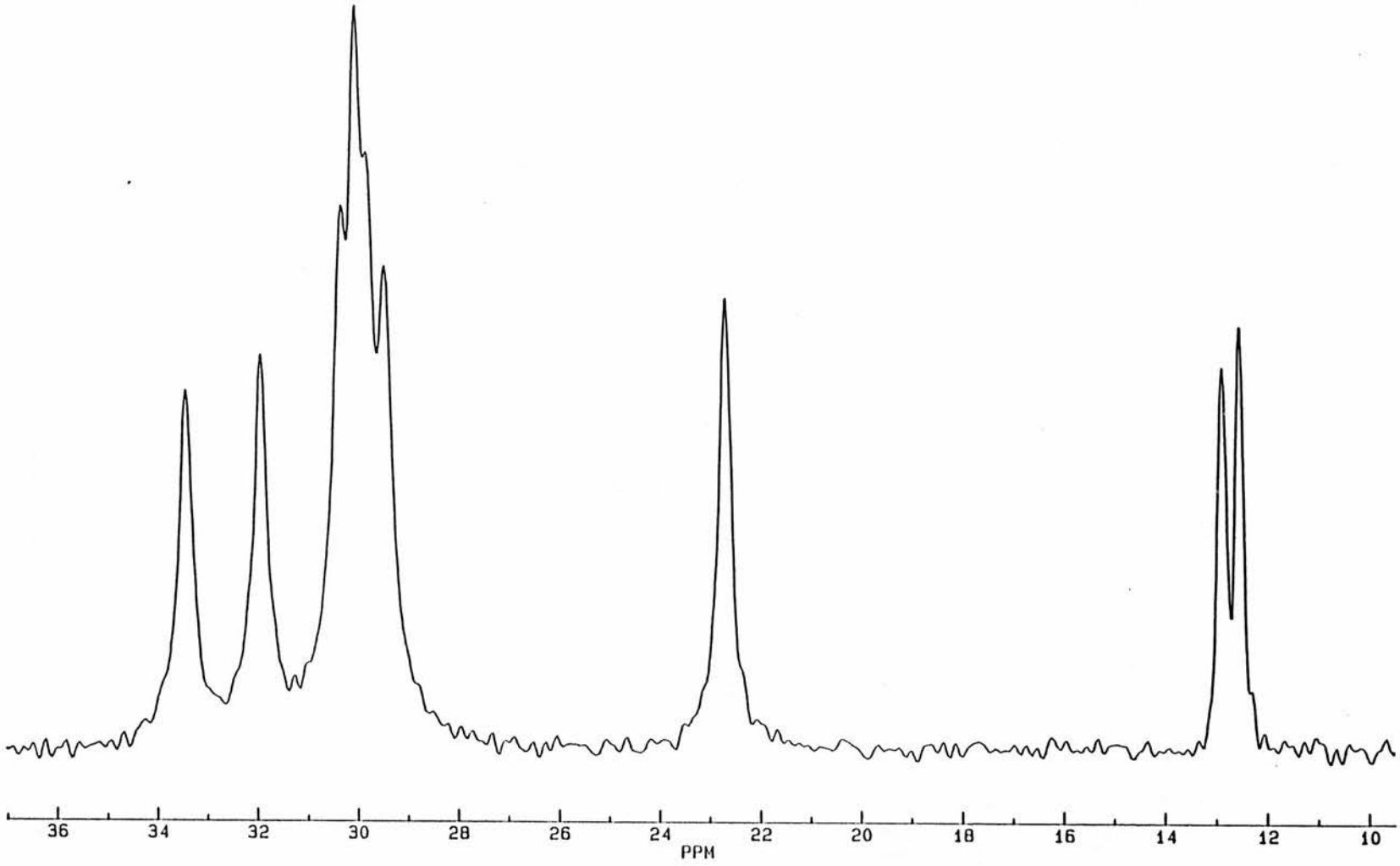

Fig. 3.7 Solid state ^{13}C NMR spectrum of 1-bromodecane/urea.

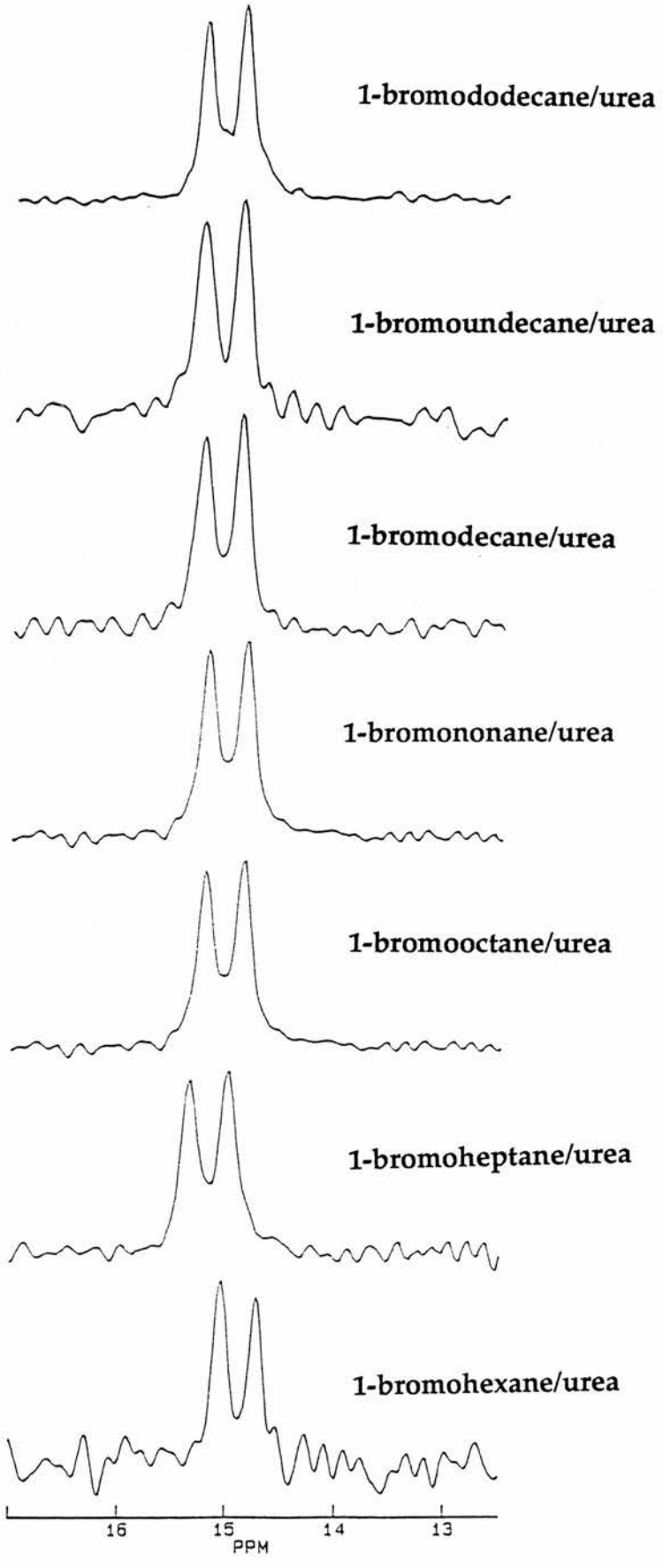

Fig. 3.8 Solid state ^{13}C NMR spectra of 1-bromoalkanes; $CH_3(CH_2)_5Br$-$CH_3(CH_2)_{12}Br$ (only the CH_3 signals are shown).

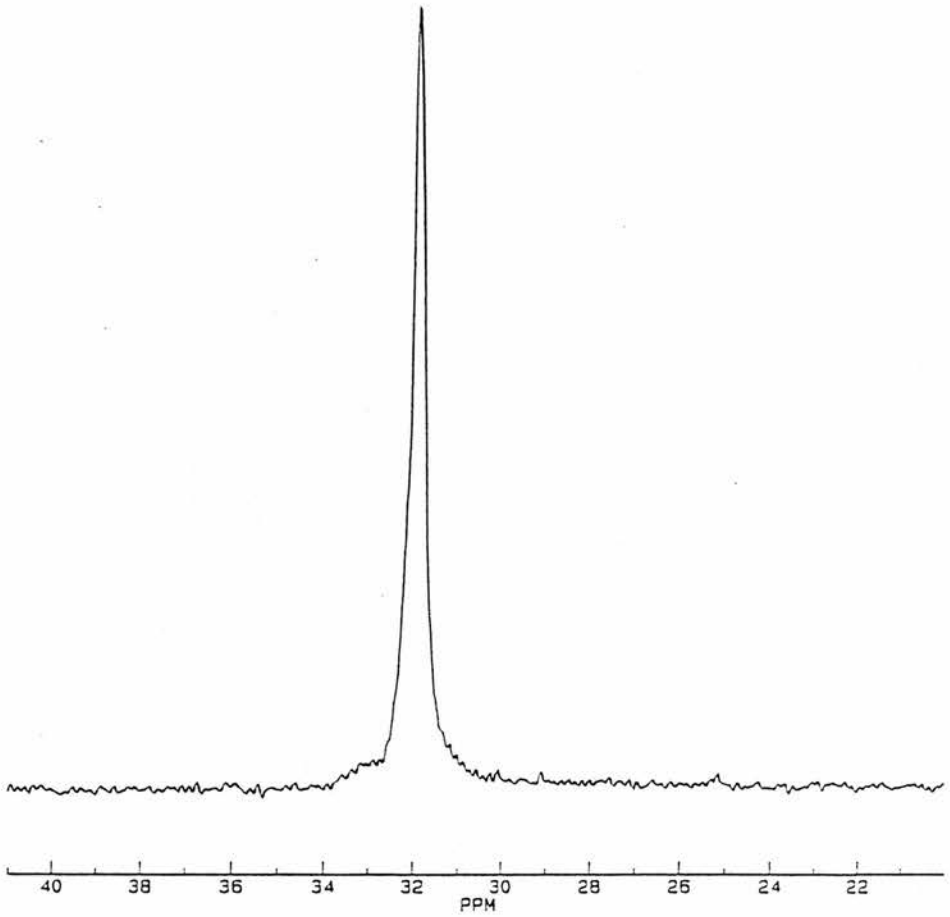

Fig. 3.9 ^{13}C NMR signal of the CH_2Br carbon of ^{13}C labelled 1-bromodecane/urea.

compound containing 1-bromodecane specifically labelled with ^{13}C in the CH_2Br position. The CH_2Br carbon signal is observed at 31.9 ppm and is the only intense signal observed in the spectrum. It is obvious that no intermolecular chemical shift effect is observed for this carbon (consistent with the conclusion for the 1-bromohexane/urea inclusion compound). This provides further evidence that this behaviour is general in 1-bromoalkane/urea inclusion compounds.

3.4.3 Characterisation of CH_3 Carbon Signals Associated With Different Intermolecular Environments

Based on the method developed in section 3.3.2.b, assignment of the two signals due to the CH_3 carbon atoms of 1-bromoalkane/urea

compounds should consider inclusion compounds containing a mixture of 1-bromoalkane and α,ω-dibromoalkane guest molecules. In such inclusion compounds, the relative number of $CH_3...CH_3$ interactions is reduced (and the relative number of $CH_3...CH_2Br$ interactions is increased) relative to the inclusion compound containing only the 1-bromoalkane guest. Hence a decrease in the intensity of the relevant signal is expected. In Fig. 3.10 the spectrum of 1-bromoheptane/urea (Fig. 3.10.a) is shown in comparison with the spectra of two inclusion compounds containing: 42.5% 1-bromoheptane, 57.5% 1,7-dibromoheptane (Fig. 3.10.b), and 58.1% 1-bromoheptane, 41.9% 1,7-dibromoheptane (Fig. 3.10.c). The intensity of the signal at 14.98 ppm is successively decreased. Hence this signal is attributed to the $CH_3...CH_3$ interaction and the signal at 15.31 ppm is therefore attributed to the $CH_3...BrCH_2$ interaction. On the basis of the results of this experiment, we conclude that in all the 1-bromoalkane/urea compounds, the CH_3 signal at higher chemical shift represents $CH_3...BrCH_2$ interaction and the CH_3 signal at lower chemical shifts represents $CH_3...CH_3$ interactions.

3.4.4 Chain Length Dependence of Chemical Shifts

^{13}C chemical shifts for CH_3 carbons of 1-bromoalkanes in their urea inclusion compounds are reported in Table 3.2. There are some noticeable facts about these values. The separation of the two signals due to CH_3 carbon atoms is constant (0.35 ± 0.02 ppm). The chemical shift of the signals in compounds containing an even number carbons (6,8,10,12) increases gradually on increasing of the chain length. In contrast, chemical shifts of signals in compounds containing odd number of carbons decrease gradually on increasing the chain length.

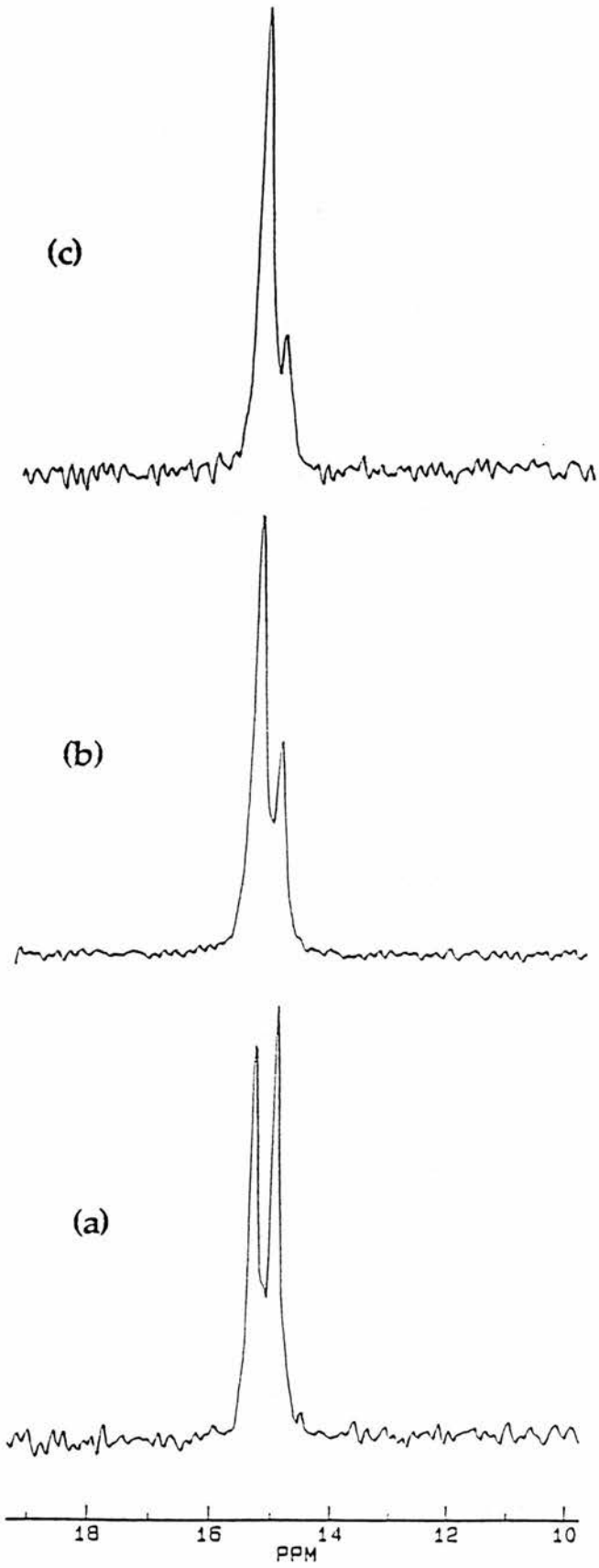

Fig. 3.10 Solid state ^{13}C NMR spectra of (a) 1-bromoheptane/urea; and urea inclusion compounds containing (b) 42.5% 1-bromoheptane, 57.5% 1,7-dibromoheptane (c) urea inclusion compound containing 58.1% 1-bromoheptane, 41.9% 1,7-dibromoheptane.

TABLE 3.2: ^{13}C Chemical shifts for CH_3 carbons 1-bromoalkanes ($CH_3(CH_2)_{n-1}Br$) in their urea inclusion compounds.[a]

	CH_3 Carbon Signals		
n	$CH_3...CH_3$	$CH_3...CH_2Br$	Δ^b
6	14.71	15.05	0.34
8	14.84	15.18	0.34
10	14.90	15.24	0.34
12	15.01	15.37	0.36
7	14.98	15.31	0.33
9	14.94	15.27	0.33
11	14.92	15.27	0.35
13	14.88	15.24	0.36

[a]Values are given in units of ppm. [b]Δ represents the chemical shift difference between the two signals associated with CH_3 carbons.

3.5 Solid State ^{13}C NMR Studies of 1-chloroalkane/Urea Inclusion Compounds

3.5.1 General Spectral Features

In Fig. 3.11 the spectrum of the 1-chlorooctane/urea inclusion compound is shown to illustrate the general spectral features of 1-chloroalkane/urea inclusion compounds. The main spectral features of the spectrum are *one* signal due to the CH_3 carbon atoms and *two* signals for the CH_2Cl carbon atoms, arising from two different intermolecular environments for the CH_2Cl carbon. These features are in contrast to the spectra of 1-bromoalkane/urea compounds for which one signal is observed for CH_2Br carbons and two signals are observed for CH_3 carbons.

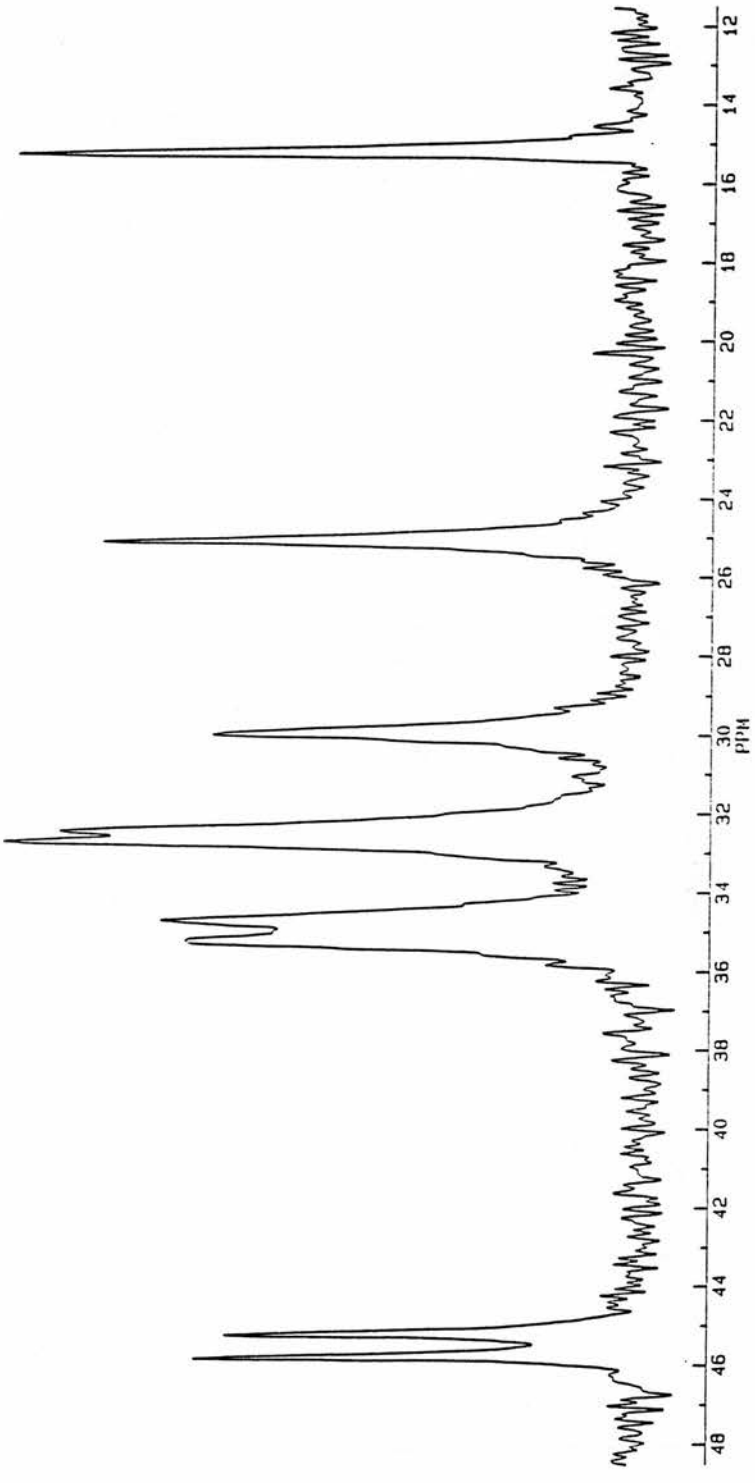

Fig. 3.11 Solid state ^{13}C NMR spectrum of 1-chlorooctane/urea.

Such spectral features are observed for all 1-chloroalkane/urea inclusion compounds. Some of the spectra for 1-chloroalkane/urea inclusion compounds are shown in Fig. 3.12. In all the spectra of these compounds, only *one* signal is observed for the CH_3 carbon atoms.

3.5.2 Characterisation of CH_2Cl Carbon Signals Associated With Different Intermolecular Environments

For characterisation of the two signals due to CH_2Cl carbons in 1-chloroalkane/urea inclusion compounds, inclusion compounds containing a mixture of: 1-chloroalkane and n-alkane guest molecules are appropriate. In such compounds, the relative number of $CH_2Cl...CH_2Cl$ interactions is decreased in comparison with the inclusion compound containing only the 1-chloroalkane guest, and therefore a decrease in relative intensity of the signal due to the $CH_2Cl...CH_2Cl$ interaction is expected. Fig. 3.13 shows the spectrum of the inclusion compound containing 65.4% 1-chlorooctane and 34.6% decane (Fig. 3.13.b) in comparison with the spectrum of the 1-chlorooctane/urea the inclusion compound (Fig. 3.13.a). The relative intensity of the signal at 45.70 ppm for the inclusion compound containing the two guest molecules is decreased. Therefore this signal is assigned to the $CH_2Cl...CH_2Cl$ interaction, and the signal at 45.12 ppm is assigned to the $CH_2Cl...CH_3$ interaction.

These results suggest that in all 1-chloroalkane/urea inclusion compounds, the CH_2Cl signals at higher chemical shift represent the $CH_2Cl...CH_2Cl$ interaction, and signals at lower chemical shift represent the $CH_2Cl...CH_3$ interaction.

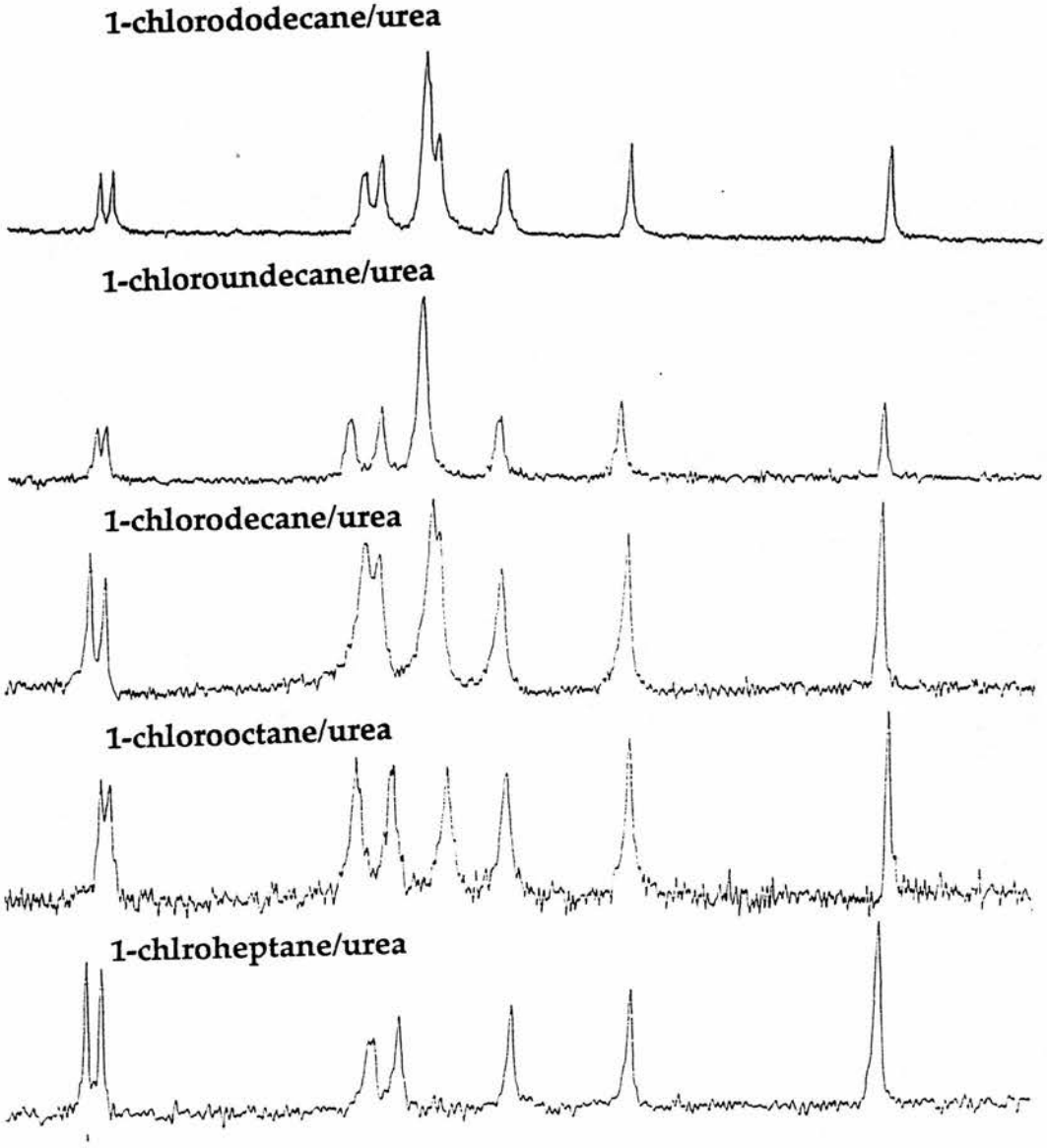

Fig. 3.12 Solid state ^{13}C NMR spectra of 1-chloroalkane/urea inclusion compounds.

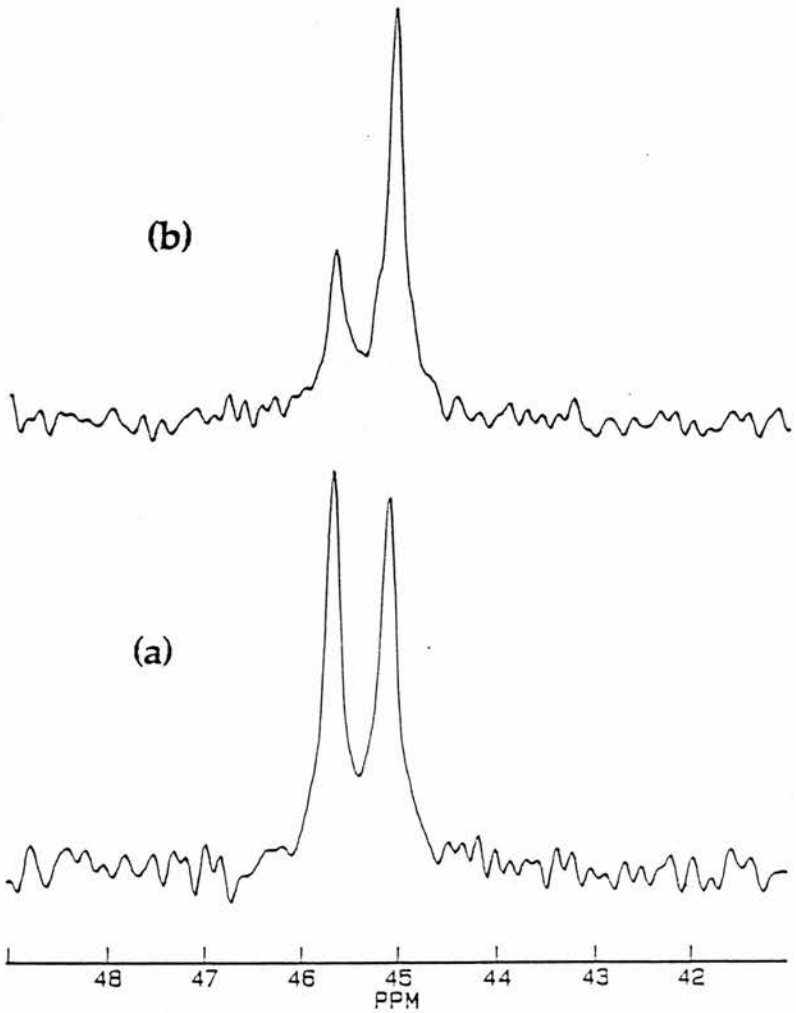

Fig. 3.13 Solid state ^{13}C NMR spectra of (a) 1-chlorooctane/urea and (b) urea inclusion compound containing 1-chlorooctane (65.4%) and n-decane (34.6%).

3.5.3 Chain Length Dependence of Chemical Shifts

Table 3.3 illustrates the chemical shifts of 1-chloroalkane/urea inclusion compounds. The noticeable fact about the values presented in this table is that the chemical shifts for the CH_2Cl carbon next to the CH_3 end-group decrease within both even and odd series; whereas the chemical shifts for the CH_2Cl carbon next to CH_2Cl end-group decrease only within the even series. In addition, the separation of the two signals due to the CH_2Cl carbon is not constant.

TABLE 3.3: ^{13}C NMR chemical shifts for CH_2Cl carbons of 1-choloroalkanes ($CH_3(CH_2)_{n-1}Cl$) in their urea inclusion compounds.[a]

	CH_2Cl Carbon signals		
n	$CH_2Cl...CH_3$	$CH_2Cl...CH_2Cl$	Δ^b
6	45.24	45.82	0.58
8	45.12	45.70	0.58
10	44.97	45.44	0.47
12	44.86	45.16	0.30
7	44.92	45.27	0.35
9	44.86	45.20	0.34
11	44.82	45.22	0.40

[a] Values are given in units of ppm. [b]Δ represents the chemical shift difference between the signals associated with CH_2Cl carbons.

3.6 Solid State ^{13}C NMR Studies of 1-fluoroalkane/Urea Inclusion Compounds

3.6.1 General Spectral Features

Fig. 3.14.a shows the ^{13}C NMR spectrum of the 1-fluorononane/urea inclusion compound. In the spectrum of this compound *two* signals exist for CH_3 carbon atoms (Fig. 3.14.b), and *four* signals are observed for CH_2F carbon atoms (Fig. 3.14.c). The existence of two signals for the CH_3 carbon is explained by the presence of two intermolecular environments for this end-group, specifically $CH_3...CH_3$ and $CH_3...CH_2F$.

Different intermolecular environments for the CH_2F end group ($CH_2F...CH_3$ and $CH_2F...CH_2F$) also generates two signals. For the CH_2F

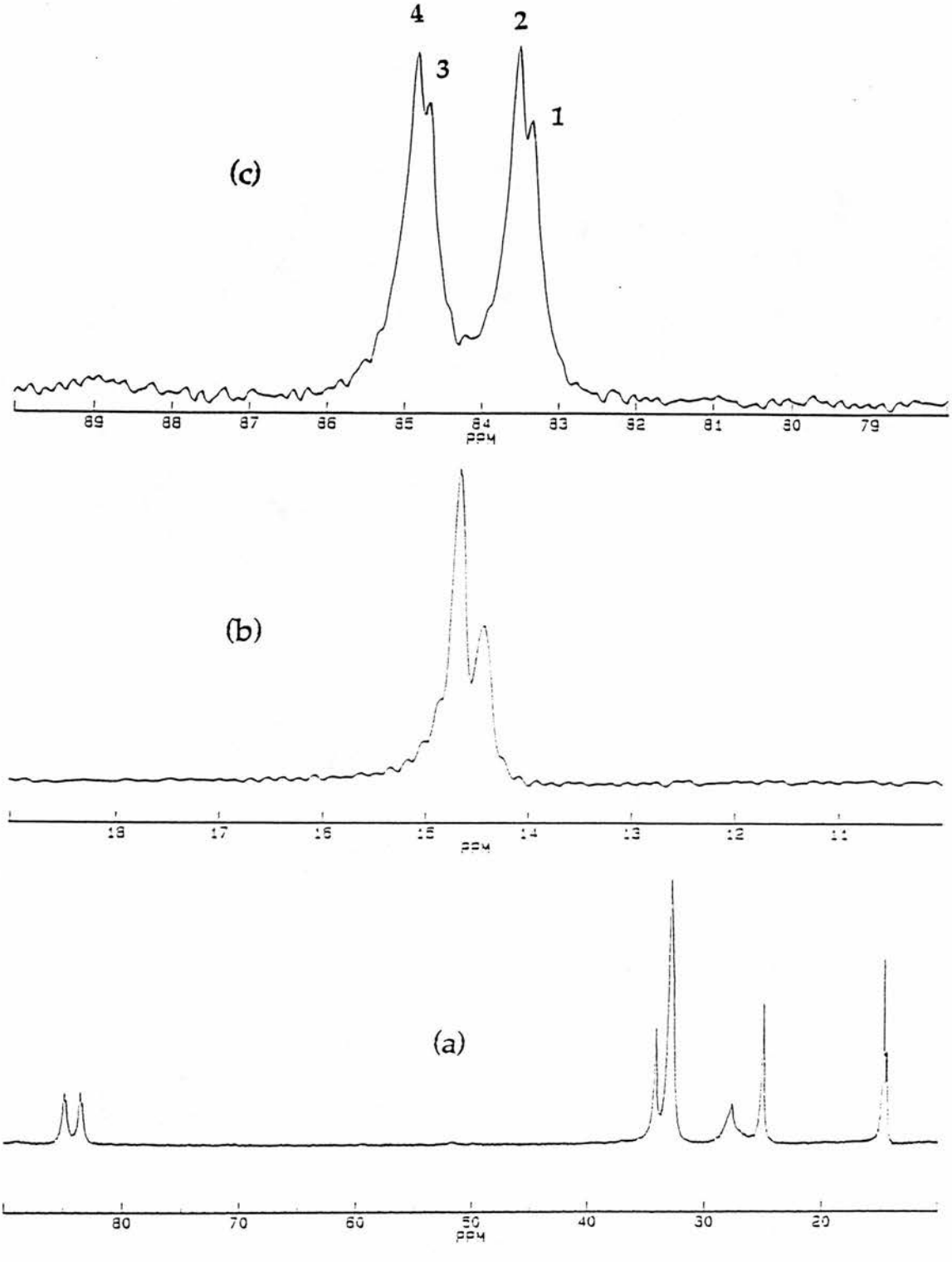

Fig. 3.14 (a) Solid state ^{13}C NMR spectrum of 1-fluorononane/urea (b) expanded region of the CH_3 carbon signals (c) expanded region of the CH_2F carbon signals.

carbon signal, coupling between ^{13}C and ^{19}F generates another two signals with equal intensities. The separation between peaks 1 and 3 (163.41 Hz) and between peaks 2 and 4 (153.35 Hz), and consideration of the intensities of these peaks, suggest that these peaks (1,3 and 2,4) are due to coupling between ^{13}C and ^{19}F nuclei (coupling constant between ^{13}C and ^{19}F in CH_3F is 157.5 Hz [10]). Therefore peaks 1 and 3 arise from CH_2F in one particular environment, whereas peaks 2 and 4 represent CH_2F in a different intermolecular environment.

Similar spectral features are observed for other 1-fluoroalkanes in their urea inclusion compounds. Table 3.4 reports chemical shift values for these compounds.

3.6.2 Characterisation of Signals Associated With Different Intermolecular Environments

3.6.2.a Characterisation of CH_3 Carbon Signals

The appropriate combination of guest molecules for characterization of the CH_3 signals in 1-fluoroalkane/urea compounds is a combination of 1-fluoroalkane and α,ω-difluoroalkane guest molecules. Since α,ω-difluoroalkanes are not commercially available, we have used mixture of α,ω-dichloroalkane and 1-fluoroalkane guest molecules to assign the CH_3 signals. Based on previous experiments on 1-chloroalkane/urea compounds (section 3.5.1), we know that the CH_3 chemical shift in the $CH_3...CH_2Cl$ interactions is the same as that in the $CH_3...CH_3$ interaction. Therefore we can use α,ω-dichloroalkane guest molecules for characterisation of CH_3 peaks because there will not be any contribution from CH_2Cl carbons to the CH_3 signals. In such inclusion compounds the relative number of CH_3 groups in $CH_3...CH_3$ *plus* $CH_3...CH_2Cl$ interactions (which have the same chemical shift) is increased relative to that in the inclusion compound containing only

TABLE 3.4: ^{13}C NMR Chemical shifts for CH_3 and CH_2F carbons of 1-flouroalkanes ($CH_3(CH_2)_{n-1}F$) in thier urea inclusion compounds.[a]

	CH_3 Carbon Signals			CH_2F Carbon Signals		
n	CH_3...CH_2F	CH_3...CH_3	Δ_1[b]	CH_2F...CH_3	CH_2F...CH_2F	Δ_2[c]
6	14.84	15.11	0.27	83.67 & 84.97	83.90 & 85.12	0.23 & 0.15
9	14.47	14.72	0.25	83.43 & 84.78	83.61 & 84.92	0.18 & 0.14
13	14.68	14.96	0.28	83.48 & 84.81	83.67 & 84.98	0.19 & 0.17

[a]Values are given in units of ppm. [b]Δ_1 represents the chemical shift differences between the signals associated with CH_3 carbons. [c]Δ_2 represents the chemical shift differences between the signals associated with CH_2F carbons.

the 1-fluoroalkane guest molecule, therefore we expect a relative increase in the intensity of the signal representing these interactions. Fig. 3.15 shows the ^{13}C NMR spectra of inclusion compounds containing 41.3% 1-fluorononane and 58.7% 1,8-dichlorooctane (Fig. 3.15.b), and 20.2% 1-fluorononane and 79.8% 1,8-dichlorooctane (Fig. 3.15.c), in comparison with the spectrum of the 1-fluorononane/urea inclusion compound (Fig. 3.15.a). In these spectra the relative intensity of the signal at 14.72 ppm is successively increased as the proportion of 1,8-dichlorooctane is increased, therefore this signal is assigned as CH_3 in the CH_3...CH_3 interaction and the signal at 14.47 ppm is assigned as CH_3 in the CH_3...CH_2F interaction.

3.6.2.b Characterisation of CH_2F Carbon Signals

For characterisation of the signals due to CH_2F carbon atoms, study of inclusion compounds containing 1-fluoroalkanes and n-alkanes is appropriate. In these compounds the relative number of CH_2F...CH_2F interactions will decrease (or the relative number of CH_2F...CH_3 interactions will increase) in comparison with the 1-fluoroalkane/urea inclusion compound. Hence we expect a decrease in the relative intensity of the signal due to CH_2F...CH_2F interaction, as the proportion of n-alkane guest molecules is increased. In Fig. 3.16 the spectra of inclusion compounds containing 75.6% 1-fluorononane and 24.4% decane (Fig. 3.16.b) and 62.7% 1-flourononane and 37.3% decane (Fig. 3.16.c) are shown in comparison with the spectrum of the 1-flourononane/urea inclusion compound (Fig. 3.16.a).

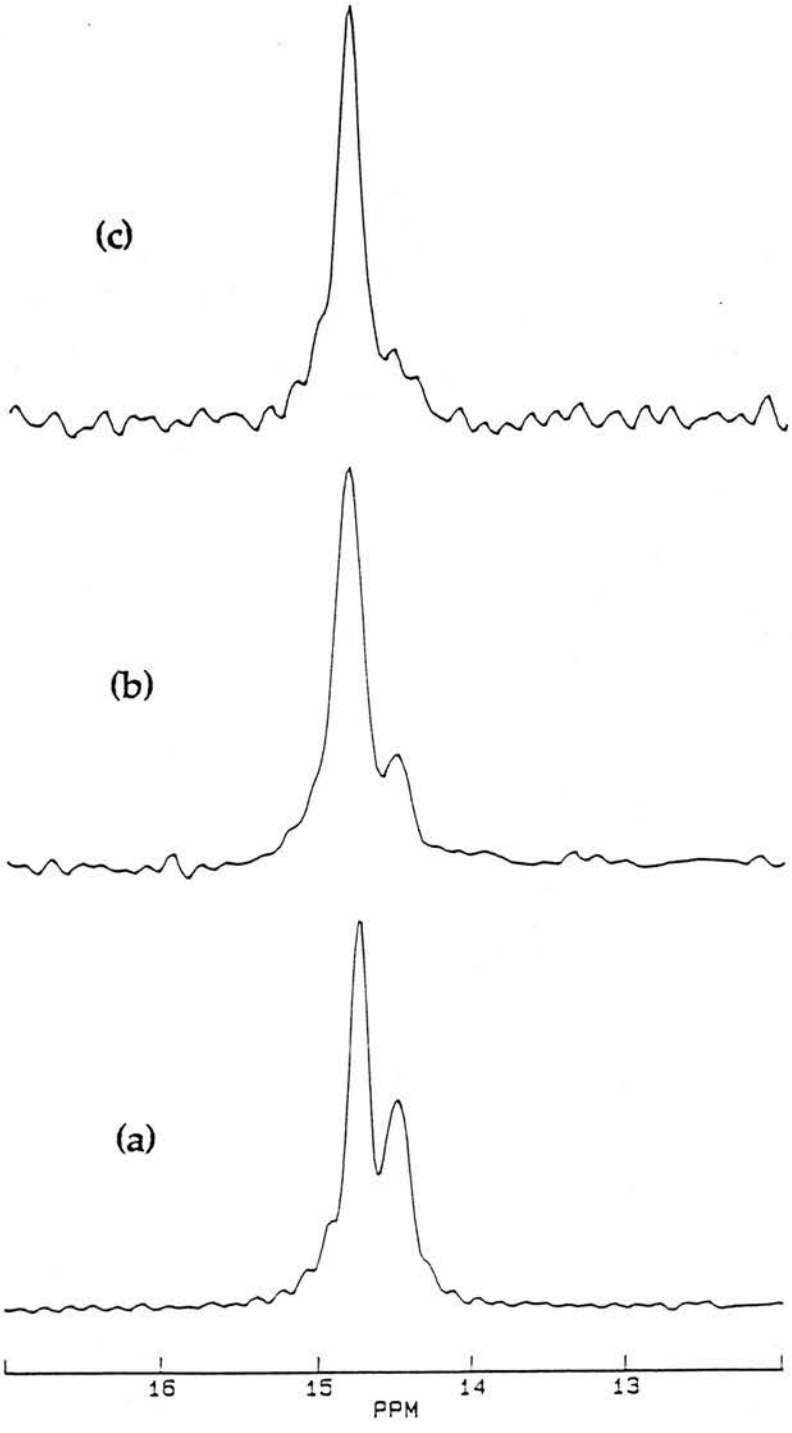

Fig. 3.15 Solid state ^{13}C NMR spectra of (a) 1-fluorononane/urea (only the CH_3 carbon signal is shown); and (b) urea inclusion compounds containing 41.3% 1-fluorononane; 58.7% 1,8-dichlorooctane and (c) 20.2% 1-fluorononane; 79.8% 1,8-dichlorooctane.

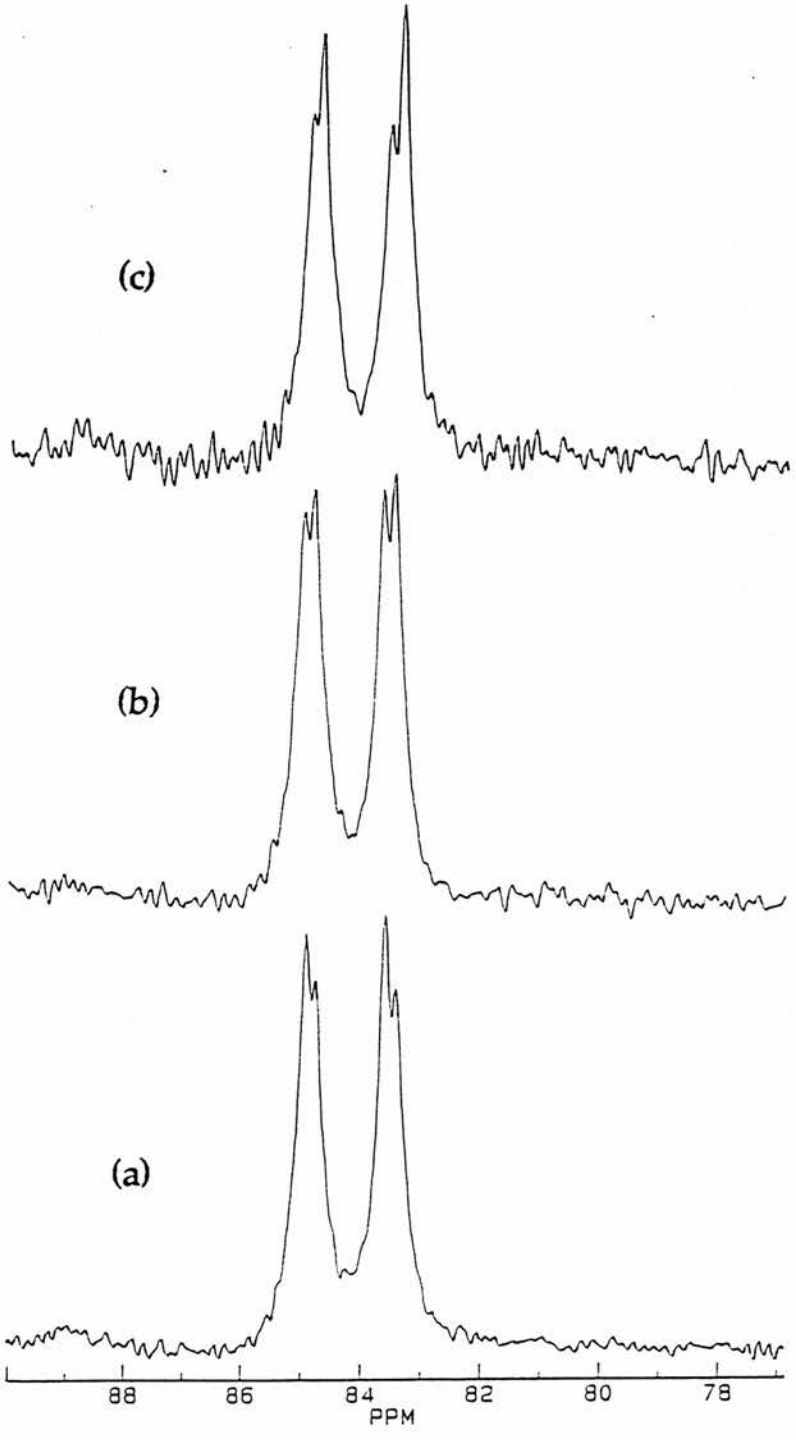

Fig. 3.16 Solid state ^{13}C NMR spectra of (a) 1-fluorononane/urea (only the CH_2F carbon signal is shown); and urea inclusion compounds containing (b) 75.6% 1-fluorononane and 24.4% n-decane and (c) 62.7% 1-fluorononane and 37.3% n-decane.

The relative intensities of the signals at 83.61 ppm and 84.92 ppm are decreased on increasing the proportion of n-alkane guest molecules, therefore we attribute these signals to the $CH_2F...CH_2F$ interaction and the signals at 83.43 ppm and 84.78 ppm to $CH_2F...CH_3$ interaction.

3.6.3. Chain Length Dependence of Chemical Shifts

The available chemical shift data for the three 1-fluoroalkanes (C_6, C_9, C_{13}; the only 1-fluoroalkanes which are commercially available) cannot provide the required information for investigating the chain length dependence or odd and even effect in 1-fluoroalkane /urea inclusion compounds.

References:

[1] Gilson, D. F. R., McDowell, C. A. *Mol. Phys.* 1961, **4**, 125.

[2] Umemoto, K., Danyluk, S. S. *J. Phys. Chem.* 1967, **71**, 3757.

[3] Harris, K. D. M., Jonsen, P. *Chem. Phys. Lett.* 1989, **154**, 593.

[4] Guillaume, F., Sourisseau, C., Dianoux, A. J. *J. Chem. Phys.* 1990, **93**, 3536.

[5] Harris, K. D. M., Thomas, J. M. *J. Chem. Soc., Faraday Trans.* 1990, **86**, 2985.

[6] Harris, K. D. M., Hollingsworth, M. D., *Proc. Royal Soc. A*, 1990, **431**, 245.

[7] Parsonage, N. G., Staveley, L. A. K. "Disorder in crystals", Oxford University Press, Oxford, 1978.

[8] Laves, F., Nicoloides, N., Peng, K. C. *Zeitschrift fur Kristallographie*, 1965, **121**, 258.

[9] Harris, K. D. M., Gameson, I., Thomas, J. M. *J. Chem. Soc., Faraday Trans.* 1990, **86**, 3135.

[10] Breitmaier, E., Voelter, W. "^{13}C NMR Spectroscopy", Weinheim: VCH 1989.

CHAPTER IV

INVESTIGATION OF WEAK INTERMOLECULAR INTERACTIONS BETWEEN FUNCTIONAL GROUPS IN UREA INCLUSION COMPOUNDS: SOLID STATE NMR AND A STATISTICAL ANALYSIS STUDIES

Introduction

In chapter III we demonstrated that different end-group interactions for guest molecules (specifically 1-haloalkanes) in urea inclusion compounds manifest themselves as different NMR signals in the spectra of these compounds. It is clear that measurement of the area under these signals in spectra measured under *quantitative* conditions will provide information regarding the relative numbers of these different end-group interactions. The factor that determines these relative numbers is the relative strength of interactions between end-groups. Therefore this information ultimately will lead to a knowledge about intermolecular interactions between end-groups within the solid phase.

The major difficulty in measuring the relative strength of functional group interactions (a knowledge of which is imperative in the field of crystal engineering), is that in many cases it is not possible to isolate these interactions [1]. Several characteristic features of urea inclusion compounds provide environments within which the interaction between particular functional groups is essentially isolated. First, the small internal diameter [2] of the urea tunnel, prohibits the interaction between other parts of the guest molecules and only the

end-groups are in contact with each other. Second, urea inclusion compounds are incommensurate structures [3]. The consequence of this fact is that the interaction between the host structure and the guest molecules is different for each guest molecule in the structure (i.e., each guest molecule is in a slightly different environment with respect to the host structure). Therefore the main factor that dictates the orientation of the guest molecules is the interaction between functional groups.

In this chapter we begin by presenting a simple mathematical description of the orientation of unsymmetric guest molecules in the urea tunnel structure. The result of this simple analysis shows that due to the intrinsic constraint that the numbers of X...X and Y...Y interactions are equal (X and Y are two different end-groups of the unsymmetric guest molecule), it is *not* possible to separate the relative importance of these two interactions, and hence gain any information about their relative strengths. Quantitative analysis of the NMR spectra of 1-haloalkane/urea inclusion compounds are subsequently discussed.

A theoretical statistical analysis based on a Markov chain model [4] is invoked to investigate the possibility of obtaining information regarding the intrinsic relative preferences of different end-group interactions using quantitative NMR measurements on inclusion compounds containing *two types* of guest molecule. The results of applying this model show that, for such measurements, the required information concerning end-group interactions can be obtained. The details of this statistical model, and the results for inclusion compounds containing two types of guest molecule based on the application of this model are subsequently reported.

This mathematical model has been developed in collaboration with Dr. Peter E. Jupp of the Mathematics Department, University of St. Andrews.

4.1 A Mathematical Analysis of Guest-Guest Interactions in One-Dimensional Inclusion Compounds

For an inclusion compound containing unsymmetric guest molecules of the type $X(CH_2)_nY$ (such as 1-haloalkanes), the following parameters are defined:

$N_{X\text{-}X}$ = number of X...X interactions.

$N_{Y\text{-}Y}$ = number of Y...Y interactions.

$N_{X\text{-}Y}$ = number of X...Y interactions.

Considering all the guest molecules present in the system we define:

N_X = number of X end-groups.

N_Y = number of Y end-groups.

It is obvious that for the inclusion compound containing *only* $X(CH_2)_nY$ guest molecules: $N_X = N_Y$

By definition, the following relations exist in the system:

$$N_X = N_{X\text{-}Y} + 2N_{X\text{-}X} \qquad (1)$$

$$N_Y = N_{X\text{-}Y} + 2N_{Y\text{-}Y} \qquad (2)$$

Since $N_X = N_Y$, therefore:

$$N_{X\text{-}X} = N_{Y\text{-}Y} \qquad (3)$$

If the ^{13}C NMR spectrum of the $X(CH_2)_nY$/urea inclusion compound has two signals for the X end-group (due to the two possible end-group interactions X...X and X...Y), we then denote *the area* of the two signals by $A_{X\text{-}X}$ and $A_{X\text{-}Y}$ respectively.

Then it is clear that:

$$\frac{A_{X\text{-}X}}{A_{X\text{-}Y}} = \frac{2N_{X\text{-}X}}{N_{X\text{-}Y}} \qquad (4)$$

The factor "2" arise because there are two X end-groups per X-X interaction.

The ratio of the number of "head-head + tail-tail" interactions to the number of "head-tail" interactions is:

$$\frac{\text{number of head-head + number of tail-tail}}{\text{number of head-tail}} = \frac{N_{X\text{-}X} + N_{Y\text{-}Y}}{N_{X\text{-}Y}} \qquad (5)$$

Considering (3) we therefore have:

$$\frac{\text{number of head-head + number of tail-tail}}{\text{number of head-tail}} = \frac{2N_{X\text{-}X}}{N_{X\text{-}Y}} = \frac{A_{X\text{-}X}}{A_{X\text{-}Y}}$$

On the basis of the above discussion, it is obvious that because of the fundamental constraint that $N_{X\text{-}X} = N_{Y\text{-}Y}$, studies of these inclusion compounds allow us to compare the relative preference of two X-Y interactions versus one X...X interaction plus one Y...Y interaction; from such information we cannot gain any insight into the relative preferences for X-X versus X-Y interactions (or Y-Y versus X-Y interactions).

In section 4.4 we develop a theoretical model which allows these preferences to be determined using measurement on inclusion compounds containing two types of guest molecule.

4.2 Experimental Considerations

Quantitative measurements of the areas under the peaks in the NMR spectra require that the experiments are performed under reliable quantitative conditions. Specifically, in cross polarisation experiments, it must be proven that the *relative* intensities of the signals due to different end-group interactions (for a given end-group) do not change as a function of cross polarization contact time (in spite of changes in the absolute intensities of the individual signals).

Table 4.1 shows the results of variable contact time cross polarisation experiments on 1-bromononane/urea. The results of these experiments clearly confirm that the relative areas of the signals due to $CH_3...CH_3$ and $CH_3...BrCH_2$, do not change appreciably as a function of contact time and therefore quantitative measurements of the areas under these NMR resonances obtained by the cross polarisation technique can provide the required information. Moreover, the relative intensities of the signals associated with different end-group interactions in spectra recorded using the "single pulse technique" is comparable to the results obtained in cross polarisation experiments, indicating that these two techniques are equally adequate for quantifying the relative amounts of the different end-group interactions.

Areas under the appropriate signals of the spectra of 1-haloalkane/urea inclusion compounds were measured *via* lineshape

Table 4.1: Relative intensities of the CH_3 signals of 1-iodoheptane/urea as a function of cross polarization contact time.

Contact Time	Relative Intensities of CH_3 Signals
0.1 ms	1.72
0.5 ms	1.66
1.0 ms	1.64
2.0 ms	1.67
3.0 ms	1.64
4.0 ms	1.67
7.0 ms	1.65
8.0 ms	1.58

fitting in an iterative fashion, using the LINESIM program. Fig. 4.1 shows a typical fit between simulated and experimental spectra.

4.3 Results and Discussion

Table 4.2 summarises the results obtained from the spectra of 1-iodoalkane/urea inclusion compounds for CH_3 and CH_2I carbon signals. In these compounds, a strong preference is observed for $CH_3...CH_3$ plus $CH_2I...CH_2I$ interactions versus two $CH_2I...CH_3$ interactions. The relative preferences of these interactions are nearly the same for all 1-iodoalkane/urea inclusion compounds investigated, except for 1-iodohexane/urea which exhibits a relatively higher preference for $CH_2I...CH_3$ interaction in comparison with the other 1-iodoalkane/urea inclusion compounds. It is noteworthy that the CH_2I

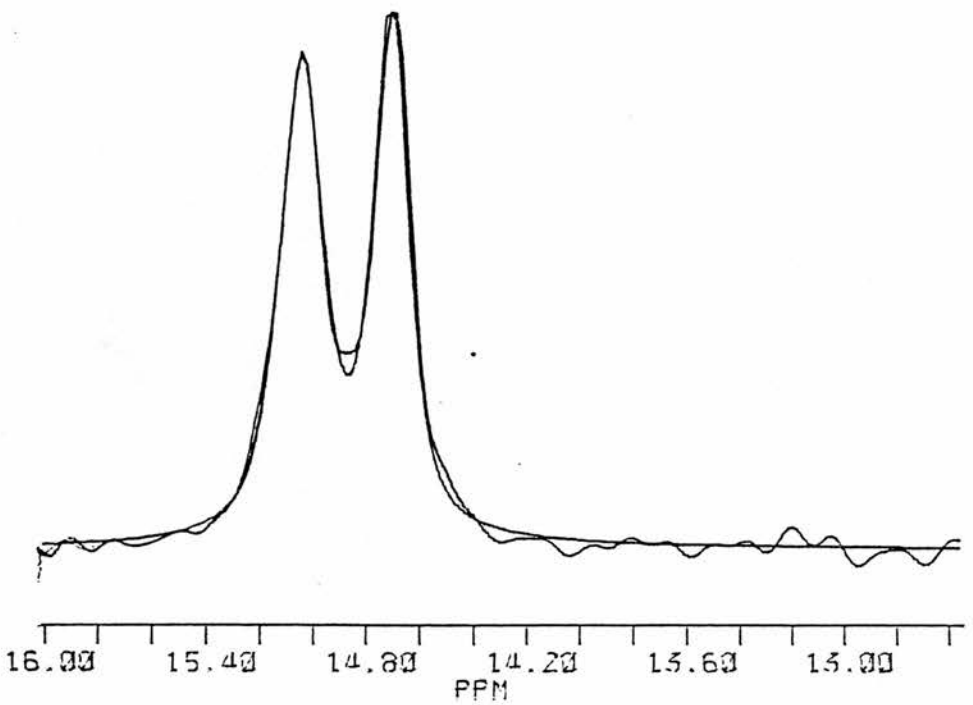

Fig. 4.1 Solid state ^{13}C NMR and the simulated signals for CH_3 carbon of 1-bromoundecane/urea inclusion compound.

signals contain the same information as the CH_3 signals, therefore the relative areas of the CH_2I signals, in principle, must be equal to the relative areas for the corresponding CH_3 signals (however, the total area of the CH_2I signals need not necessarily be equal to the total area of the CH_3 signals as a consequence of different cross polarization efficiencies for the CH_3 and CH_2I carbons). The results presented in Table 4.2 confirm this assumption.

1-fluoroalkane/urea inclusion compounds exhibit similar spectral characteristics to the 1-iodoalkane/urea inclusion compounds. Table 4.3 reports the results of lineshape fitting for the CH_3 and CH_2F signals for these compounds. For all 1-fluoroalkane/urea inclusion

compounds studied, there is a strong preference for $CH_3...CH_3$ plus $CH_2F...FCH_2$ interactions versus two $CH_3...FCH_2$ interactions.

Table 4.2 Relative areas of signals associated with CH_3 and CH_2I carbons of 1-iodoalkanes ($CH_3(CH_2)_{n-1}I$; n=6-12) in urea inclusion compounds[a].

n	CH_3 Carbon Signals		CH_2I Carbon Signals	
	$CH_3...CH_3$	$CH_3...CH_2I$	$CH_2I...CH_3$	$CH_2I...CH_2I$
6	53.8	46.2	44.8	55.2
7	60.5	39.5	40.2	59.8
8	58.3	41.7	43.3	56.7
9	60.5	39.5	39.4	60.6
10	58.6	41.4	39.5	60.5
11	60.2	39.8	41.6	58.4
12	59.1	40.9	40.3	59.7

[a] Areas of the signals have been estimated using the iterative program Linesim.

Table 4.3 Relative areas of signals associated with CH_3 and CH_2F carbons of 1-fluoroalkanes ($CH_3(CH_2)_{n-1}F$; n=6,9,13) in urea inclusion compounds[a].

n	CH_3 Carbon Signals		CH_2F Carbon Signals	
	$CH_3...CH_3$	$CH_3...CH_2F$	$CH_2F...CH_3$	$CH_2F...CH_2F$
6	59.9	40.1	37.4	62.6
9	60.8	39.2	36.4	63.6
13	62.1	37.9	36.1	63.9

[a] Areas of the signals have been estimated using the iterative program Linesim.

The results of lineshape fitting for the CH_2Cl signals of 1-chloroalkane/urea inclusion compounds are presented in Table 4.4. These results show that the relative preference for $CH_3...CH_3$ plus $CH_2Cl...ClCH_2$ interactions versus two $CH_3...ClCH_2$ interactions is nearly equal. Furthermore, the variation of these ratios is not significantly different in different 1-chloroalkane/urea inclusion. compounds, suggesting that chain length does not affect this distribution strongly.

The results of lineshape fitting for the CH_3 signals of the spectra for 1-bromoalkane/urea inclusion compounds is presented in Table 4.5. The relative population of two $CH_3...BrCH_2$ versus $CH_3...CH_3$ plus $CH_2Br...BrCH_2$ end-group interactions is also nearly equal, and this distribution is essentially constant for different 1-bromoalkanes.

4.4 A Markov Chain Model for Intermolecular Guest-Guest Interactions in One-dimensional Inclusion Compounds

4.4.1 Introduction

The simple mathematical analysis in section 4.1 demonstrated a fundamental constraint for the inclusion compounds containing unsymmetric guest molecules of the type $X(CH_2)_nY$ (such as 1-haloalkanes); specifically, for such compounds,
$N_{X-X} = N_{Y-Y}$. Therefore it is not possible using measurements from NMR spectra of these inclusion compounds to separate the relative probabilities of X-X and Y-Y interactions.

We now attempt to separate these relative probabilities and derive separate values for the X-X and Y-Y interactions. The motivation underlying our effort is that these probabilities are intrinsically related to the different energetics of these interactions, and

Table 4.4 Relative areas of signals associated with CH_2Cl carbons of 1-chloroalkanes ($CH_3(CH_2)_{n-1}Cl$; n=7-12) in urea inclusion compounds[a].

n	$CH_2Cl...CH_3$	$CH_2Cl...CH_2Cl$
7	49.0	51.0
8	51.2	48.8
9	49.2	50.8
10	48.3	51.7
11	44.5	55.5
12	47.2	52.8

[a] Areas of the signals have been estimated using the iterative program Linesim.

Table 4.5 Relative areas of signals associated with CH_3 carbons of 1-bromoalkanes ($CH_3(CH_2)_{n-1}Br$; n=6-13) in urea inclusion compounds[a].

n	$CH_3...CH_3$	$CH_3...CH_2Br$
6	50.6	50.4
7	51.0	49.0
8	48.7	51.3
9	48.6	51.4
10	48.5	51.5
11	48.3	51.7
12	48.4	51.6
13	47.5	52.5

[a] Areas of the signals have been estimated using the iterative program Linesim.

a knowledge of the relative energies of such interactions is an issue of tremendous importance in the field of crystal engineering.

Here we present a statistical analysis which clearly shows that it is indeed possible to separate the intrinsic probabilities of X-X and Y-Y interactions, provided measurements are performed on inclusion compounds containing **two** different guest molecules (e.g. $X(CH_2)_nY$ and $X(CH_2)_nX$). Synthesis of these inclusion compounds is straightforward and we can prepare inclusion compounds containing different ratios of the guest molecules. The ratio of the different guest molecules in the inclusion compound can be determined independently of the NMR measurements, using microanalysis.

4.4.2 Basic Definitions Utilised in the Model.

Consider a one-dimensional inclusion compound containing guest molecules of the types $X(CH_2)_nY$ and $X(CH_2)_nX$. We aim to construct a Markov chain model for such a system. In order to set up a standard notation, consider first the more general case in which the guest molecules are of the types XX, XY, YX and YY (with XY and YX denoting different orientations of the guest molecule). The proportions of XX, XY, YX and YY molecules are denoted m_{XX}, m_{XY}, m_{YX} and m_{YY}. The proportions of X-X, X-Y, Y-X and Y-Y interactions are denoted $r_{X\text{-}X}$, $r_{X\text{-}Y}$, $r_{Y\text{-}X}$ and $r_{Y\text{-}Y}$. Therefore we have:

$$m_{XX} + (m_{XY} + m_{YX}) + m_{YY} = 1 \qquad (6)$$

and

$$r_{X\text{-}X} + (r_{X\text{-}Y} + r_{Y\text{-}X}) + r_{Y\text{-}Y} = 1 \qquad (7)$$

The proportion of the different types of end-group interaction r_{X-X}, ($r_{X-Y} + r_{Y-X}$) and r_{Y-Y} cannot be measured directly but *via* parameters c_X and c_Y defined as:

$$c_X = \frac{r_{X-X}}{r_{X-Y}+r_{Y-X}} \qquad c_Y = \frac{r_{Y-Y}}{r_{X-Y} + r_{Y-X}}$$

Measurements of the NMR spectra yield the values of c_X and c_Y (sometimes only c_X or c_Y but sometimes both c_X and c_Y. for each compound). The values of m_{XX}, ($m_{XY}+m_{YX}$) and m_{YY} are determined via microanalysis.

4.4.3 The Markov Chain Model

Random processes evolve through the time in a manner that is not completely predictable. By imposing certain simplifying assumptions, it is possible to handle mathematically such processes relatively easily. A subset of all random processes, in which certain conditions are imposed, are called Markov processes. The basic methodology was developed initially by the Russian mathematician A. A. Markov, around the beginning of the 20th century [4-6]. A Markov chain is a sequence of random events in which the outcome of any particular event depends on the outcome of the immediately preceding event (but is independent of the outcome of any event earlier than this).

The physical state of guest molecules in the urea tunnel structure resembles a Markov chain, since, to a good approximation the orientation of each guest molecules is only influenced only by its nearest neighbours and not by any other guest molecule in the tunnel structure (the incommensurate nature of the structure effectively eliminates the influence of the host structure on the guest orientation).

Here we apply a Markov chain model to describe the state of guest molecules in one-dimensional inclusion compounds. In this model, it is assumed that guest molecules are inserted successively into the tunnel from one side (for instance from the right hand side). Therefore the first inserted molecule is located at the left end of the tunnel. For constructing the model, the following assumption is made;

I. The probability of the n^{th} guest molecule (entering the tunnel) being of a given type and orientation depends on the guest molecules already in the tunnel only through the type and orientation of the $(n-1)^{th}$ guest molecule (already inside the tunnel).

II. The probabilities in **I.** depend only on (a) the abundance of available guests, (b) the interaction energy between the host structure and the n^{th} guest molecule, (c) the interaction energy between the right hand end-group of the $(n - 1)^{th}$ guest molecule and the left hand end-group of the n^{th} guest molecule

III. The host-guest interaction for XY molecules does not depend on the orientation of the XY molecule.

IV. The number of guest molecules in the tunnel is large.

V. Guest molecules in any tunnel are chosen and oriented independently of the guest molecules in other tunnels.

Based on assumption **I.**, the sequence of oriented guest molecules in a tunnel forms a homogeneous Markov chain. The Markov chain is determined by its probability transition matrix

$$\begin{bmatrix} P_{11} & P_{12} & P_{13} \\ P_{21} & P_{22} & P_{23} \\ P_{31} & P_{32} & P_{33} \end{bmatrix}$$

where p_{ij} (where i = 1, 2, 3 and j = 1, 2, 3) denotes the probability of an oriented molecule of type j being included immediately after an

oriented molecule of type i. In this work, the definitions of i and j in terms of the particular guest molecule orientations are; i=1: YX, i=2: XX, i=3: XY, j=1: YX, j=2: XX, j=3: XY. Note that these probabilities must satisfy the following equation for all i:

$$p_{i1}+p_{i2}+p_{i3} = 1 \qquad (8)$$

From assumptions **II.** and **III.** it follows that the probability transition matrix is of the form:

$$P = \begin{bmatrix} \frac{\kappa}{1+\kappa+\gamma} & \frac{\gamma}{1+\kappa+\gamma} & \frac{1}{1+\kappa+\gamma} \\ \frac{\kappa}{1+\kappa+\gamma} & \frac{\gamma}{1+\kappa+\gamma} & \frac{1}{1+\kappa+\gamma} \\ \frac{1}{1+\lambda(\gamma+1)} & \frac{\gamma\lambda}{1+\lambda(\gamma+1)} & \frac{\lambda}{1+\lambda(\gamma+1)} \end{bmatrix}$$

so that for example, if at any stage the last guest to be inserted into the tunnel is YX the probability of the next guest being XY is $1/(1+\kappa+\gamma)$. The only restrictions on κ, λ and γ are that they are positive. The interpretation of these parameters is considered in the next section.

4.4.4 Interpretation of Parameters

If host-guest interactions are negligible, the interpretation of the parameter γ is that $\gamma/(1+\gamma)$ and $1/(1+\gamma)$ represent the proportions of XX and XY molecules respectively among potential guest in the solution. The interpretation of the parameters κ and λ is that:

1- an incoming XY molecule arriving to find a free X end-group takes orientation X-Y with probability $1/(1+\kappa)$ and orientation Y-X (to form an X...Y orientation) with probability $\kappa/(1+\kappa)$;

---X X---Y	$1/(1+\kappa)$
---X Y---X	$\kappa/(1+\kappa)$

2- an incoming XY molecule arriving to find a free Y end-group takes orientation Y-X (to form a Y...Y interaction) with probability $1/(1+\lambda)$ and orientation X-Y (to form a Y...X interaction) with probability $\lambda/(1+\lambda)$;

---Y Y---X	$1/(1+\lambda)$
---Y X---Y	$\lambda/(1+\lambda)$

Consequently κ and λ are, respectively, the odds that an incoming XY molecule arriving to find a free X end-group forms an X...X interaction and the odds that an incoming XY molecule arriving to find a free Y end-group forms a Y...Y interaction.

Therefore the intrinsic parameters of interest in the Markov chain model presented above are κ and λ. These are the parameters that are related to guest-guest interaction energies, and represent the intrinsic interaction between end-groups. The usual experimental approach for obtaining these values is as follows: we take measurements of m and c on each of k samples in order to obtain the values $m_1, c_1, \ldots, m_k, c_k$. It is assumed that the parameters κ and λ are the same for each sample, whereas γ may vary between samples. The parameters κ and λ can then be estimated by applying standard results

on the properties of Markov chains together with considerable algebraic manipulation.

4.4.7 Results and Discussion

Based on the model presented above, if we aim to derive intrinsic information on functional group interactions, this requires measurements on inclusion compounds containing two types of guest molecule. Hence we prepared several inclusion compounds containing two guests and the ratio of different guests in these inclusion compounds were determined using microanalysis. Also the area under the relevant signals in the ^{13}C NMR spectra of these compounds were measured using the LINESIM program. The results of these measurements for different mixed 1-haloalkane/urea inclusion compounds are presented in Table 4.6.

The results presented in Table 4.6 provide the values of m and c (as defined in 4.4.2) for each particular compound. Utilising these values together with the values of m and c for inclusion compounds containing only one type of guest molecule (the concentration of the second type of guest molecule in these inclusion compounds is considered as 0), the parameters κ and λ have been derived for each class of compound[1].

Table 4.7 shows the intrinsic probabilities for $CH_3...CH_3$ (defined as $1/1+\kappa$) interaction in comparison with $CH_3...XCH_2$ (defined as $\kappa/1+\kappa$) interaction for different halogens. This result shows that in the 1-fluoroalkane/urea inclusion compounds, the relative probabilities of these two interactions are equal. In 1-chloroalkane/urea inclusion compounds, the $CH_3...ClCH_2$ interaction is preferred to the $CH_3...CH_3$

---

[1] The detail mathematical procedure for deriving these values has been done by Dr Peter E. Jupp of Mathematics department, University of St. Andrews. Here we only focus on the results of these calculations.

Table 4.6: The percentage of the guests and the relative areas under the appropriate signals for urea inclusion compounds containing two types of guest molecule.

Precentage of the two Guest Components[a]		Relative Areas Under the Signals for CH_2Cl Carbons[b]	
1-chlorooctane	decane	$CH_2Cl...CH_3$	$CH_2Cl...CH_2Cl$
84.6	15.4	52.6	47.4
57.4	42.6	60.6	39.4
26.2	73.8	87.8	12.2
		Relative Areas Under the Signals for CH_3 Carbons[b]	
1-bromoheptane	1,7-dibromoheptane	$CH_3...CH_3$	$CH_3...CH_2Br$
78.2	21.8	45.9	54.1
59.4	40.6	35.6	64.4
34.5	65.5	28.0	72.0
		Relative Areas Under the Signals for CH_3 Carbons[b]	
1-iodooctane	1,8-diiodooctane	$CH_3...CH_3$	$CH_3...CH_2I$
84.5	15.5	45.9	54.1
63.9	36.1	35.5	64.4
22.1	77.9	28.0	72.0
		Relative Areas Under the Signals for CH_2I Carbons[b]	
1-iodooctane	n-undecane	$CH_2I...CH_3$	$CH_2I...CH_2I$
78.1	23.9	52.3	47.7
52.6	47.4	67.5	32.5
38.3	61.7	80.5	19.5
		Relative Areas Under the Signals for CH_2F Carbons[b]	
1-fluorononane	n-decane	$CH_2F...CH_3$	$CH_2F...CH_2F$
28.4	71.6	60.4	39.6
43.7	56.3	55.1	44.8
54.0	46.0	51.5	48.5

[a]The percentage of the two guest components has been determined by microanalysis.

[b]The relative areas of the signals have been estimated using the iterative program Linesim.

Table 4.7: The intrinsic probability of $CH_3...CH_3$ interaction (defined as $1/1+\kappa$) and the intrinsic probability of $CH_3...XCH_2$ interaction (defined as $\kappa/1+\kappa$) for different halogens.

Interaction	κ	Intrinsic probabilities
$CH_3...CH_3$ $CH_3...FCH_2$	0.98	0.50 0.50
$CH_3...CH_3$ $CH_3...ClCH_2$	1.65	0.38 0.62
$CH_3...CH_3$ $CH_3...BrCH_3$	0.23	0.81 0.19
$CH_3...CH_3$ $CH_3...ICH_2$	1.22	0.55 0.45

interaction, although this preference is not strong. In 1-bromoalkane/urea inclusion compounds, there is a strong preference for the $CH_3...CH_3$ interaction over the $CH_3...BrCH_2$ interaction. This behaviour is contrary to the expectation that a trend may exist in the behaviour of the series of halogens. For 1-iodoalkane/urea inclusion compounds the $CH_3...CH_3$ interaction is slightly preferred in comparison with $CH_3...ICH_2$ interaction.

Table 4.8 presents the intrinsic probabilities of $CH_2X...XCH_2$ (defined as $1/1+\lambda$) and $CH_3...XCH_2$ (defined as $\lambda/1+\lambda$) interactions. In the case of 1-bromoalkane/urea inclusion compounds, the $CH_2Br...CH_3$ interaction is preferred to the $CH_2Br...BrCH_2$ interaction. Here also 1-bromoalkanes exhibit different behaviour in comparison to the other 1-

Table 4.8: The intrinsic probability of $CH_2X...XCH_2$ interaction (defined as $1/1+\lambda$) and the intrinsic probability of $CH_3...XCH_2$ interaction (defined as $\lambda/1+\lambda$) for different halogens.

Interaction	λ	Intrinsic Probabilities
$CH_2F...FCH_2$ $CH_2F...CH_3$	0.22	0.82 0.18
$CH_2Cl...ClCH_2$ $CH_2Cl...CH_3$	0.38	0.73 0.27
$CH_2Br...BrCH_2$ $CH_2Br...CH_3$	1.82	0.35 0.65
$CH_2I...ICH_2$ $CH_2I...CH_3$	0.15	0.87 0.13

haloalkanes. In 1-iodoalkane/urea inclusion compounds we encounter the strongest preference for $CH_2X...XCH_2$ interaction versus $CH_3...XCH_2$ interaction (0.87 compared with 0.13).

The exceptional behaviour for 1-bromoalkane/urea inclusion compounds is interesting and undoubtedly warrants further investigation. Similar solid-state NMR investigations of other inclusion systems containing 1-bromoalkanes, and comparing the results obtained with the results for 1-bromoalkane/urea inclusion compounds, will clearly give more insight regarding this issue.

References:

[1] Desiraju, G. R. "Crystal engineering: the design of organic solids", Elsevier, Amsterdam, 1989.

[2] Takemoto, K.; Soneda, N. in "Inclusion Compounds", (Ed. Atwood, J. L.; Davies, J. E. D.; MacNicol, D. D. Vol. 2, Academic Press, 1984., p. 47.

[3] Harris, K. D. M.; Thomas, J. M. *J. Chem. Soc., Faraday Trans.* 1990, **86**, 2985.

[4] Dynkin, E. B. "Theory of Markov processes", New York, Pergamon, 1960.

[5] Isaacson, D. L.; Madsen, R. W. "Markov chains, Theory and applications", New York-London, Wiley, 1976.

[6] Daniel, R. D. "Markov Chains", Amsterdam-New York, North-Holland, 1984.

CHAPTER V

STUDY OF DIFFUSION OF GUEST MOLECULES INTO THE TUNNEL STRUCTURE OF UREA INCLUSION COMPOUNDS

Introduction

Current interest in the science of crystalline organic inclusion compounds (typified by urea and thiourea inclusion compounds) originates mainly from their representation, in many respects, as structural analogues of microporous inorganic solids, such as zeolites and aluminophosphates.

As discussed in chapter II, in the absence of suitable guest molecules, urea crystallises in a tetragonal structure which differs substantially from the host structure in urea inclusion compounds and, in particular, does not contain "empty" tunnels [1]. Also, it has been shown that the empty tunnel structure of urea is unstable with respect to recrystallization as the "pure" crystal form of urea [2,3].

In topologically similar zeolitic systems such as theta-1, mordenite and zeolite-L, which possess one-dimensional tunnel structures, empty zeolites can exist as stable structures and guest molecules can therefore readily diffuse into and out of the zeolite host framework [4]. In fact many applications of zeolitic materials originate from this particular property. Here we present the first conclusive evidence which proves that in spite of the instability of the empty urea host structure, it is possible to carry out an exchange of the guest molecules in a urea inclusion compound without destroying the host framework in the course of this process. The system that has been

investigated is the exchange of 1,8-dichlorooctane and n-decane in their urea inclusion compounds.

5.1 Evidence for Diffusion of Molecules into the Tunnel Structure of Urea Inclusion Compounds

5.1.1 Experimental

The 1,8-dichlorooctane/urea and n-decane/urea inclusion compounds used in our study were prepared by the method described in chapter III. Single crystals of 1,8-dichlorooctane/urea (0.4 g) were immersed in liquid n-decane (10 g) in a closed bottle and left at room temperature (24 ± 2 °C) for seven days (sample I). After this period, the crystals were collected by filtration and then washed with 2,2,4-trimethylpentane to remove any molecules adsorbed on their external surfaces. These crystals were then dried in air. The high-resolution solid-state ^{13}C NMR spectrum of this sample is shown in Fig. 5.1.c.

5.1.2 Results and Discussion

Fig. 5.1 shows the ^{13}C NMR spectra of 1,8-dichlorooctane/urea, decane/urea and sample I. The spectrum of sample I indicates the existence of n-decane in the solid phase *in addition to* 1,8-dichlorooctane. We attribute the existence of n-decane in this sample to the migration of the n-decane molecules from the liquid phase into the tunnel structure of the inclusion compound. In this proposed mechanism, it is assumed that the tunnel structure of the urea inclusion compound is maintained while the guest species are diffusing into and out of the material.

It might be argued that the presence of n-decane/urea in the solid phase (sample I) could arise from alternative mechanisms. These alternative mechanisms could be for instance, partial dissolution of the

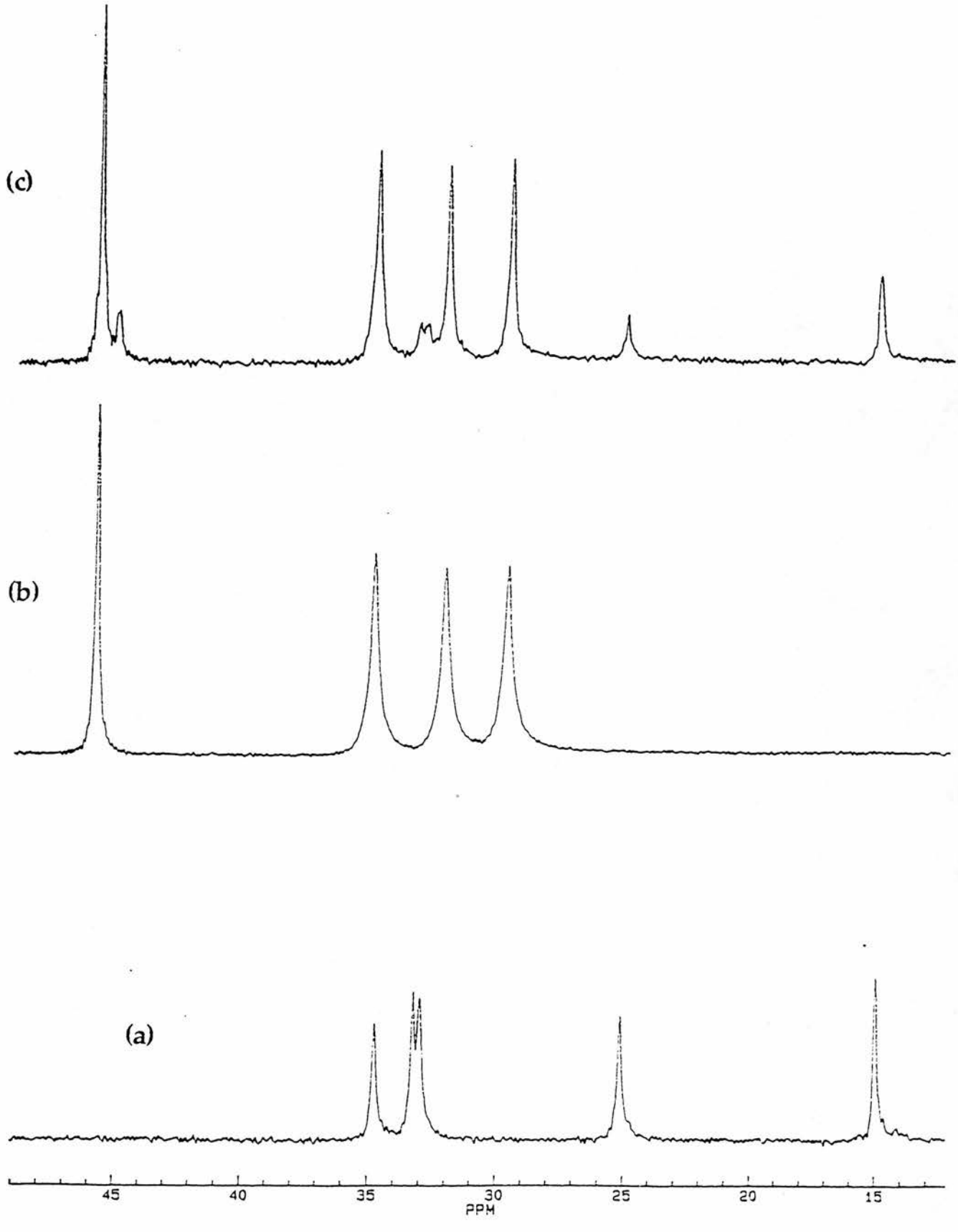

Fig. 5.1 Solid state ^{13}C NMR spectra of (a) decane/urea (b) 1,8-dichlorooctane/urea (c) sample I.

1,8-dichlorooctane/urea inclusion compound followed by recrystallization of the dissolved urea to form the decane/urea inclusion compound, or surface adsorption of n-decane on the crystals of 1,8-dichlorooctane/urea. In the following section we present evidence which eliminates these alternative explanations for this observation.

Finally we note that in the spectrum of sample I there are *two* peaks at 45.2 and 45.7 ppm due to the CH_2Cl carbon, whereas in the spectrum of 1,8-dichlorooctane/urea (Fig. 5.1.b) there is only *one* peak at 45.7 ppm due to the CH_2Cl carbon. In section 5.2.2 we describe how this spectral feature can provide evidence for the exchange mechanism.

5.2 Assigning the Exchange Mechanism from the Experimental Results

5.2.1 Introduction

In this section we adopt two approaches in order to verify the proposed exchange mechanism. While these approaches differ substantially in nature, they provide complementary and consistent results. We therefore believe that the results of these investigations, in principle, eliminate other possible conceivable mechanisms that could explain the observations described above.

5.2.2 Optical Microscopic Investigation on Single Crystals

5.2.2.a Introduction

While optical microscopy by itself cannot probe details at the atomic level (due to its low resolution), it can nevertheless indicate significant changes in the integrity of individual single crystals [5]. For example the collapse of an organic host (urea or thiourea), upon removing

guest molecules, is readily observed even by low-power optical microscopy. The morphology of single crystals of thiourea or urea inclusion compounds is distinctly different from that of pure crystalline thiourea or urea. The decomposition of unstable inclusion compounds like the n-octane/urea inclusion compound can be observed easily by optical microscopy.

The aim of exploiting optical microscopy here is to detect any significant changes in the morphology of single crystals of urea inclusion compounds immersed in an external liquid phase. If the prime reason for observing species from the external liquid phase within the solid is the diffusion of these molecules into the tunnel structure of the urea inclusion compound, it is required that the integrity of these single crystals is maintained while they are immersed within the liquid phase. Thus, during the period for which single crystals are immersed in the liquid phase, there should (if the exchange mechanism occurs) be no change in the external morphology of these single crystals.

In contrast, considerable changes in the morphology of the single crystals are expected if other mechanisms like partial dissolution or recrystallisation are primarily involved, since these mechanisms will lead to the collapse of the host structure of the urea inclusion compound.

An optical microscopic investigation can therefore provide evidence (although not conclusive) to support the proposed exchange mechanism. In order to compare and contrast the experimental results, optical microscopic investigations of both *pure* urea single crystals and urea inclusion compound single crystals in external liquid phases have been carried out.

5.2.2.b Experimental

High quality single crystals of pure urea (i.e. crystals which possess well-defined tetragonal morphology and extinguish polarised light uniformly) were chosen and immersed in 10 g of pure liquid n-decane at room temperature in a closed sample bottle. The morphology and surface structure of these single crystals were examined using optical microscopy within the period of one week. Two photographs were taken for this sample. One photograph was taken immediately after immersion and the other photograph was taken after one week.

High quality single crystals of 1,8-dichlorooctane/urea (i.e. crystals with well-defined hexagonal morphology) were chosen and immersed in 10 g of liquid n-decane in a closed sample bottle. The sample bottle was left undisturbed for a period of one month at room temperature (24 ± 2 °C). The morphology and surface structure of these single crystals were examined regularly and carefully by optical microscopy within this period. Two photographs of these single crystals were taken ; one immediately after immersion into the liquid phase, and the other at the end of the observation period.

5.2.2.c Results and Discussion

Fig. 5.2.a shows the photograph of urea single crystals immediately after immersion into the liquid n-decane. The external surfaces of this crystal are transparent and the characteristic morphology of pure urea crystals is readily recognised. Fig. 5.2.b shows the photograph of these single crystals in n-decane after one week. The external surface of this crystal has entirely been covered by polycrystalline material. Moreover, this "crystal" extinguishes polarised light in all orientations. Powder X-ray diffraction on this material shows the existence of urea inclusion compound in addition to the pure urea phase.

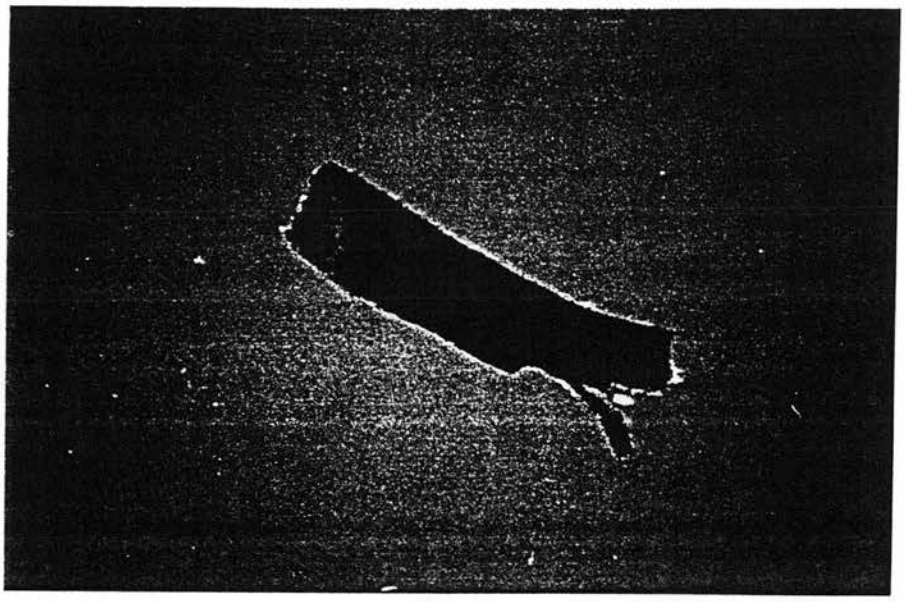

(b)

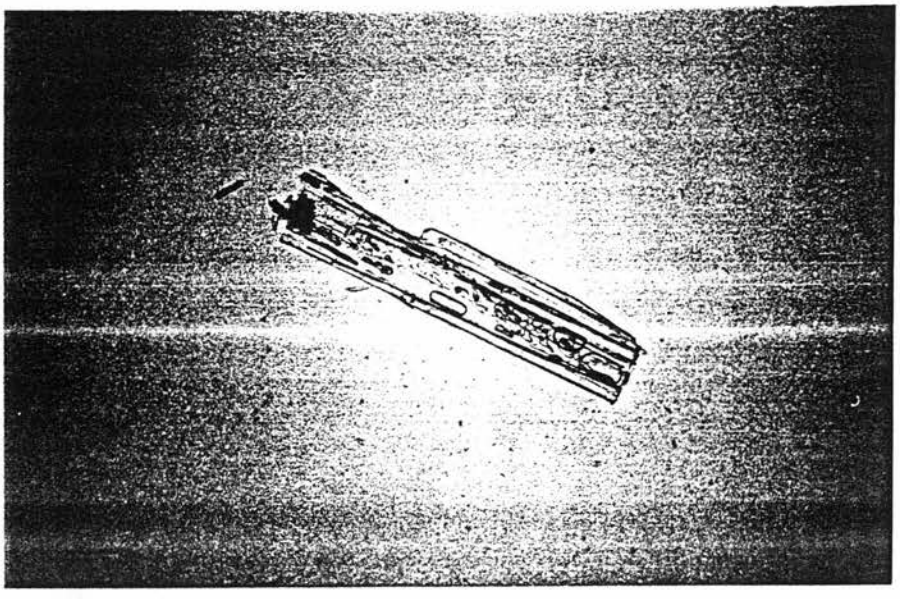

(a)

Fig. 5.2 The photographs of (a) the urea single crystals immediately after immersion into the liquid n-decane (b) the same sample after one week.

This observation can be explained by proposing that the tetragonal structure of urea is not stable in the presence of appropriate guest species (such as n-decane); contact between urea crystals and the guest species will lead to recrystallisation of the tetragonal structure of urea as the hexagonal structure of the urea inclusion compound. The instability of urea single crystals in liquid n-decane, and the formation of a polycrystalline material (decane/urea inclusion compound), is the concomitant result of this fact. Clearly in this system recrystallization and/or partial dissolution are the major mechanisms for the formation of the inclusion compounds.

In conclusion, the loss of single crystal integrity (and the formation of polycrystalline material) is the macroscopic indication of this recrystallisation. Nevertheless, the main reason of performing this experiment here was to demonstrate the feasibility of optical microscopy to investigate this issue.

Fig. 5.3.a illustrates a photograph of 1,8-dichlorooctane/urea single crystals immediately after immersion into liquid n-decane. A photograph of the same sample after one month is shown in Fig. 5.3.b. Comparison of these two photographs shows no detectable changes in the external morphology of these single crystals. The solid state ^{13}C NMR spectrum of this sample indicates the existence of n-decane in the solid phase. Therefore we can conclude (based on the previous discussion) that the tunnel structure of the urea inclusion compound is maintained during immersion of the urea inclusion compound crystals in the liquid n-decane, and the existence of n-decane in the solid phase is related to the diffusion of these molecules into the tunnel structure.

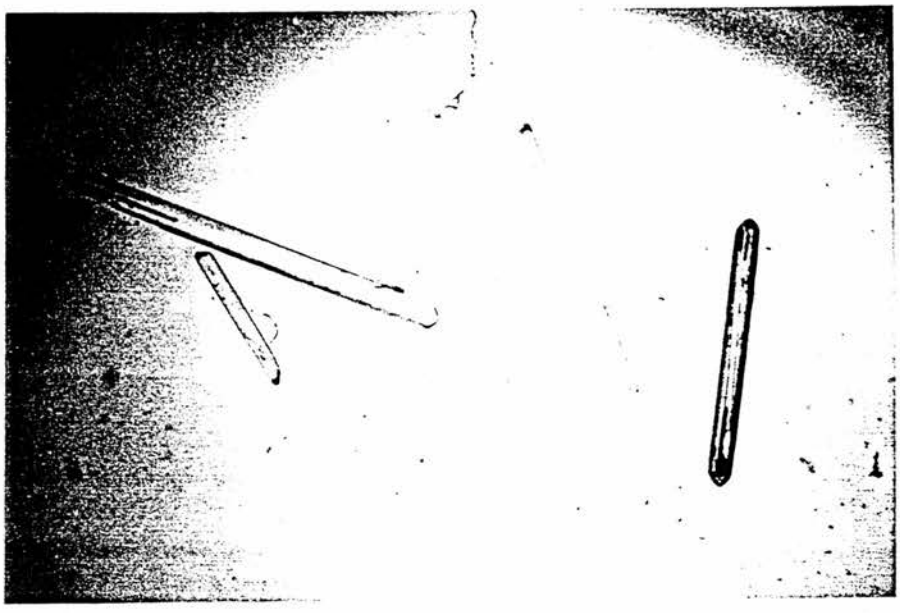

(b)

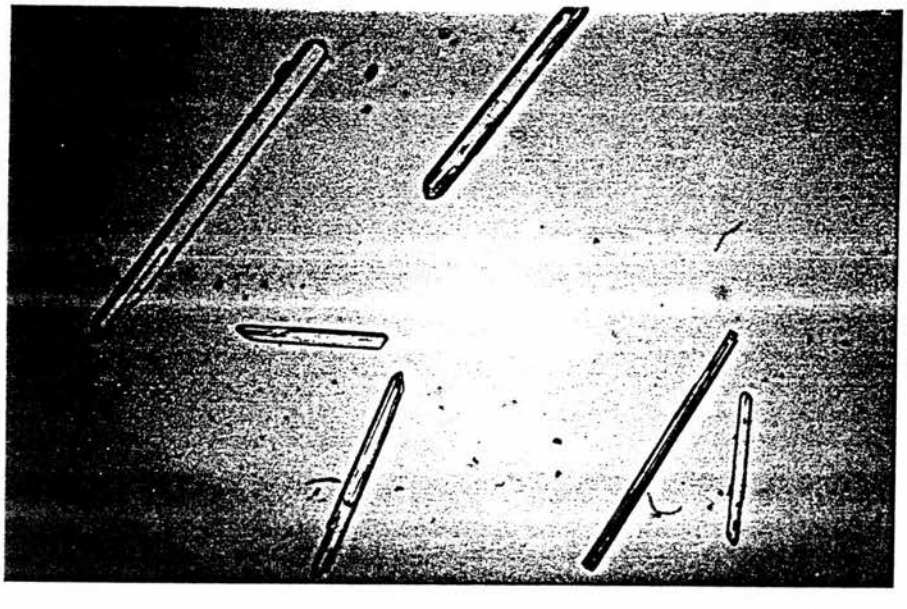

(a)

Fig. 5.3 The photographs of (a) the 1,8-dichlorooctane/urea single crystals immediately after immersion into pure liquid n-decane (b) the same sample after one month.

5.2.3 Solid State ^{13}C NMR Evidence

We recall that in the solid state ^{13}C NMR spectrum of sample I, two signals in 45.2 and 45.7 ppm are observed for the CH_2Cl carbon atom. The intensity of the peak at 45.2 ppm is much smaller than the peak at 45.7 ppm. In contrast, in the spectrum of 1,8-dichlorooctane/urea there is only *one* signal for the CH_2Cl carbon, at 45.7 ppm.

In chapter III we demonstrated that in ^{13}C NMR spectra of 1-chloroalkane/urea inclusion compounds, two signals exist for CH_2Cl carbon atoms. The presence of two signals was explained by the existence of two intermolecular environments for the CH_2Cl end-group; specifically, $CH_2Cl...CH_2Cl$ and $CH_2Cl...CH_3$. The chemical shifts of these two signals were 45.3 ± 0.4 ppm and 45.5 ± 0.3 ppm depending on the chain length of the guest molecule, and the relative intensities of these signals are proportional to the relative numbers of end-groups involved in each of these two interactions. The signal at 45.7 ppm was assigned to the $CH_2Cl...CH_2Cl$ interaction and the signal at lower chemical shift was assigned to the $CH_2Cl...CH_3$ interaction.

The occurrence of two signals for the CH_2Cl carbon atoms in sample I indicates that two intermolecular environments *must* exist for the CH_2Cl carbon atoms. The chemical shifts for these two signals suggest that these intermolecular environments are $CH_2Cl...CH_2Cl$ and $CH_2Cl...CH_3$. The only possible explanation for the existence of the methyl group in this inclusion compound is that n-decane guest molecule are present. Therefore, these results suggest that there are n-decane molecules in the vicinity of 1,8-dichlorooctane molecules within the urea tunnel structure.

If partial dissolution of urea followed by recrystallization were the mechanism for this observation, it is probable that this process would produce the n-decane/urea compound, and the NMR spectrum

of sample I should then simply be the spectrum of a physical mixture of 1,8 dichlorooctane/urea and n-decane/urea. In such a case essentially no n-decane molecules would be located in the same tunnels as 1,8-dichlorooctane molecules.

Also it is obvious that surface adsorption of n-decane molecules would not lead to the accommodation of n-decane molecules in the vicinity of 1,8-dichlorooctane molecules. In addition, washing the collected materials with 2,2,4-trimethylpentane will ensure that the amount of surface-adsorbed n-decane on the materials used in the NMR experiments is negligible.

Therefore these alternative mechanisms do not lead to the accommodation of n-decane molecules in the vicinity of 1,8-dichlorooctane molecules. However, the exchange mechanism is completely consistent with the accommodation of n-decane molecules in the vicinity of 1,8-dichlorooctane molecules. The diffusion of the n-decane molecules from the external liquid phase leads to the accommodation of n-decane molecules within the same tunnels as 1,8-dichlorooctane molecules are located, which clearly generates two types of intermolecular environment for the CH_2Cl carbon.

5.3 Time Dependence and Particle Size Dependence of the Exchange Process

5.3.1 Introduction

The amount of exchange in the system comprising a urea inclusion compound immersed in the liquid phase of a potential guest species may be influenced by changing several factors. These may include, for instance, particle size, time, agitation or temperature. For example, if the sample is kept at higher temperature, a greater extent of exchange may be expected to occur within the system. Here we only focus on two

factors; time and particle size, and discuss the experimental results in detail.

5.3.2 Experimental

EXPERIMENT A: crystals of 1,8-dichlorooctane/urea were ground into fine particles (sample II) and very fine particles (sample III) and then immersed in 10 g of liquid n-decane in two separate closed bottles and left at room temperature for seven days. After this period, the solid materials were collected, washed with 2,2,4-trimethylpentane and dried. Solid-state ^{13}C NMR spectra of these samples are presented in Fig. 5.4

EXPERIMENT B: crystals of 1,8-dichlorooctane/urea were ground thoroughly and divided in four equal portions. Each portion (0.4 g) was then immersed in 10 g of liquid n-decane in a closed sample bottle and left for one day (sample IV), five days (sample V), fifteen days (sample VI), and 30 days (sample VII) respectively. After each period of time, the solid materials were collected, washed with 2,2,4-trimethylpentane and dried. Solid-state ^{13}C NMR spectra of these samples are presented in Fig. 5.5.

5.3.3 Results and discussion

^{13}C NMR spectra of sample I (single crystals), sample II (fine particles) and sample III (very fine particles) are shown in Fig. 5.4. It is apparent that the amount of n-decane in the solid phase is directly related to the size of the particles. This observation is consistent with the exchange process discussed above. For small particles there are more ends of tunnels facilitating migration of molecules from the external liquid phase into the tunnels. The amount of exchange is directly related to the number of ends of tunnels available for the new guest molecules to

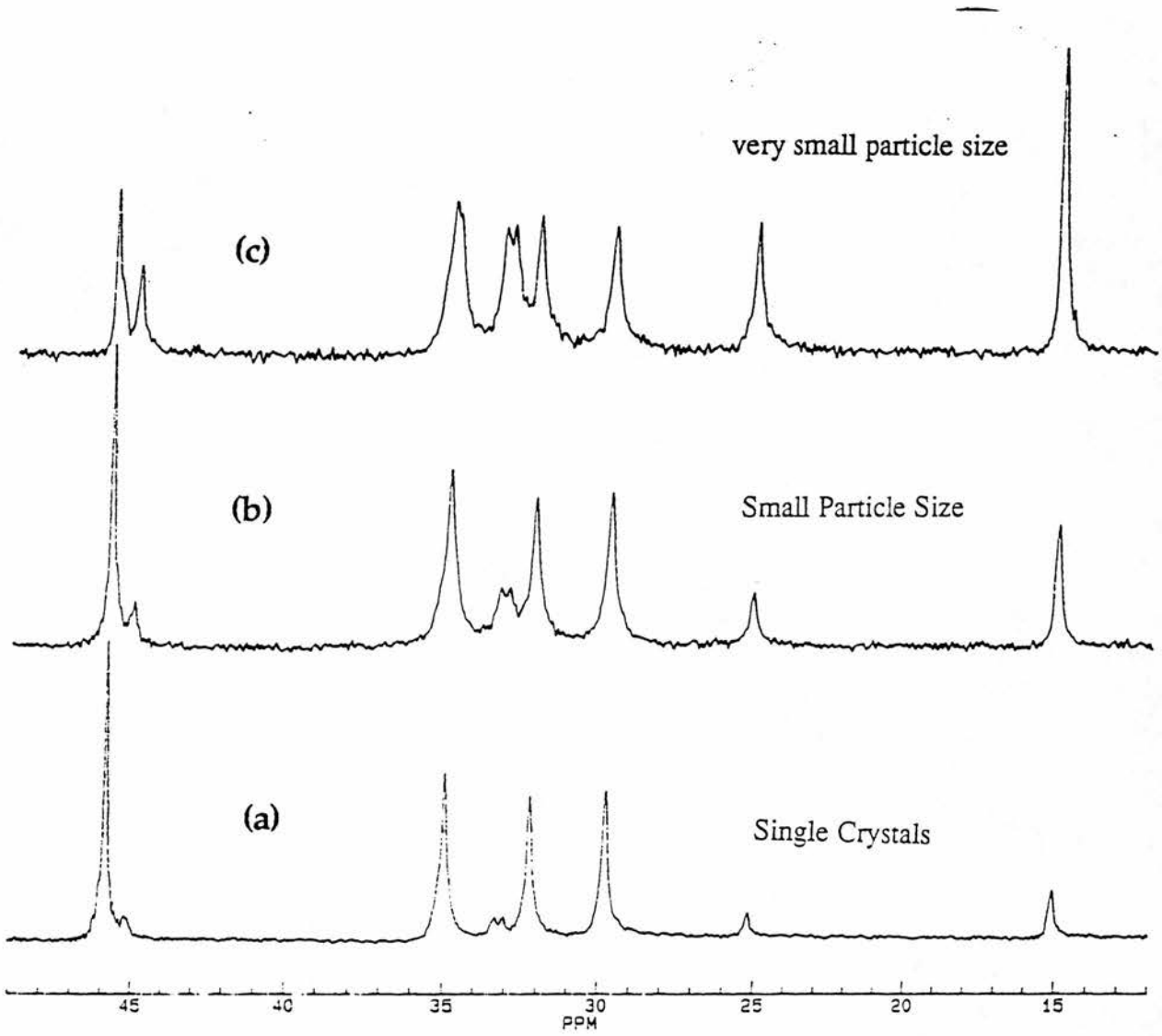

Fig. 5.4 Solid state ^{13}C NMR spectra of (a) single crystals of 1,8-dichlorooctane/urea immersed in liquid n-decane (b) sample II (c) sample III.

enter. When the particle size becomes smaller, more "ends" are produced and, therefore, more diffusion of molecules from the external liquid phase into the inclusion compound occurs.

An interesting and informative feature in the spectra of these compounds concerns the relative intensities of the CH_2Cl carbon signals. In these spectra the intensity of the signal due to the $CH_2Cl...CH_3$ interaction increases relative to the intensity of the signal due to the $CH_2Cl...CH_2Cl$ interaction . This feature can be explained by the fact that, in the course of the exchange process, the ratio $N_{(CH_3...CH_2Cl)}$ / $N_{(CH_2Cl...CH_2Cl)}$, where N denotes the number of a particular type of end-group interaction, is continually increasing and the relative intensities of the corresponding signals change accordingly.

This provides further evidence in support of the exchange mechanism. If other mechanisms were responsible for the existence of the n-decane in the solid phase, the observed variation in the relative intensities of these two peaks would not be expected.

Fig. 5.5 shows the spectra of samples IV, V, VI and VII. In these samples, the amount of n-decane within the solid phase increases as a function of time. This increase is not a linear function of time; exchange is faster at the start of the experiment and becomes slower at the end of the experiment (Fig. 5.6).

The relative intensities of the signals due to the CH_2Cl carbon in these samples behave in a similar manner to the spectra of the samples in experiment A; i.e., as the amount of n-decane in the inclusion compound increases, the intensity of the signal due to the $CH_2Cl...CH_3$ interaction increases relative to the signal due to the $CH_2Cl...CH_2Cl$ interaction. This feature is consistent with the occurrence of the exchange mechanism as outlined above.

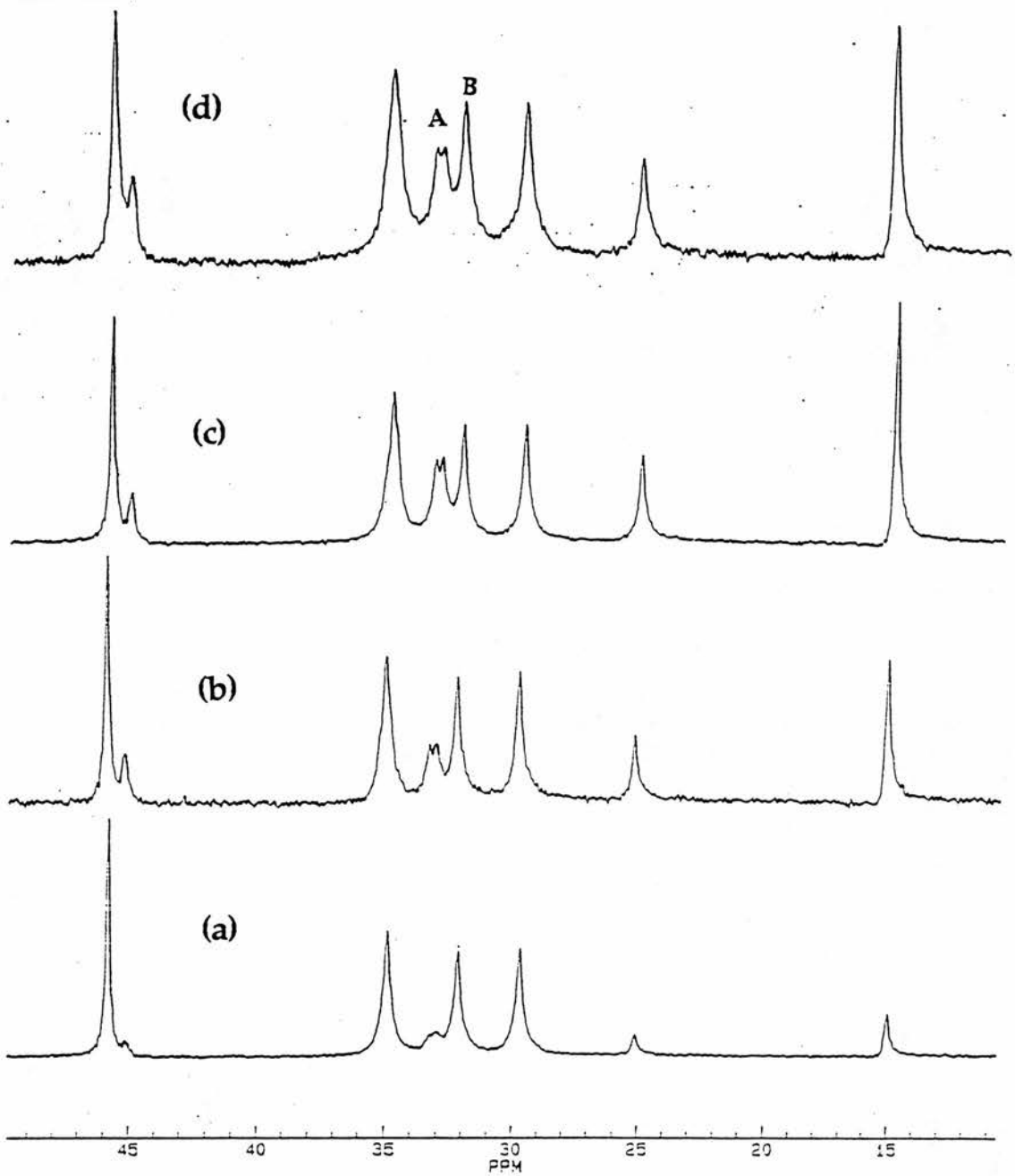

Fig. 5.5 Solid state ^{13}C NMR spectra of (a) sample IV (b) sample V (c) sample VI (d) sample VII.

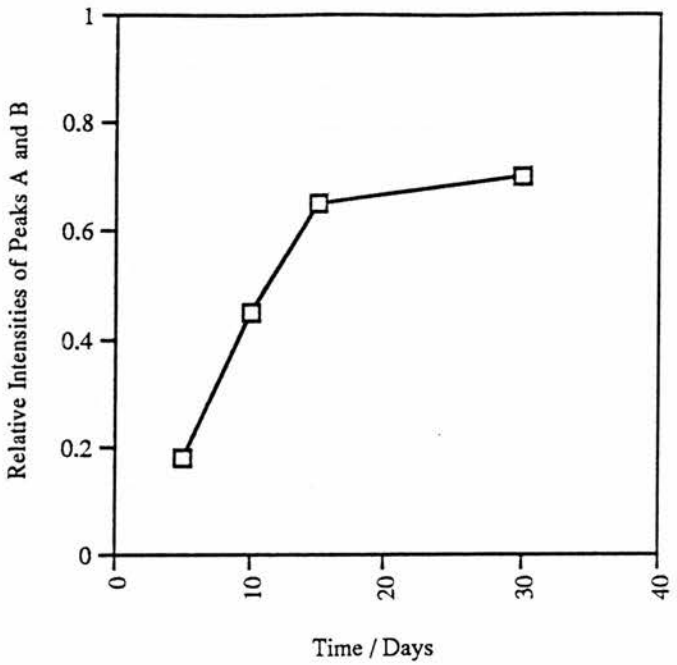

Fig. 5.6 The change in the relative intensities of ^{13}C NMR signals of 1,8-dichlorooctane/urea as a function of the immersion time in pure liquid n-decane (days).

5.5 Discussion of Possible Driving Forces for the Exchange Process

5.5.1 Introduction

In this section we attempt to seek those essential factors which govern the exchange of guest species in urea inclusion compounds. While a profound understanding of these factors cannot be obtained without possessing comprehensive experimental results on a diverse range of guest species, and also other attributes concerning physical characteristics of the system (such as temperature, particle size, etc.), it is nevertheless not premature to attempt to rationalise the experimental results presently available. We believe that the exchange of the guest molecules can be explained on the basis of two major factors.

5.5.2 Establishment of Equilibrium Between Urea Inclusion Compounds and the External Liquid Phase

In many respects, a system containing crystals of a urea inclusion compound immersed in an external liquid phase containing potential guest molecules resembles two interconnected reservoirs of different liquids. Although there are severe constraints imposed by the host framework on the guest molecules, experimental results indicate that the guest molecules experience a high degree of mobility within the tunnel structure of urea inclusion compounds. Hence the physical state of the guest molecules in urea inclusion compounds can be assumed as a semi-liquid state; the similarity between such a system and two interconnected reservoirs of liquids is therefore justified.

In the presence of a concentration gradient in such a system, there will be a driving force to equalise the chemical potential in different parts of the system. A similar driving force is expected in a system comprising a urea inclusion compound in a potential liquid guest; thereby guest species from the external liquid phase diffuse into the tunnel structure and the guest molecules inside the tunnel migrate into the external liquid phase. If the concentration of the external guest species is much higher than the amount of guest molecules originally inside the inclusion compound, then, in the absence of any other over-riding factors, the exchange process should lead to essentially complete replacement of the guests.

Due to other influences, the real behaviour of the system, , is usually more complicated. If A and B denote two different guests, then the A/urea and B/urea inclusion compounds possess different thermodynamic stabilities. Therefore, the tendency of the system to form the more stable inclusion compound will be another factor

influencing the exchange process. The contribution of this factor to the exchange process is discussed in the following section.

If the nature of the two guests A and B is not significantly different, the exchange process can satisfactorily be explained on the basis of the tendency for the system to equalise the concentration of the guests throughout the system. However, if the nature of the different guest molecules is substantially different, the following factor may be dominant.

5.3.3 Thermodynamic stabilities of urea inclusion compounds

Formation of an inclusion compound is a result of host-guest interaction. The host structural framework is formed only based on sufficiently strong host-guest interactions. These are the interactions between the host molecules and the guest species that make such structures stable. For example the empty host structure of urea is not stable and will collapse to the pure urea phase (see chapter II). Therefore the nature of the guest species (e.g. the length and the chemical nature of the guests) has a crucial effect on the relative stabilities of urea inclusion compounds. There are several experimental results which confirm this fact. For instance, the stabilities of n-alkane/urea compounds decrease by decreasing the length of the n-alkane; it is not feasible (at ambient temperature and pressure) to synthesise urea inclusion compounds containing n-alkanes shorter than n-octane. In contrast, longer chain n-alkanes generally form very stable inclusion compounds with urea. This diversity in thermodynamic behaviour of n-alkane urea inclusion compounds is based on the stronger host-guest interaction, per unit length of tunnel, in inclusion compounds containing longer n-alkanes.

Functional groups also have a significant effect on the relative stabilities of inclusion compounds. For example, experimental evidence [6] indicates that if crystallisation of urea inclusion compounds occurs from a solution containing two type of potential guest molecules, an α,ω-diiodoalkane and an n-alkane with comparable chain lengths, there is a strong preference for the inclusion of the α,ω-diiodoalkane. This preference originates from the strong interaction between the iodine atoms in the guest molecule and the host framework.

Hence, it is conceivable that immersion of a urea inclusion compound containing a guest species which forms an inclusion compound that is less stable than that of the potential guest molecules in the liquid phase surrounding the crystals, should, in principle, lead to the migration of the molecules from the external environment into the tunnel structure.

It is worthwhile to mention that the contribution of this factor to the exchange process depends critically on the nature of the system. In certain systems, such thermodynamic differences are very subtle and this factor cannot be considered as the major driving factor for the exchange process. For example, thermodynamic stability is unlikely to be the main driving force for the exchange of the guests in decane/urea immersed in liquid n-undecane. The difference in chain length of these two guests is so small that only a small thermodynamic difference is anticipated.

The following experiment clearly demonstrates the role of this factor in the exchange process. Fig. 5.7.a presents the ^{13}C NMR spectrum of the 1,8-diiodooctane/urea inclusion compound which was left for 2 months in n-decane (sample I). Fig. 5.7.b shows the spectrum of 1,8-dichlorooctane/urea immersed for the same period of time, and

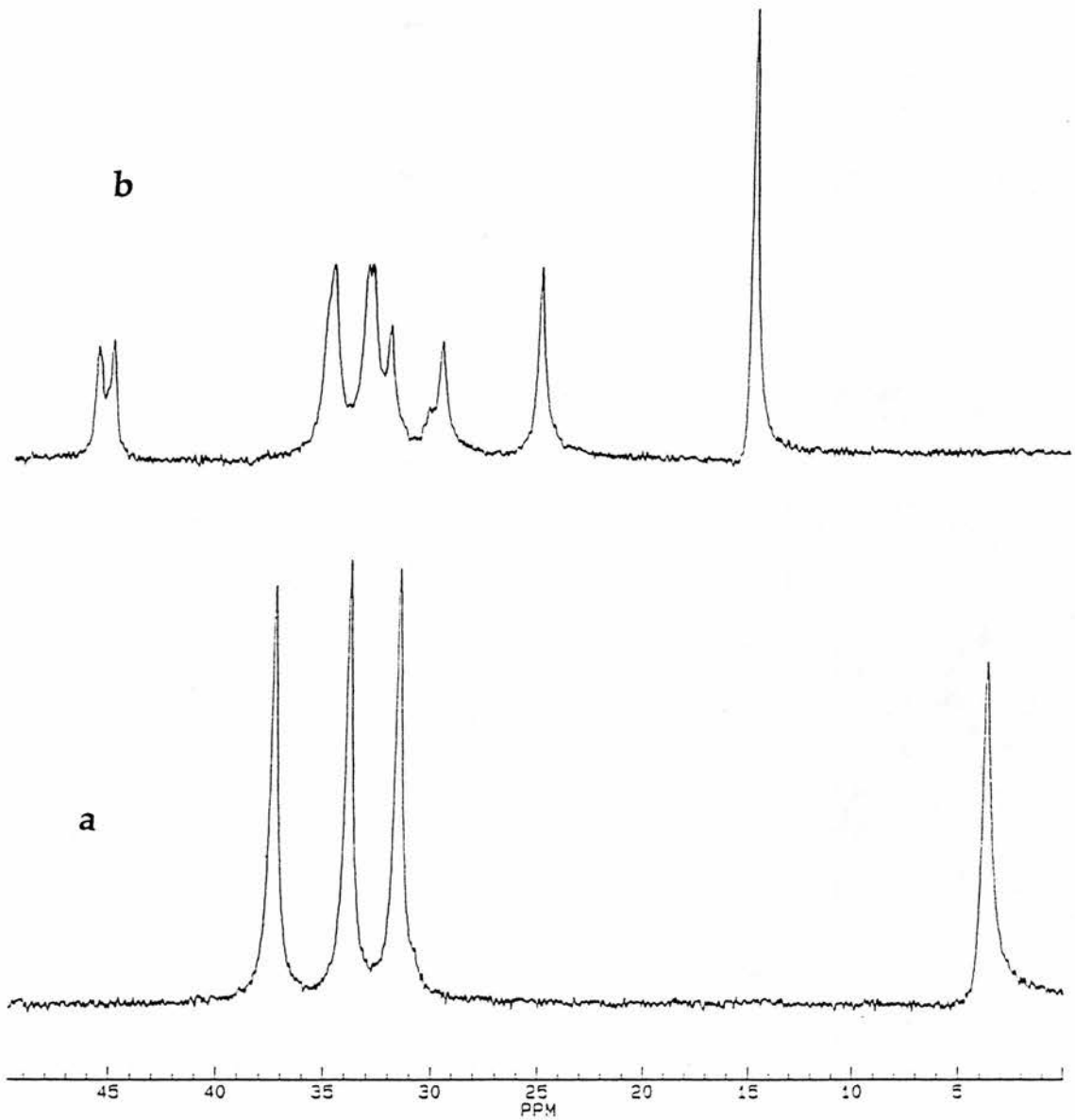

Fig. 5.7 Solid state ^{13}C NMR spectra of (a) 1,8-diiodooctane/urea immersed in n-decane for 2 months (b) 1,8-dichlorooctane/urea immersed in n-decane for 2 months.

under identical conditions, in liquid n-decane (sample II). Whereas a considerable amount of n-decane has entered the urea tunnel structure in sample II, no noticeable exchange has occurred in sample I.

The result of this experiment is consistent with the fact that the thermodynamic stability of 1,8-diiodooctane/urea is much higher than n-decane/urea, and therefore the diffusion of the n-decane from the liquid phase into the tunnel structure is prohibited.

In addition to thermodynamic factors, this result is also consistence with kinetic considerations. The kinetic barrier for 1,8-diiodooctane to escape from the tunnel structure is higher than this barrier for n-decane. This is the result of higher compatibility between 1,8-diiodooctane molecule and the shape of the tunnel compare with n-alkane molecule.

References:

[1] Wyckoff, R. W. G., Corey, R. B. *Z. Kristallogr.* 1934, **89**, 7117.

[2] McAdie, H. G. *Can. J. Chem.* 1963, **41**, 2144.

[3] Harris, K. D. M. *J. Phys. Chem. Solids.* 1992, **53**, 529.

[4] Thomas, J. M. *Angew. Chem., Int. Ed. Engl.* 1988, **27**, 1673.

[5] Thomas, J. M., Harris, K. D. M. in "Organic Solid State Chemistry". Ed. Desiraju, G. R., Elsevier, Amsterdam, 1987.

[6] Mahdyarfar, A., Harris, K. D. M. Unpublished results.

CHAPTER VI

^{2}H NMR INVESTIGATION OF GUEST DYNAMICS IN TRI-ORTHO-THYMOTIDE INCLUSION COMPOUNDS

Introduction

The investigation of dynamics in the solid state has been particularly appealing to chemists not only because such knowledge is fundamentally important, but also because many important physical properties are influenced by such motion. The nature of large amplitude motion in the solid state and its origin, which is strongly influenced by molecular and environmental characteristics, are topics which are still open to debate and discussion. The recent development of experimental solid state NMR methodologies [1-3], advances in theoretical formulation of the dynamic effects in NMR lineshapes [4-7], and progress in the chemistry of selective isotope labelling have made this technique a particularly valuable tool for studying the dynamics of crystalline compounds (see chapter II and also references 8-11).

In this chapter we first briefly introduce the theoretical basis of the ^{2}H NMR technique and the way that appropriate motion can affect the ^{2}H NMR spectrum. Dynamic investigations of benzene-d_6 and pyridine-d_5 in tri-ortho-thymotide (TOT) inclusion compounds are then presented.

6.1 Basic Theory of ^{2}H NMR Spectroscopy

Within the solid state, the nuclear quadrupolar interaction is the dominating interaction for ^{2}H nuclei located in non-cubic environments [12]. Other interactions such as dipole-dipole interaction and chemical

shift anisotropy are comparatively small and can be neglected in comparison with the quadrupolar interaction.

The quadrupolar interaction originates from the interaction between non-spherically symmetric nuclear charge distributions and the electric field gradient (EFG) at the nucleus, generated by asymmetric electron distributions in molecules or lattice sites.

The electric field gradient at the nuclear site is represented by a second rank traceless tensor (denoted V). The magnitude and orientation of the electric field gradient tensor is entirely described by the components of this tensor. By choosing an appropriate coordinate system (Principal Axis System), the electric field gradient is immensely simplified since the tensor is converted to diagonal form and the characteristic features of electric field gradient are described by three diagonal elements; V_{xx}, V_{yy}, and V_{zz} (with $V_{xx}+V_{yy}+V_{zz} = 0$). The principal axis are assigned such that $|V_{zz}| \geq |V_{yy}| \geq |V_{xx}|$, and the asymmetry parameter is defined according to the following equation:

$$\eta = \frac{|Vxx - Vyy|}{|Vzz|} \qquad (1)$$

In addition, another important parameter, the quadrupolar coupling constant, is defined as:

$$\chi = \frac{e^2qQ}{h} \qquad (2)$$

where $V_{zz} = eq_{zz}$ (e is the charge of the electron) and Q is the ^2H nuclear quadrupole moment.

Each particular nucleus in a specific environment possesses characteristic values of η and χ. These values may be evaluated directly from NMR spectra of single crystals or from a polycrystalline sample (in

both cases sufficiently low temperature is required). If the electric field gradient has axial symmetry, then $V_{XX} = V_{YY}$ and therefore $\eta = 0$. In this situation the interaction is denoted as "axially symmetric".

For a nucleus with spin I = 1 such as ^2H, in the presence of a strong applied magnetic field B_0, the quadrupolar interaction perturbs the Zeeman energy levels and leads to an orientation-dependent splitting between the two allowed NMR transitions; i.e. m =0 <--> m = 1 and m =0 <-> m = -1. In the absence of molecular motion, the orientation-dependence of the separation of the two transitions is given by the following equation:

$$\Delta\upsilon(\theta,\phi) = (3/2)\,\chi\,[1/2(3\cos^2\theta - 1) - 1/2\,(\eta\sin^2\theta\cos^2\phi)] \qquad (3)$$

The orientation of the electric field gradient tensor in the applied magnetic field is described by θ and ϕ, where θ is the angle between B_0 and V_{ZZ}. Therefore, in the solid state NMR spectrum of a single crystal of static deuterons with all deuterons in the unit cell oriented in the same way, a specific doublet exists for these deuterons; the separation of the doublet depends upon the orientation of the principal axis with respect to the applied magnetic field and the linewidths of the peaks in the doublet are determined by the spin-spin relaxation time (T_2) and are proportional to $1/T_2$.

In a polycrystalline sample, the existence of all possible orientations of crystallites relative to the applied magnetic field generates a superposition of these doublets due to different crystal orientations. A typical resultant spectrum for a static sample, a so-called "powder pattern", is shown in Fig. 6.1.

The spectrum is symmetric about the Larmor frequency υ_0 and the dominant features of this lineshape are two strong peaks disposed symmetrically about υ_0 and separated by $(3/4)\chi(1-\eta)$, and two extreme

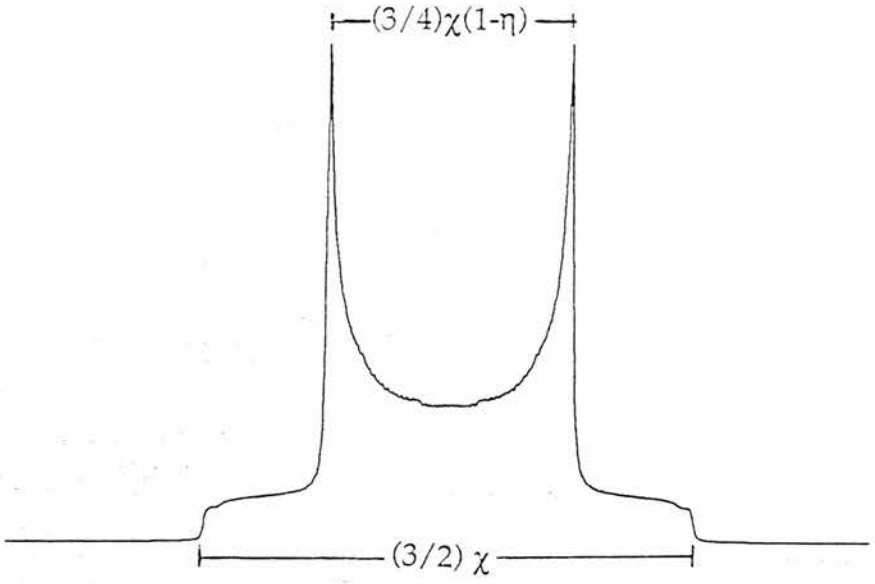

Fig. 6.1 A typical resultant spectrum for a static sample (powder pattern).

shoulders separated by (3/2) χ. The former corresponds to $\theta = 90°$ orientations (we refer subsequently to these as the "perpendicular peaks"), and the latter to $\theta = 0$ orientations (denoted "parallel peaks").

Appropriate molecular motion within the solid can affect the ^2H NMR spectrum. In general, large-scale motion which occurring at a frequency of greater than *ca.* 10^3 Hz, will significantly affect the ^2H NMR spectrum.

Based on the qualitative effect of a particular motion on the ^2H NMR spectrum, it is convenient to define three motional regimes:

I. Slow motional regime: motions with rates up to about 10^3 Hz. In this regime, the motion is unable to affect the ^2H NMR lineshape and the spectrum essentially resembles a static powder pattern. Therefore no insight concerning the dynamics can be obtained for a system experiencing motion within this region.

II. Intermediate motional regime: motions with the rates between *ca.* 10^3-10^7 Hz. Motions which occur within this regime can significantly affect the ^2H NMR lineshape (provided they cover appropriate orientations relative to the applied magnetic field). In principle, it is possible to obtain detailed mechanistic and kinetic information concerning a particular motion which occurs in this regime.

III. Fast motional regime: motions with rates greater than ca. 10^7 Hz. The existence of fast motion induces a change in the spectrum, in comparison with that of the static deuteron, but the overall shape of the spectrum in this region is not sensitive to the rate of the motion. Therefore while it is possible to recognise from the spectrum that the system undergoes rapid motion, it is not possible to obtain detailed mechanistic information about the particular motion occurring in this range.

If molecules in the rapid motional regime undergo isotropic molecular reorientation similar to the motion in isotropic fluids, the NMR lineshape will be independent of crystal orientation. In this case, a single sharp line is observed at the centre of the spectrum[13]. This lineshape can also result from certain types of jump mechanism, provided the jump motion have appropriate symmetry.

Dynamic NMR studies have indicated that motion in the solid state often comprises discrete jumps between specific position in space rather than continuous diffusion [14].

6.2 Experimental Aspects of ^2H NMR Spectroscopy

Spectra of quadrupolar nuclei (like ^2H) in powder are extremely broad (within the range of hundreds of kilohertz). Therefore in order to excite the whole range of the spectrum, short high-power pulses are required. Utilising such strong pulses usually causes a phenomenon called "pulse breakthrough" which originates from the effect of a strong pulse on the

initial data points, resulting in distortion of the free induction decay. The first data points in the free induction decay are very crucial since they define the outer limits of the spectra.

A technique invented by Bloom and co-workers [15], which overcomes this problem is the "quadrupolar spin-echo" technique. Due to the fact that ^2H nuclei possess three available spin states, it is not possible to illustrate different stages of the quadrupolar spin-echo sequence using the magnetisation vector representation. However, the basic principle of this technique is relatively simple and is shown in Fig. 6.2. The sequence starts with a 90° pulse which tips the ^2H magnetisation vector into the XY plane. This pulse is followed by a delay time, τ, and then another 90° degree pulse is applied. The effect of the second 90° pulse is to refocus the magnetisation, and after a total time of 2τ from the start of the pulse sequence an echo of the original free induction decay is observed. From this echo, the final spectrum can be obtained.

The reason that the quadrupolar echo-pulse sequence provides, in principle, undistorted spectra lies in the fact that such spectra are obtained from the echo signals. These signals (due to the presence of the delay time) are sufficiently removed in time from the RF pulse, and the distorting effect of the RF pulse is thereby prevented.

6.3. Dynamic Investigation of the TOT/ Benzene-d_6 Inclusion Compound

6.3.1. Introduction

The dynamic behaviour of benzene has been investigated in various solid environments (including its pure solid phase). The highly symmetric structure of the molecule and its capability of undergoing large amplitude motion have been the main reasons for these investigations. Some of these studies include the dynamics of benzene in its pure solid phase [16], the

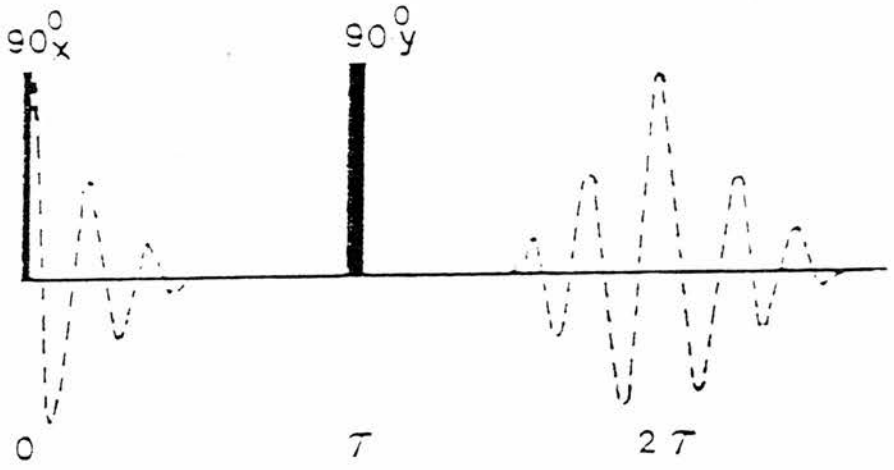

Fig. 6.2 Simple illustration of "quadrupolar spin-echo" technique.

motion of benzene in benzene-cyclophosphazene [17], benzene adsorbed on graphite and boron nitride [18], and benzene in different zeolite frameworks [19]. Here we have studies the mobility of benzene-d_6 in its TOT inclusion compound (see chapter II for general information about TOT inclusion compounds). The objective of this investigation is two-fold; first to study the mobility of benzene in a different type of solid environment (i.e., the cage structure of TOT) and to compare the results with the mobility of benzene in other solid environments. Such comparisons will provide insights regarding the role of the solid environment in influencing the mobility of particular species. Second, this work will allow us to compare and contrast the dynamic behaviour of benzene with the structurally similar molecule pyridine in the same solid environment (cage structure of TOT inclusion compounds). This will provide knowledge concerning the role of molecular symmetry and host-guest interactions on the dynamic behaviour.

6.3.2. Experimental

6.3.2.a. Preparation of TOT/ Benzene-d_6 Inclusion Compound

TOT and benzene-d_6 were purchased from Aldrich and were used without further purification. The benzene-d_6 /TOT inclusion compound was prepared using the following method: 0.5 g of TOT was dissolved in 4 ml benzene-d_6. The solution was slightly heated in order to dissolve completely the TOT. Well-defined large hexagonal-shaped crystals of benzene-d_6 /TOT were obtained by slow evaporation (within two weeks) of this solution at room temperature under a nitrogen atmosphere. The crystals were collected and washed sparingly with cold 2,2,4 trimethylpentane in order to remove any surface-adsorbed benzene. The collected crystals were then dried in a nitrogen atmosphere. The crystals were ground thoroughly into fine powders and packed into a 5mm NMR tube. The tube was carefully sealed in order to eliminate the possibility of penetration of atmospheric water into the sample.

6.3.2.b. Experimental Aspects of Recording the ^2H Spectra

^2H NMR spectra were recorded at 76.8 MHz on a Bruker MSL-500 spectrometer, using a standard Bruker high power variable-temperature solenoid probe. A Bruker BVT-1000 variable temperature unit with a nitrogen gas flow as the coolant was used for recording spectra at temperatures below ambient temperature. The recorded temperatures are uncalibrated.

All spectra were recorded using classical quadrupolar echo pulse sequence (QE). This pulse sequence is:

$$[\pi/2]_x \ , \ \tau_1 \ , \ [\pi/2]_y \ , \ \tau_2 \ , \ \text{acquisition.}$$

While ^2H spectra recorded using composite quadrupole echo pulse sequences (CQE) [20] are often of superior quality, no attempt was made to record and compare spectra using this alternative approach, since the spectra recorded using the classical quadrupolar echo technique had acceptable lineshapes. The delay times used in the experiment were τ_1 = 13.0 μs and τ_2 = 10.0 μs. The free induction decays obtained by these delays were left shifted before Fourier transformation in order that the first point in the FID corresponded to the echo maximum.

The sample was not subjected to any external mechanical rotation during the experiment. At each temperature usually 200 acquisitions were collected for an acceptable signal to noise ratio. The ^2H $\pi/2$ pulse length was 2.4 μs for all experiments. A 5s recycle delay was chosen, based on several test experiments, as sufficiently long to prevent saturation.

6.3.3. Results

Fig 6.3 shows the ^2H NMR spectra recorded for benzene-d_6 /TOT at different temperatures. The spectra at all temperatures can be described as well-defined powder patterns which are qualitatively similar to the theoretical spectrum presented at Fig. 6.1 for a static deuteron. The shape of the spectrum does not change noticeably as a function of temperature. While general spectral features are invariant within the range of temperatures studied, there is nevertheless a continuous small change in the splitting between the perpendicular peaks at different temperatures. The measured values of the splitting for benzene-d_6 in TOT are presented in Table 6.1.

At the lowest temperature (130 K), the separation between the perpendicular peaks is 68.6 kHz and the separation between the parallel peaks is 136.96 kHz. At room temperature the separation of the

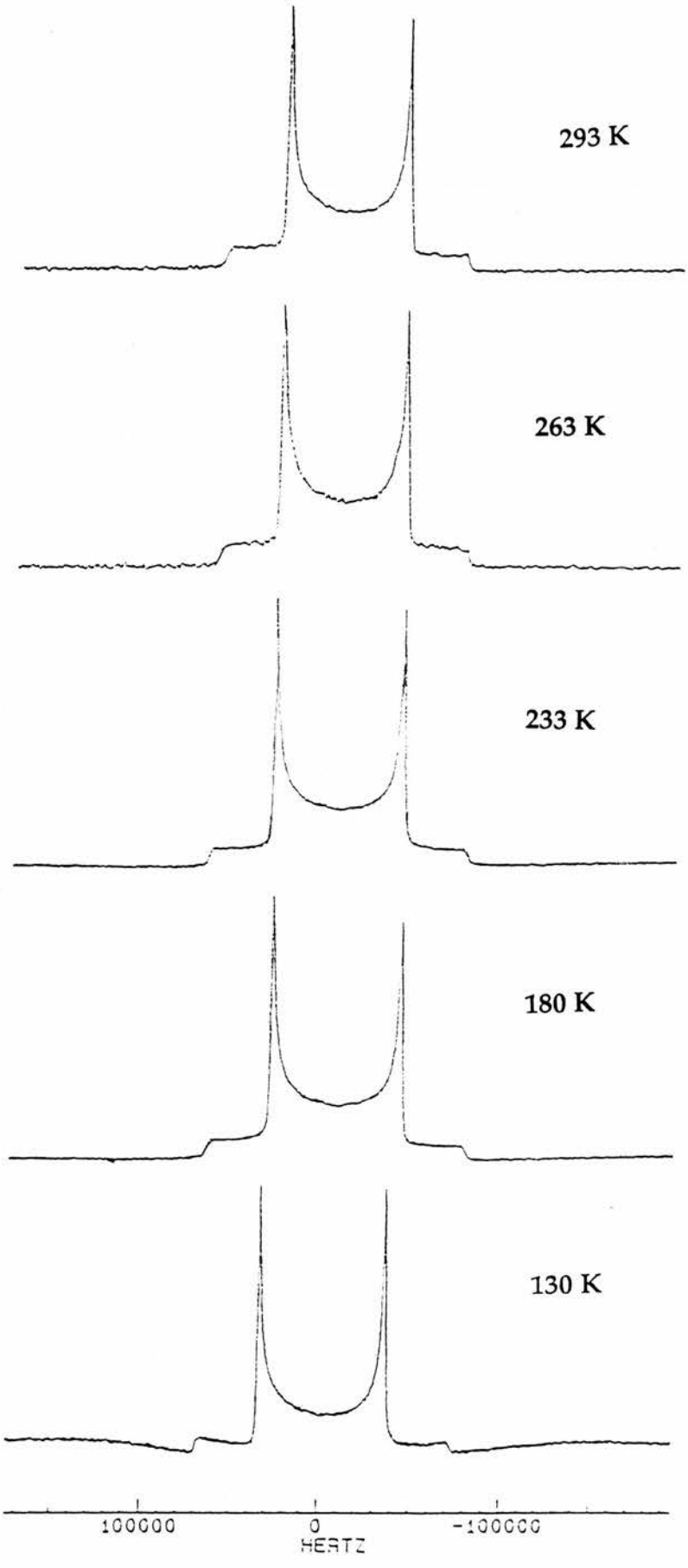

Fig. 6.3 ^{2}H NMR spectra of benzene-d_6/TOT at different temperatures.

Temperature (K)	Splittings (kHz)	
	AA´	BB´
130	68.60	136.96
180	68.60	136.84
233	67.50	131.71
263	65.31	121.09
293	63.23	124.88

Table 6.1 The values for splittings in ^2H NMR spectra of benzene/TOT at different temperature.

perpendicular peaks is 63.23 k Hz and the separation of the parallel peaks is 124.88 k Hz.

We discuss subsequently the origin of such changes in the lineshape. Due to instrumental restrictions it was not possible to record spectra at temperatures lower than 130 K.

6.3.4. Computer Simulation of ^2H NMR Spectra

The general procedure followed in dynamic investigations using ^2H NMR is based on calculation of a theoretical spectrum, using computer simulation, then comparing the simulated spectrum with the experimental one. The agreement between simulated and experimental spectra is the necessary criterion for accepting a proposed motional model. The simulation program used here implicitly assumes a jump mechanism rather than diffusive motion. In the program, the jump is assumed to be instantaneous with the time for the deuteron to pass between steps

assumed to be essentially zero. The frequency of the jump process is defined as the inverse of the residence time in each site.

The program calculates theoretical ^2H NMR spectrum using formula (3) and then averaging it over all possible orientations (powder averaging). The required parameters in the program are:

1- the Euler angles (α, β, γ), which specify the orientation of each deuteron. Specifically, the Euler angles define the transformation from the principal axis system of the electric field gradient tensor to a fixed reference frame called the molecular axis system.

2- A matrix (exchange matrix) to indicate which pairs of sites the deuteron can jump between. The rows and the columns of this matrix represent the particular sites of the exchange. Each entry of the matrix shows the possibility of the exchange between the two sites (1, if exchange is possible and, 0 if exchange is not possible).

3- The relative population of each deuteron site.

4- The intrinsic NMR linewidth which is proportional to $1/T_2$ (T_2 denotes spin-spin relaxation time). In the simulation procedure it is assumed that the spin-spin relaxation time is not affected by the exchange process.

5- The angle increment ($\Delta\alpha$) used in calculating the powder average. The quality of the simulated spectra is improved using smaller $\Delta\alpha$. Smaller $\Delta\alpha$ requires longer computational time.

6- The quadrupole coupling constant χ as defined in (2), and the asymmetry parameter η defined in (1) for the *static* deuteron. These values can be obtained from the spectra of the samples in the slow motional regime or alternatively can be obtained from the literature (and may have been obtained from other experimental approaches).

7- The rate of the specific motion (Hz).

6.3.5 Dynamic Model for the Motion of Benzene in TOT

We first intend to probe the existence of motion for benzene in the cage structure. Therefore a theoretical spectrum was simulated based on the assumption that the benzene molecules are static. Values of 180.7 kHz for the quadrupole coupling constant and 0.041 for the asymmetry parameter were used in simulation program for this system [21]. The simulated spectrum for static benzene and the experimental spectrum recorded at 130 K presented in Fig. 6.4. It is clear that the benzene molecule in the cage structure at this temperature *is not static*. Although the experimental lineshape is similar in general appearance to the simulated spectrum for static benzene, nevertheless the splitting between the perpendicular peaks in the experimental spectrum is about half the value for simulated spectrum. Following this result, we therefore intend to establish an appropriate motional model for the mobility of benzene in the TOT inclusion compound. We first focus on the interpretation of the features of the spectrum at 130 K. We subsequently propose three different motional models and the simulated spectra related to these models over different motional regimes are presented. These motional models have been chosen on the basis of the molecular symmetry of benzene. It is clear that the mobility of benzene in the cage structure (similar to other physicochemical properties), may also be influenced by the symmetry of the cage (C_2 symmetry).

a- Model I

Model I is based on 180° jumps of benzene along the two-fold symmetry axis passing through two carbon atoms (Fig. 6.5). The Euler angles are defined in Table 6.2. The orientation of the electric field gradient tensor (EFG) components in the principal axis system and the molecular reference frame for benzene are shown in Fig. 6.6.

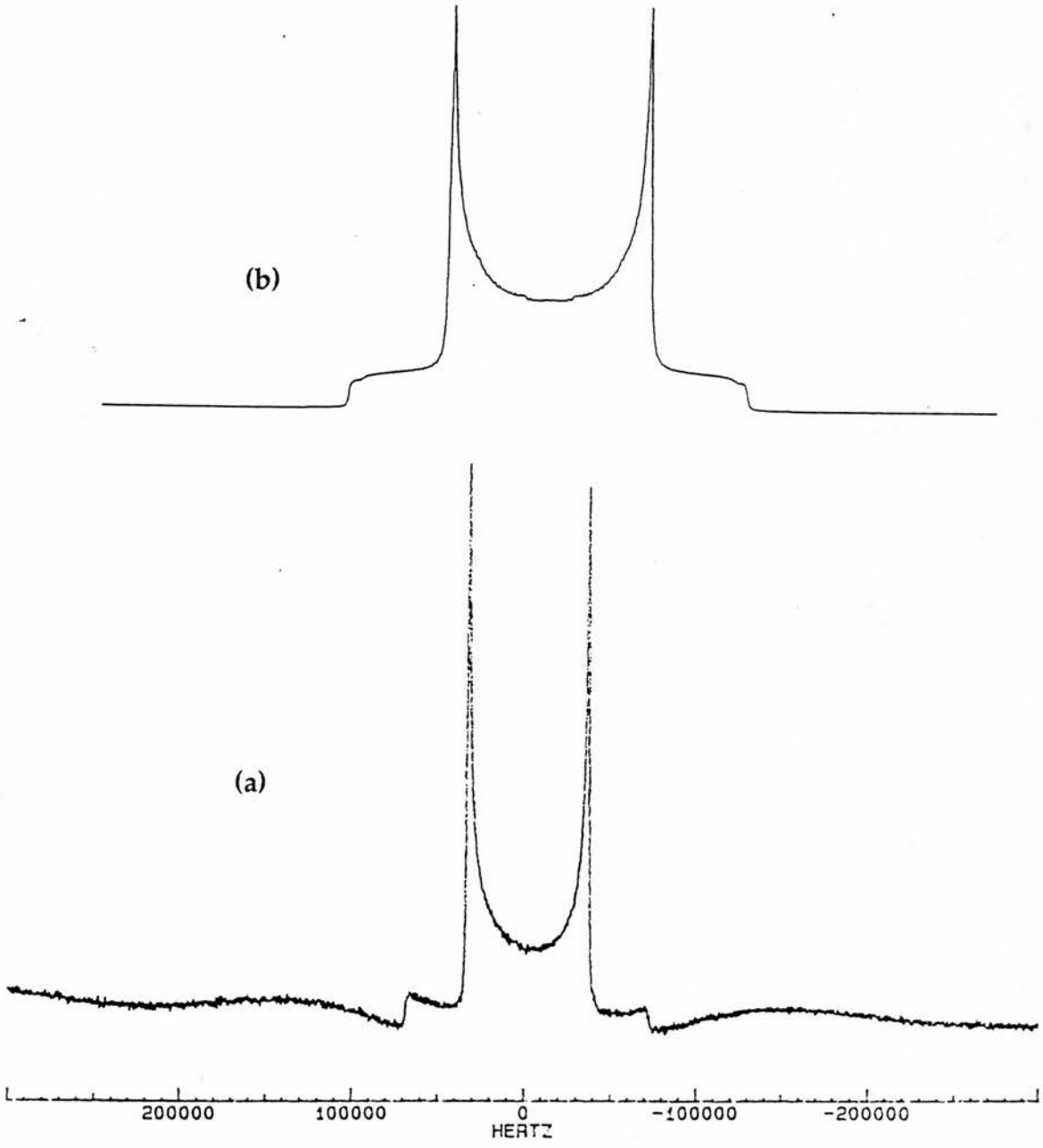

Fig. 6.4 (a) ^2H NMR spectrum of benzene-d_6/TOT recorded at 130 K (b) simulated spectrum for static benzene.

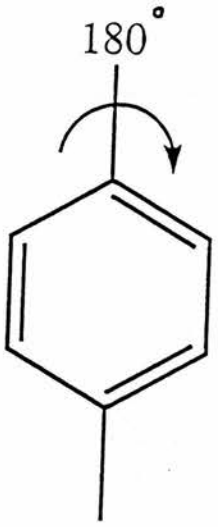

Fig. 6.5 180° jump of benzene along the two-fold symmetry axis passing through two carbon atoms (model I).

Carbon No.	α	β	γ
1	0	0	0
2	0	60	0
3	0	120	0
4	0	180	0
5	0	240	0
6	0	300	0

Table 6.2 Euler angles (degrees) for different carbons of benzene, which define the orientations of the principal axis systems of the electric field gradient tensors relative to a space fixed molecular reference frame.

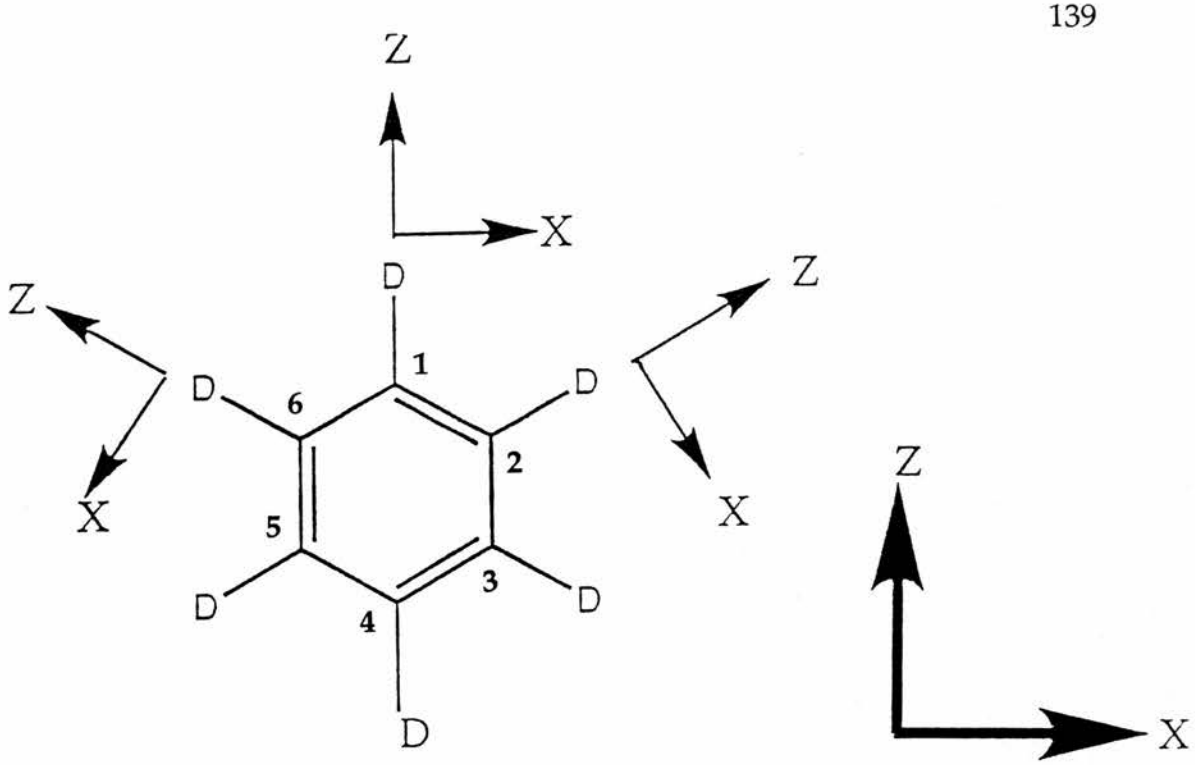

Fig. 6.6 The orientation of the electric field gradient tensor components in the principal axis system and the molecular reference frame for benzene.

In this definition, we assume that the Z component of the EFG tensor is along the C-D bond, the X component is in the molecular plane and the Y component is perpendicular to this plane. Since the asymmetry parameter for deuterons in benzene molecule is not zero, in principle it is important whether the X component is in the plane or perpendicular to it. However, simulation of spectra based on both different cases showed no detectable difference. The orientation of the two deuterons that lie on the jump axis does not change during the jump motion and therefore, in the simulated spectra, they resemble static deuterons. The exchange matrix that has been constructed for this jump motion is:

	1	2	3	4	5	6
1	0	0	0	0	0	0
2	0	-1	0	0	0	1
3	0	0	-1	0	1	0
4	0	0	0	0	0	0
5	0	0	1	0	-1	0
6	0	1	0	0	0	-1

Spectra were simulated for different motional rates (0-10^{10} Hz), and some of the simulated spectra are shown in Fig. 6.7.

Comparison of the experimental spectrum recorded at 130 K with the simulated spectra based on this motional model shows that none of these spectra reproduce the lineshape of the experimental spectrum. Therefore this model can not be accepted as a reasonable model for explaining the motion of benzene in the cage structure.

b- Model II

This model is based on 180° jumps of the molecule along the two-fold symmetry axis which passes through the midpoints of opposite C-C bonds (see Fig. 6.8).

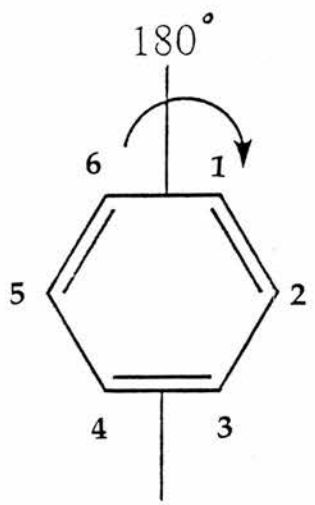

Fig. 6.8 180° jumps of the benzene along the two-fold symmetry axis which passes through the midpoints of opposite C-C bonds (model II).

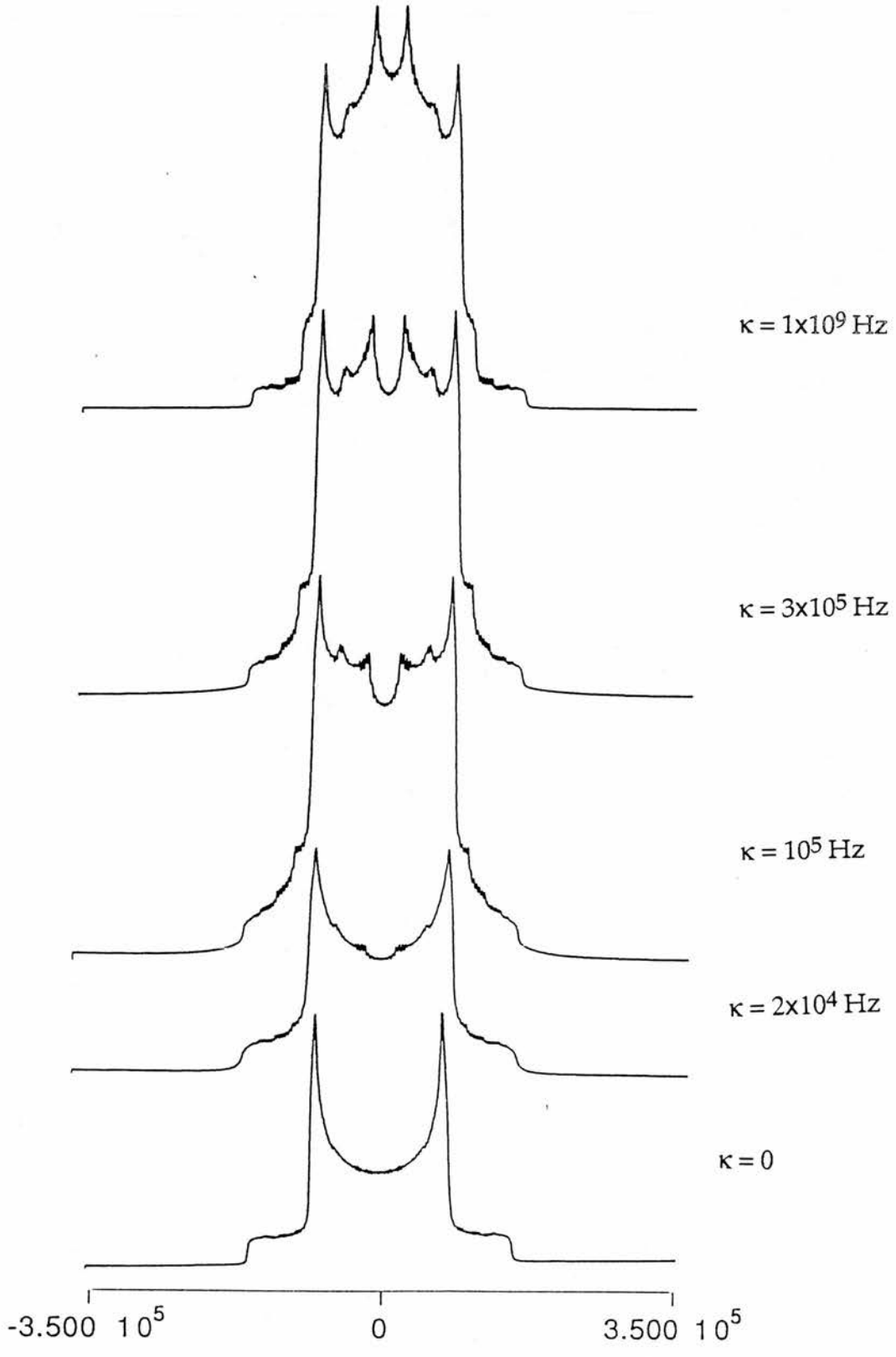

Fig. 6.7 Simulated spectra for the motion of benzene based on model I.

The exchange matrix for this motion is:

$$\begin{vmatrix} -1 & 0 & 0 & 0 & 0 & 1 \\ 0 & -1 & 0 & 0 & 1 & 0 \\ 0 & 0 & -1 & 1 & 0 & 0 \\ 0 & 0 & 1 & -1 & 0 & 0 \\ 0 & 1 & 0 & 0 & -1 & 0 \\ 1 & 0 & 0 & 0 & 0 & -1 \end{vmatrix}$$

The simulated spectra based on this motional model using different motional rates is presented in Fig. 6.9. The spectral lineshape for this motional model does not resemble the experimental spectra, therefore this model does not provide a satisfactory explanation for the mobility of benzene in this particular solid environment.

c- Model III

In this model, six fold jumps of the benzene molecule about the six-fold symmetry axis perpendicular to the molecular plane is considered (Fig. 6.10).

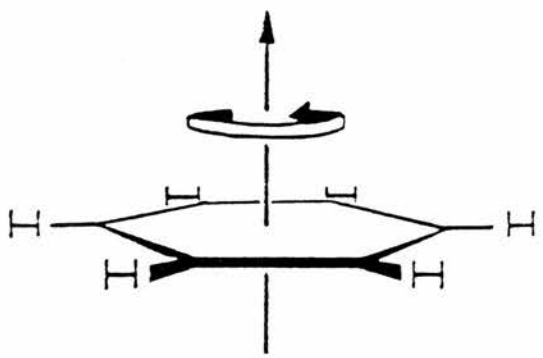

Fig. 6.10 Six-fold jumps of benzene about the six-fold symmetry axis perpendicular to the molecular plane.

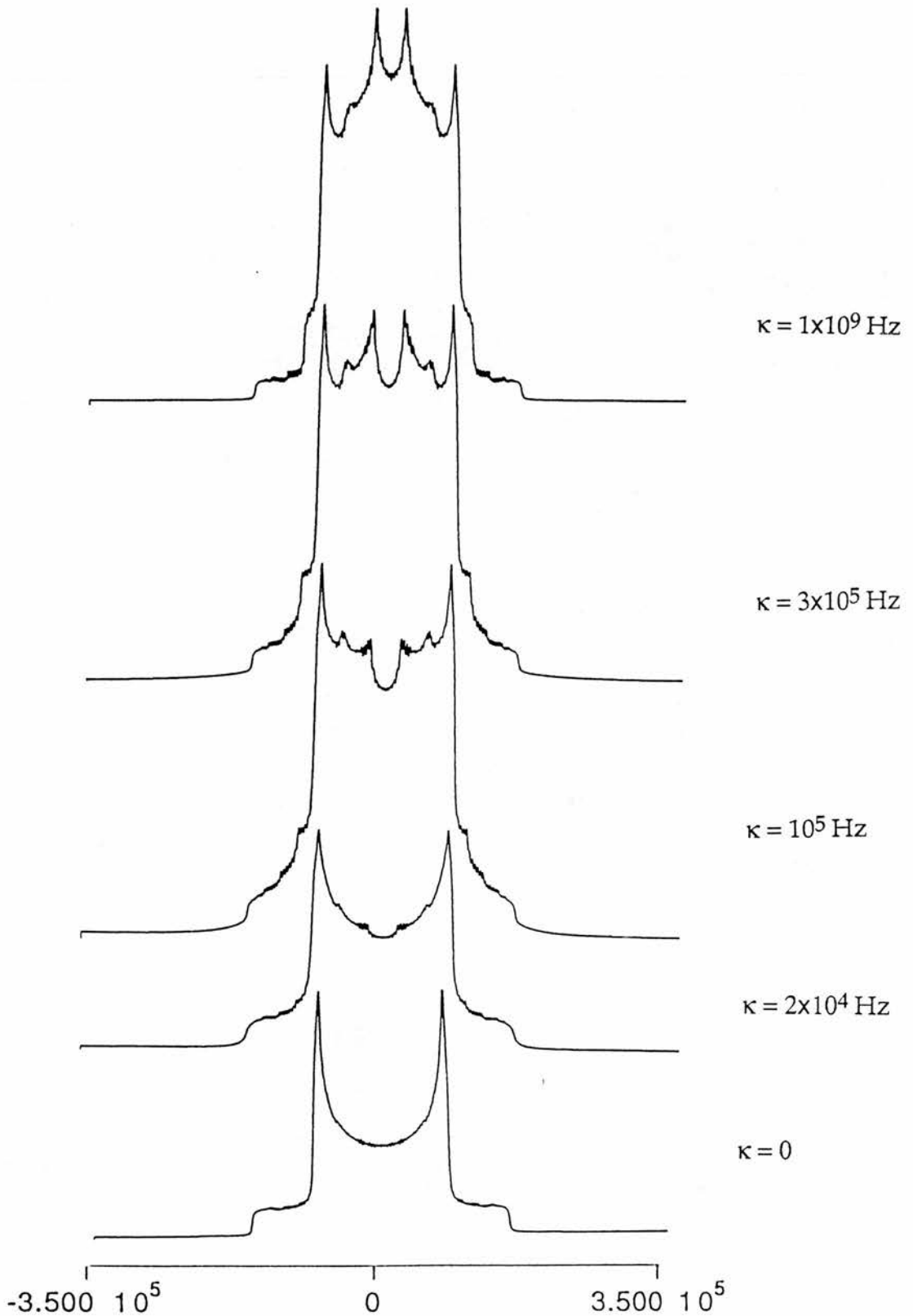

Fig. 6.9 Simulated spectra of the motion of benzene based on the model II.

The exchange matrix for this model of motion is:

$$\begin{vmatrix} -2 & 1 & 0 & 0 & 0 & 1 \\ 1 & -2 & 1 & 0 & 0 & 0 \\ 0 & 1 & -2 & 1 & 0 & 0 \\ 0 & 0 & 1 & -2 & 1 & 0 \\ 0 & 0 & 0 & 1 & -2 & 1 \\ 1 & 0 & 0 & 0 & 1 & -2 \end{vmatrix}$$

The spectra simulated for this motional model are presented in Fig. 6.11. The important feature of the spectra for this motional model is that the general spectral shape in the static motional regime is *identical* to the fast motional regime, but the splitting between perpendicular peaks in the fast motional regime is exactly half of that in the slow motional regime.

The experimental spectrum at 130 K resembles the simulated spectrum based on this model in the fast motional regime. The fit between experimental and theoretical spectra is excellent. Therefore we assign the model for benzene in the TOT cage structure as six fold jumps of the molecule, with rate faster than *ca.* 10^7 Hz (i.e., fast motional regime). This implies that the exact value for the jump rate cannot be determined from the ^{2}H NMR technique, since in the fast motional regime, the ^{2}H NMR lineshape is insensitive to the exact rate of motion.

6.3.6 Interpretation of Spectral Characteristics at Temperatures Above 130 K

As described earlier, by increasing the temperature the general lineshape of the experimental spectra remains unaltered, but the splitting of the perpendicular peaks exhibit a small continuous decrease. Considering the fact that benzene molecules in the cage structure undergo a six fold jump motion in the fast motional regime (deduced from simulation), no change

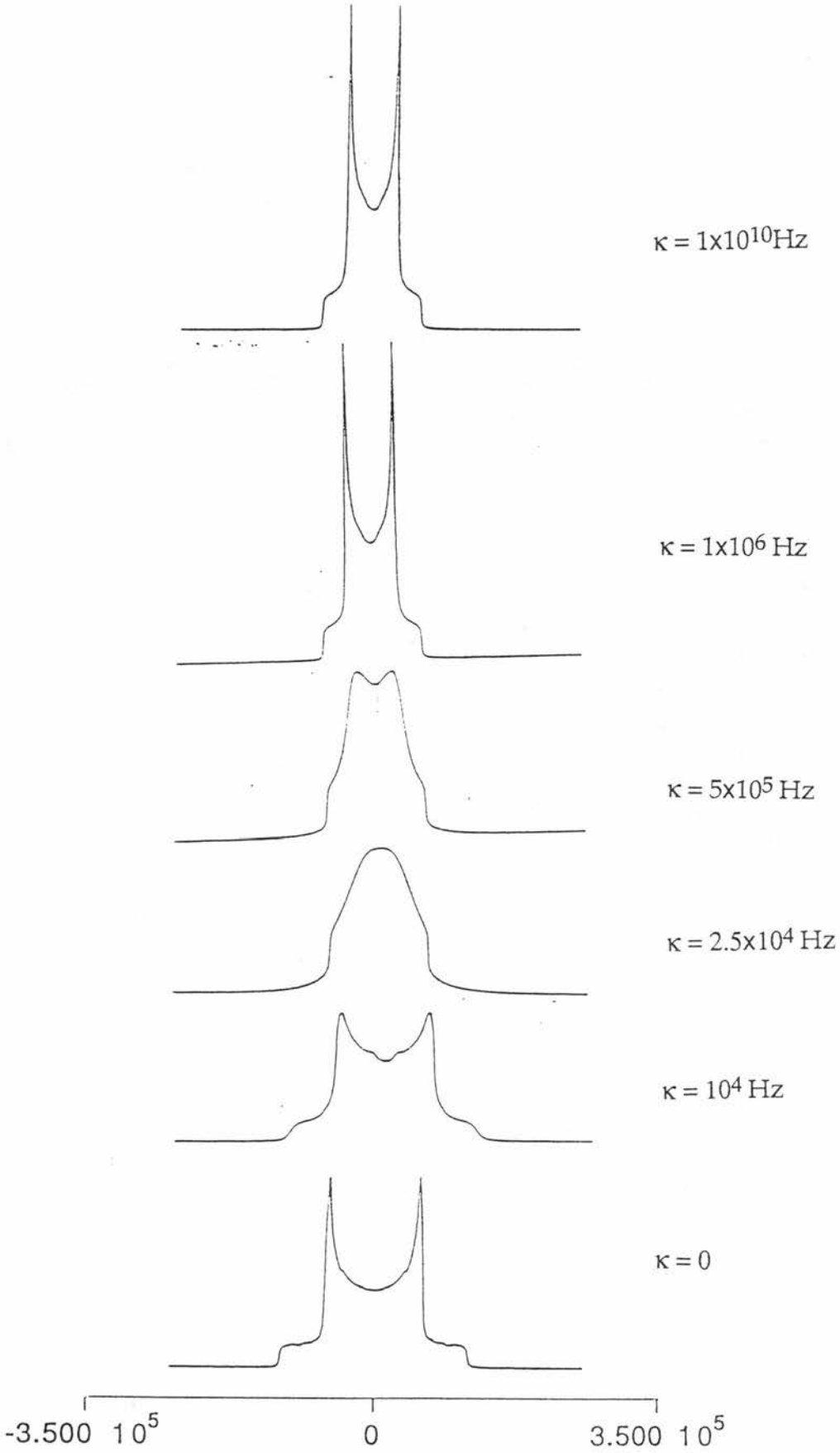

Fig. 6.11 Simulated spectra for the motion of benzene based on model III.

is expected in the lineshape of the spectrum as a result of increase in temperature.

Therefore this relatively small decrease in the value of the splitting must be due to the existence of an additional motion. The additional motion that we invoke here in order to explain this spectral feature is based on small angle molecular liberation [22].

Thus it is proposed that, in addition to the six fold jump motion of benzene, the plane of the molecule librates rapidly through a small angle. The angle of libration and/or the rate of vibration are increased by increasing the temperature, and this explains the continuous decrease in the value of the observed splitting between perpendicular peaks. The suggestion that the amplitude of this motion increases by increasing the temperature is consistent with our experimental results. The existence of this low amplitude motion for the benzene molecule in the cage structure illustrates high degree of freedom for the molecule in this environment. Furthermore, the fact that fast motional regime ^2H NMR spectra are observed down to 130 K implies a weak potential barrier for the jump motion.

The overall physical picture for the mobility of benzene in TOT that emerges from this analysis is that the guest-host interaction between the benzene molecule and the wall of the cage structure in the TOT inclusion compound is insensitive to the orientation of the benzene molecule, giving a low energy barrier for the reorientation of the benzene molecule. Benzene in this structure undergoes rapid six fold jumps even at 130 K; at higher temperatures the plane of the molecule librates within a relatively low angle, superimposed on the rapid six fold jumps of the molecule.

6.4 Dynamic Investigation of the Pyridine-d_5 /TOT Inclusion Compound

6.4.1 Introduction

The structure of the pyridine /TOT inclusion compound is similar to benzene /TOT inclusion compound in that they both possess cage type structures. Our dynamic investigation of pyridine in the TOT cage structure using ^2H NMR allows us to compare and contrast its behaviour with the behaviour of benzene in the same solid environment.

The existence of nitrogen in pyridine alters the symmetry of the molecule and it is anticipated that this may also alter the nature of the host-guest interaction. Since the nature of the dynamics in the solid state is greatly influenced by the molecular symmetry and intermolecular interactions, this comparison should be informative with regard to our general aim of understanding the correlation between structure and dynamics.

6.4.2. Experimental Considerations

The pyridine-d_5/TOT inclusion compound was synthesised using the general synthetic method followed in the preparation of the benzene/TOT inclusion compound (section 6.3.2.a). ^2H NMR spectra were also recorded by a similar experimental approach and the parameters used in recording the ^2H NMR spectra were the same as those used for benzene /TOT.

6.4.3. Results

Fig. 6.12 shows ^2H NMR spectra of pyridine-d_5 /TOT as a detailed function of temperature (130 K - 298 K). ^2H NMR spectra were also recorded at other temperatures not illustrated in this figure, and will also be considered in our discussion of the observed spectral features.

We commence by describing the spectral features observed at 130 K. The spectrum at 130 K consists of three separate recognisable powder

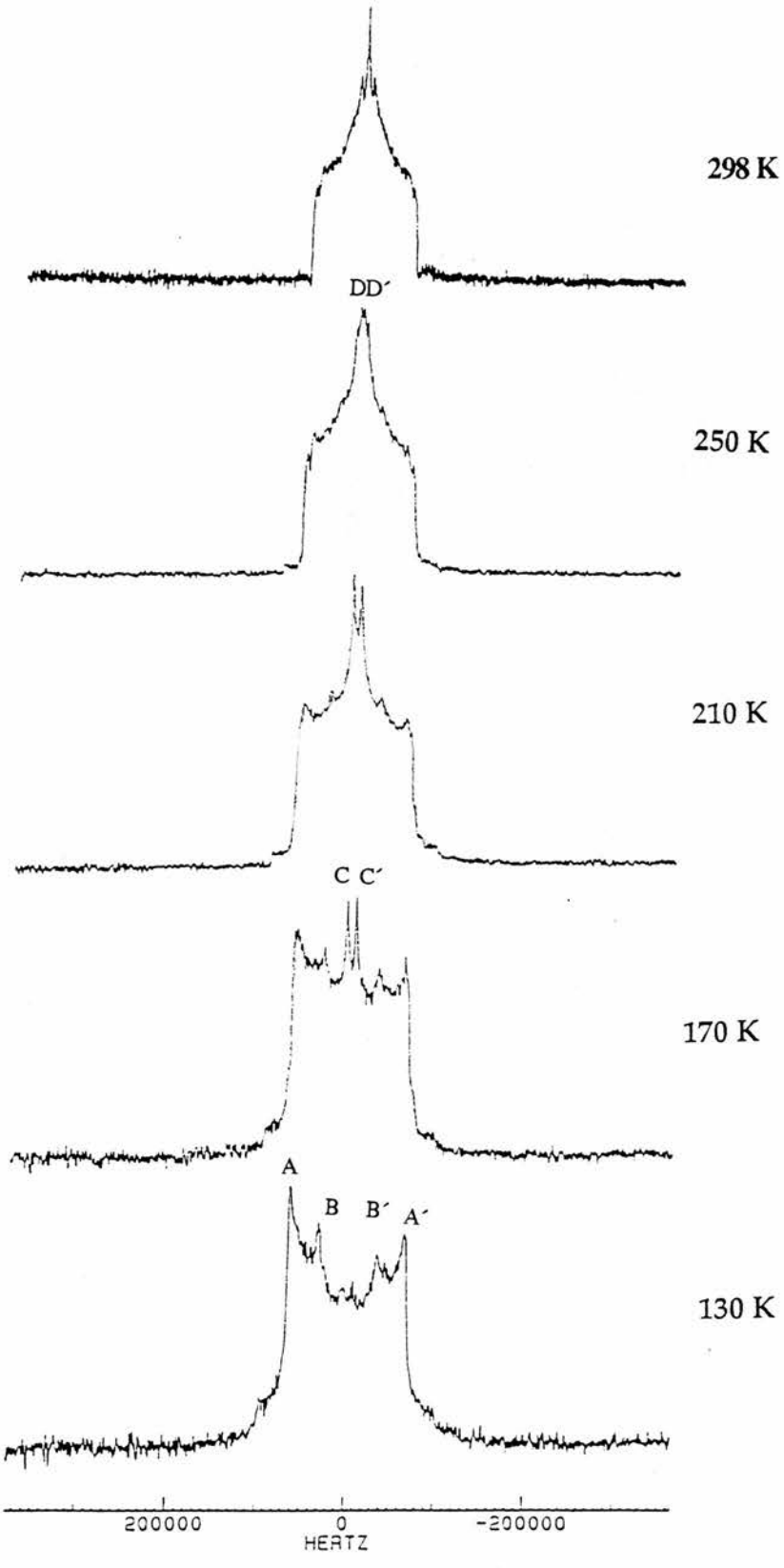

Fig. 6.12 ^{2}H NMR spectra of pyridine-d_5/TOT at different temperatures.

patterns. The splitting denoted AA′ is 128.1 kHz, which is consistent with the expected splitting for static deuterons of pyridine. Splitting BB′ is 63 kHz which is approximately half of the AA′ splitting (the value of splitting BB′ is clearly important with regard to understanding the motion experienced by pyridine). The splitting CC′ is 10.3 kHz.

The experimental result at this temperature confirms the hypothesis that motion in the solid state is affected by the host-guest interaction and also by the symmetry of the molecule.

The main spectral change from 130 K to 170 K is the significant increase in the intensity of the splitting CC′ compared to the other two splittings. The important feature about the CC′ splitting is that while the intensity of this splitting increases, the size of the splitting is essentially constant (9.7 kHz). The splittings BB′ and AA′ are reduced to 60.7 kHz and 120 kHz respectively over this temperature range.

At 210 K, splitting CC′ has remained relatively constant (9.2 kHz). The sizes of the splittings BB′ and AA′ have decreased 56.9 kHz and 109.3 kHz.

At 250 K a new feature is observed in the spectrum. A new powder pattern is observed within the splitting CC′ with the size of 3.3 kHz (denoted DD′). The intensity of BB′ and AA′ at this temperature is very low and can not be detected readily. The value of splitting CC′ (12.6 kHz) at this temperature does not differ considerably from the value for lower temperatures. In the spectrum of the sample at room temperature (298 K), the splitting DD′ has become a single line at the centre of the spectrum. The splitting CC′ at room temperature is about 11.3 kHz.

We have also recorded the ^{2}H NMR spectrum of this sample at 330 K to investigate the possibility of further changes in the spectrum. However the ^{2}H NMR spectrum of the sample recorded at 330 K does not show any noticeable change compared with the spectrum recorded at

room temperature; it is probable that at room temperature the sample is in the fast motional regime and therefore increasing the rate of the motion (by increasing the temperature) does not have any effect on the lineshape.

6.4.4. Investigation of the Dynamic Model for the Motion of Pyridine in TOT

The initial model that we consider for the motion of pyridine in the cage structure of TOT is based on the symmetry of the pyridine molecule (C_{2v}) and is a 180° jump motion of the molecule along the two-fold axis which passes through the nitrogen atom (Fig. 6.13). The orientation of the principal components of the electric field gradient tensors for the deuterons in pyridine is similar to that for the benzene molecule. The exchange matrix for the 180° jump model of pyridine along its two-fold axis is:

	1	2	3	4	5
1	0	0	0	0	0
2	0	-1	0	0	1
3	0	0	-1	1	0
4	0	0	1	-1	0
5	0	1	0	0	-1

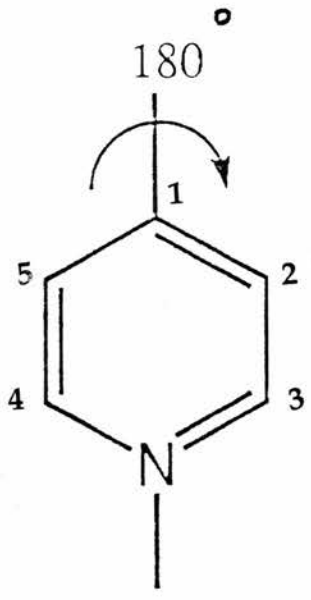

Fig. 6.13 180° jump of pyridine along the two-fold axis which passes through the nitrogen atom.

Fig. 6.14 shows the spectra calculated for this motional model using computer simulation for different jump rates (0-10^{12} Hz).

In the simulated spectra, two distinguishable components are observed. The shape and the size of the first component (the outer splitting) are constant within different jump rates. This component arises from the single deuteron that is along the jump axis. The orientation of z axis of the electric field gradient for this deuteron does not change in 180° jump model for pyridine. The other four deuterons give rise to the second component of the spectrum (the middle splitting), which changes in shape and size as the motional rate changes .

In the experimental spectrum recorded at 130 K a "static" powder pattern (AA′) is observed in the spectrum. This static contribution gradually decreases both in intensity and the size. At room temperature, this contribution has been essentially removed from the spectrum.

Within the confines of our motional model the deuteron that lies on the two-fold jump axis should contribute an essentially "static" powder pattern to the spectrum, and this should remain essentially unaltered within the temperature range. The fact that we do not observe such a contribution in the entire temperature range suggests that this model by itself is insufficient to explain the dynamic behaviour of the system.

However, it has been reported [24] that in 180° jump motions of phenyl rings, the static deuteron possesses a longer spin-lattice relaxation time than with the mobile deuterons. Therefore, recording the ^2H NMR spectrum of the sample with a relatively long recycle delay could in principle reveal such a possibility for pyridine/TOT. The ^2H NMR spectrum of the sample was recorded using a recycle delay of 60 s. No appreciable change is observed between this spectrum and the spectrum recorded using a recycle delay of 5 s. Hence the absence of a static

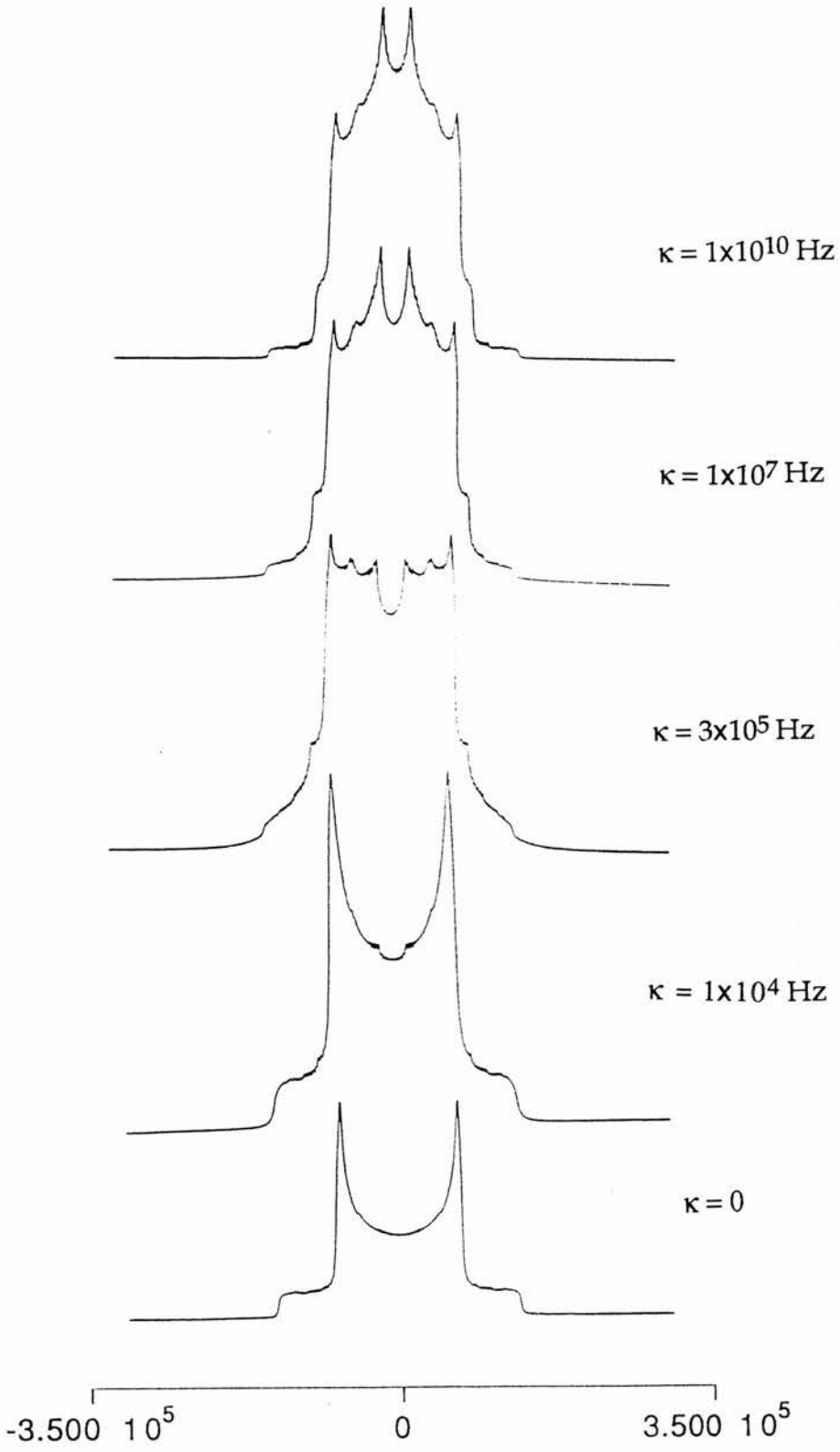

Fig. 6.14 simulated spectra for the motion of pyridine based on 180° jump model.

contribution in the experimental spectra can not be attributed to the difference in relaxation times of the static and mobile deuterons in the pyridine molecule.

Hence the fit between the proposed motional model and the experimental results is unsatisfactory, and further assumptions are required. It might be argued that a more realistic and complete approach including both site and molecular symmetry i.e., incorporation of the structure of the cage in addition to the geometry of the mobile molecule as the determinants of the dynamic behaviour could be more appropriate. It may be expected that, guest molecules can hop among the three positions, and this process will be augmented by any motion about the molecular axis. The simulated spectrum resembles the spectrum of a system undergoing only a simple six fold rotation.

In another approach we have considered the fact that the actual angles between carbons and nitrogen in the ring structure of pyridine deviates from the ideal angle of 120° [25]. The new Euler angles calculated based on the experimentally measured angles is presented in Table 6.3.

Simulated ^2H NMR spectra based on these new Euler angles do not show any new spectral features in addition to the spectral features for the spectra simulated on the basis of the ideal structure of pyridine; this implies that the small changes in bond angles in the ring structure does influence significantly the observed spectral features.

6.4.5 Concluding Remarks

Pyridine molecules trapped within the cage structure of its TOT inclusion compound experience motion on the ^2H NMR timescale. We have not yet been successful in reproducing the spectral lineshape for this motion using computer simulation.

Carbon No.	α	β	γ
1	0	61.74	0
2	0	0	0
3	0	-61.74	0
4	0	116.03	0
5	0	-116.03	0

Table 6.3 Euler angles (degrees) for different carbons of pyridine, obtained by considering the actual bond angles in the molecule [25]. The Euler angles define the orientations of the principal axis systems of the electric field gradient tensors relative to a space fixed molecular reference frame.

One reason of this failure might be the possible occurrence of a phase transition in the system. Some solid materials undergo a phase transition from one crystallographic structure to an other at a specific temperature. A solid-solid phase transition can lower the symmetry of the guest site and/or slightly contract the crystallographic unit cell in the lower temperature phase compared with the structure of the high temperature phase. Consequently the shape of the reorientational potential for the guest molecule change [13].

There has been no previous report on the variable temperature X-ray diffraction or calorimetric investigations of the pyridine /TOT inclusion compound to address whether a phase transition occurs for this compound. Such information may help us in understanding the dynamic behaviour of this system. Also, it is possible that guest molecules occupy more than one site and in each site will exhibit a different type of motion. The observed spectrum could be the superposition of spectra arising from these individual motions.

It is expected that additional experimental data, provided by other types of solid-state NMR experiments, observing nuclei such as ^{13}C, ^{1}H,

^{14}N, ^{15}N, etc. and employing other techniques will both corroborate and complement this approach.

In conclusion, our initial attempt this ^{2}H NMR to derive a model for the dynamic behaviour of the pyridine /TOT inclusion compound proved unsuccessful in reproducing the experimental spectra. The main point that should be emphasised is that the simplicity of the dynamic models used in our present approach to interpret these data might contribute to this failure.

References:

[1] Mehring, M. "High Resolution NMR Spectroscopy in Solids", 2nd ed; Springle-Verlag: New York 1983.

[2] Haeberlen, U. "High Resolution NMR in Solids"; Academic Press: New York, 1976.

[3] Griffin, R. G. in "Methods in Enzymology", Lowenstein, L. M., Ed.; Academic: New York 1981; Vol. 72, part D, section I, p 108.

[4] Freed, J. H.; Bruno, G. V.; Plonazek, C. F. *J. Phys. Chem.*. 1971, **75**, 3386.

[5] Campbell, R. F.; Meirovitch, E.; Freed, J. H. *J. Phys. Chem.*. 1979, **83**, 525.

[6] Meirovitch, E.; Freed, J. H. *Chem. Phys. Lett.* 1979, **64**, 311.

[7] Baram, A.; Luz, Z.; Alexander, S. *J. Chem. Phys.*. 1973, **58**, 4558.

[8] Schaefer, J.; Stejskal, E. O.; Mckay, R. A.; Dixon, W. T. *J. Magn. Reson.*. 1984, **57**, 85.

[9] Frey, M. H.; Opella, S. J.; Rochwell, A. L.; Gierasch, L. M. *J. Am. Chem. Soc.* 1985, **107**, 1947.

[10] Jelinsky, L. W.; Dumais, J.J.; Watnick, P. I.; Engel, A. K.; Sefcik, M. D. *Macromolecules*. 1983, **16**, 409 and references cited therein.

[11] Hentschel, D.; Sillescu, H.; Spiess, H. W. *Macromolecules.* 1981, **14,** 1605.

[12] Abragam, A. "Principle of Nuclear Magnetism"; Clarendon Press: Oxford, 1961.

[13] MacIntosh, M, R.; Fraser, B.; Gruewel, M. L. H.; Wasylishen, R. E.; Cameron, T. S. *J. Phys. Chem.* 1992, **96,** 8572.

[14] Meirovitch, E., Rananavare, B., Freed, J. H. *J. Phys. Chem.* 1987, **91,** 5014.

[15] Davis, J. H.; Jeffrey, K. R.; Bloom, M.; Valic, M. I.; Higgs, T. P. *Chem Phys. Lett.* 1976, **42,** 390.

[16] Boden, N.; Clark, L. D.; Hanlon, S. M.; Mortimer, M.; *Faraday Symposia,*. 1978, **13,** 109.

[17] Meirovitch, E; Belsky, I.; Vega, S. *J. Phys. Chem.* . 1984, **88,** 1522.

[18] Boddenberg, B.; Grosse, R. Z. *Naturforsch,* 1986, **14a,** 1361.

[19] Zibrowious, B.; Caro, j.; Pfeifer, H. *J. Chem. Soc., Faraday Trans..* 1988, **84,** 1328.

[20] Levitt, M. H.; Suter, D.; Ernst, R. R. *J. Chem. Phys.* 1984, **80,** 3064.

[21] Barnes, R. G. in "Advances in Nuclear Quadrupole Resonance"; J.A.S. Smith, Ed., Vol. 1, Heyden, 1974, p. 335.

[22] Heyes, J. S.; Dobson, M. C. *Mag. Res. Chem.* 1990, **28,** S37.

[23] Brunie, S.; Navaza, A.; Tsoucaris, G.; Declercq, P. J.; Germain, G. *Acta Cryst.* 1977, **B33,** 2645.

[24] Gall, C. M.; Di Verdi, J. A.; Opella, S. J. *J. Am. Chem. Soc.* 1981, **103,** 5039.

[25] Sorensen, G. O., Mahler, L., Rastrup-Andersen, N. *J. Mol. Struc.* 1974, **20,** 119.